Forschungszentrum Karlsruhe
Technik und Umwelt

Wissenschaftliche Berichte
FZKA 5666

Summary Report of NEPTUN Investigations into the Transient Thermal Hydraulics of the Passive Decay Heat Removal

D. Weinberg, H. Hoffmann, K. Rust,
H. H. Frey, K. Hain, W. Leiling, H. Hayafune

Institut für Angewandte Thermo- und Fluiddynamik
Hauptabteilung Ingenieurtechnik
Projekt Nukleare Sicherheitsforschung

Dezember 1995

FORSCHUNGSZENTRUM KARLSRUHE
Technik und Umwelt
Wissenschaftliche Berichte
FZKA 5666

SUMMARY REPORT OF NEPTUN INVESTIGATIONS INTO THE TRANSIENT THERMAL HYDRAULICS OF THE PASSIVE DECAY HEAT REMOVAL

D. Weinberg, H. Hoffmann, K. Rust,
H.H. Frey, K. Hain, W. Leiling
and H. Hayafune*

Institut für Angewandte Thermo- und Fluiddynamik
Hauptabteilung Ingenieurtechnik
Projekt Nukleare Sicherheitsforschung

* Power Reactor and Nuclear Fuel Development Corporation,
O-arai Engineering Center, O-arai, Ibaraki-ken 311-13, Japan

Forschungszentrum Karlsruhe GmbH, Karlsruhe
1995

Forschungszentrum Karlsruhe GmbH
Postfach 3640, 76021 Karlsruhe

ISSN 0947-8620

SUMMARY REPORT OF NEPTUN INVESTIGATIONS INTO THE TRANSIENT THERMAL HYDRAULICS OF THE PASSIVE DECAY HEAT REMOVAL

ABSTRACT

To demonstrate the capability of the passive decay heat removal system designed for an advanced pool-type sodium cooled reactor (e.g. European Fast Reactor, EFR) experiments were performed in the 1:5 scaled three-dimensional NEPTUN test facility using water as the simulant fluid. These studies were focused on the transition from nominal operation conditions under forced convection to decay heat removal operation under natural convection. The influences of different operating and design parameters on the onset of the natural convection within the primary system were investigated. The core power before scram was varied in the range of 800 to 1600 kW. The symmetrical cooling mode was compared to a highly asymmetrical decay heat removal caused by the operation of only two of four serviceable decay heat exchangers. The decay heat exchangers startup was delayed up to one hour and the effects of permeable and impermeable structures above the core were examined. In addition the pump coast down time was varied and finally the hypothetical situation where all primary flow paths via intermediate heat exchangers were blocked was simulated.

The results corroborate the findings of preceding tests with the RAMONA model, scaled 1:20. With the core power reduction at scram and the start of the decay heat exchangers operation cold fluid is delivered into the prevailing uniform temperatured upper plenum. A temperature stratification develops with distinct large temperature gradients. The onset of natural convection is mainly influenced by two effects, namely, the temperature increase on the intermediate heat exchangers primary sides as a result of which the downward pressures are reduced, and the startup of the decay heat exchangers which leads to a decrease of the buoyancy forces in the core. The temperatures of the upper plenum are systematically reduced as soon as the decay heat exchangers are in operation. Then mixed fluid in the hot plenum reaches the intermediate heat exchangers inlet windows and causes an increase in the core flow rate.

The primary pump coastdown curve influences the primary system thermal hydraulics only during the first thousand seconds after scram. The longer the pumps

operate the more cold fluid is delivered via the core to the upper plenum. The delay of the start of the decay heat exchangers operation separates the two effects which influence the core mass flow, namely the heatup of the intermediate heat exchangers as well as the formation of the stratification in the upper plenum. Increasing the power as well as the operation of only half of the available decay heat exchangers increase the system temperatures. A permeable above core structure produces a temperature stratification along the total upper plenum, and therefore a lower temperature gradient in the region between core outlet and lower edge of the above core structure, in comparison to the impermeable design. A complete flow path blockage of the primary fluid through the intermediate heat exchangers leads to an enhanced cooling effect of the interstitial flow and gives rise to a thermosiphon effect inside the core elements. The core outlet temperatures increase slightly, but the core coolability from above is feasible without any difficulty.

The comparison of numerically determined findings with the FLUTAN code and measurements generally leads to encouraging agreements. These comparisons were carried out for the steady state prescram (forced convection) and the post scram (natural convection) conditions.

The conclusion of all these investigations is that the decay heat can be removed from the primary system by means of natural convection. Always convective flow paths develop, which ensure an effective cooling of all regions. This is even proved for extreme conditions, e.g. in case of delays of the decay heat exchanger startup, failures of several decay heat removal circuits, and a total blockage of all the primary flow paths via the intermediate heat exchangers.

ZUSAMMENFASSENDER BERICHT ÜBER NEPTUN-UNTERSUCHUNGEN ZUM TRANSIENTEN THERMOHYDRAULISCHEN VERHALTEN DER PASSIVEN NACHWÄRMEABFUHR

ZUSAMMENFASSUNG

Mit Hilfe der NEPTUN-Versuchsanlage wurde die Funktion des für einen fortgeschrittenen natriumgekühlten Reaktor (z.B. des Europäischen Schnellen Reaktors, EFR) vorgesehenen, völlig passiv arbeitenden, sicherheitstechnischen Nachwärmeabfuhr-Systems nachgewiesen. NEPTUN ist ein im Maßstab 1:5 errichtetes 360°-Tankmodell. Als Modellfluid dient Wasser. Die Untersuchungen konzentrierten sich auf das thermohydraulische Geschehen beim Übergang vom Normalbetrieb bei Zwangskonvektion auf den Nachwärmeabfuhrbetrieb bei Naturumlauf. Als Versuchsparameter wurden betriebliche und geometrische Zustände verändert. Die Kernleistung im simulierten Normalbetrieb wurde zwischen 800 und 1600 kW variiert. Stark unsymmetrische Kühlungsarten des Oberplenums wurden durch den Betrieb von nur zwei der vier vorhandenen, paarweise eingebauten Tauchkühlern untersucht. Die Zeiten der Nichtverfügbarkeit der Tauchkühler nach Schnellabschaltung wurden bis zu einer Stunde variiert. Der über dem Kern befindliche Instrumentierungsstopfen wurde in durchströmbarer und nicht durchströmbarer Form eingesetzt. Schließlich wurden extreme Kühlungszustände des Kerns untersucht durch Blockade sämtlicher Primärkühlmittel-Strömungspfade der Zwischenwärmetauscher.

Die Ergebnisse bestätigen vorausgegangene Versuche mit der im Maßstab 1:20 aufgebauten RAMONA-Anlage. Mit der plötzlichen Leistungsreduktion des Kerns und dem Beginn des Tauchkühlerbetriebes wird kaltes Fluid ins gleichmäßig temperierte Oberplenum eingespeist. Damit beginnt die Ausbildung einer Temperaturschichtung mit starken Temperaturgradienten im Bereich der Tauchkühleraustrittsfenster und der Kernoberkante. Es zeigt sich, daß die transienten Übergangszustände hauptsächlich von zwei Vorgängen geprägt werden, nämlich durch den Temperaturanstieg nach Scram auf der Primärseite der Zwischenwärmetauscher (Reduktion der Abtriebskräfte) und dem Einschaltzeitpunkt der Tauchkühler nach Scram (Reduktion der Auftriebskräfte). Beide Vorgänge vermindern im Naturkonvektionsbetrieb den Massendurchsatz im Kern.

Die Oberplenumstemperatur wird systematisch abgekühlt, sobald die Tauchkühler eingeschaltet werden. Kühleres Fluid erreicht dann die Zwischenwärmetauscher-Eintrittsfenster, was eine Erhöhung der Kerndurchströmung bewirkt. Die Auslaufzeit der Primärpumpen beeinflußt das thermohydraulische Geschehen im Oberplenum nur in den ersten 1000 Sekunden nach Scram.Mit zunehmender Kernleistung steigen die Systemtemperaturen an. Der Ausfall der Hälfte der verfügbaren Tauchkühler beeinflußt das Temperaturniveau, nicht aber die charakteristische Temperaturverteilung im Oberplenum. Die Oberplenumstemperatur wird verzögert abgekühlt, wenn die Tauchkühler bis zu einer Stunde nach Scram nicht in Betrieb genommen werden können. Die dabei auftretende Erhöhung der Oberplenumstemperatur ist gering, weil die Speicherkapazitäten des Oberplenums groß sind. Sofern der Instrumentierungsstopfen über dem Kern vom heißen Kernfluid durchströmt wird, bildet sich die Temperaturstratifikation über die gesamte vertikale Erstreckung des Oberplenums aus. Das ist nicht der Fall, wenn die Durchströmung unterbunden wird. Dann bleiben die starken Temperaturgradienten zwischen Kern und Tauchkühleraustritt erhalten. Schließlich wird durch eine totale Unterbrechung der normalen Kühlmittelzufuhr zum Kern durch Blockade sämtlicher Primärkühlmittel-Strömungspfade der Zwischenwärmetauscher die Kernkühlung verändert. Der Kern wird dann hauptsächlich vom Fluid gekühlt, das über die obere Kante des Kernmantels zwischen die Kernelemente strömt. Diese Strömung ist in der Lage, ca. 60 % der freigesetzten Wärme des Kerns abzuführen. Der Rest wird durch Thermosiphons, die sich in den beheizten Elementen ausbilden, abgeführt. Die Kernaustrittstemperaturen steigen dabei leicht an, der Kern bleibt auch in diesem Extremzustand kühlbar.

Es wurden Rechnungen mit experimentellen Werten für den Normal- und Nachwärmeabfuhr-Betrieb verglichen. Die mit dem FLUTAN Rechenprogramm ermittelten Ergebnisse stimmen generell gut mit den Messungen überein.

Abschließend kann festgestellt werden, daß die Nachwärme aus dem Primärsystem sicher abgeführt werden kann. Es bilden sich immer kühlungseffektive Strömungspfade aus, die selbst in außergewöhnlichen Situationen die Kühlung des Primärsystems sicherstellen.

CONTENTS

1. INTRODUCTION

The reliable removal of decay heat after the shutdown of a nuclear reactor is an important safety criterion. For this reason, passive measures are the guiding principle for the design of the European Fast Reactor (EFR) elaborated in a French/British/German cooperation [1].

The EFR is a liquid-metal cooled plant with a total thermal power of about 3,600 MW_{th}. The primary system is based on a pool-type configuration as illustrated in Fig. 1. Sodium is circulated through the core by primary pumps (PPs). The heat is transferred to the secondary sodium by intermediate heat exchangers (IHXs). The decay heat removal (DHR) concept comprises two diverse systems:

1. Under nominal operating conditions including a scheduled reactor shutdown, the heat is removed from the primary system by intermediate heat exchangers and their cooling circuits and is transported via steam generators to the water/steam plant with turbine, generator and condenser. Figure 2 shows one of several cooling circuits with the IHXs located in the reactor vessel and the main components.
   In this heat transfer system, the fluid is transported by the PPs in a forced convection mode. After a scram, the PPs are coasted down by controlling the electric power to values given as a function of time. The coastdown characteristics determine the core mass flow rate and hence the core temperatures to meet the safety requirements.

2. In unlikely cases of unavailability of the main heat transfer route via secondary system and water/steam plant or a complete loss-of-station service power (LOSSP), the decay heat will be removed by the safety graded system [2]. This DHR system, shown in Fig. 3, is based on six direct reactor cooling (DRC) systems operating independently from each other. Each of them consists of a sodium/sodium decay heat exchanger (DHX) immersed in the upper plenum (UP) of the primary vessel and connected via an intermediate sodium loop to a heat sink formed by a sodium/air heat exchanger (AHX) arranged at the bottom end of a stack with air inlet and outlet dampers. All DRC loops are rated to a thermal power of 15 MW_{th} each under nominal conditions. The decay heat is removed by natural convection on both sodium sides and natural draft on the air side. To enforce the startup of the DRC circuits, the air dampers of the stacks

are opened initiated by an automatic signal of the reactor protection system or in case of a LOSSP mechanically by the operator staff. Except for this procedure, the DRC systems are entirely passive. During power operation of the plant, however, a certain sodium mass flow in the DRC loops is maintained by an assured minimum level of heat loss from the air-cooled stack. This guarantees the right sodium flow direction at the startup of the DRC system.

2. OBJECTIVES

The objectives of the investigations into decay heat removal by natural convection are:

1. to demonstrate the capability of the passive DRC concept by means of natural convection without exceeding the maximum permissible load values specified for the respective structures, for the whole time after scram up to long time behavior [3],
2. to study the influence of different design geometries and operating parameters on the time dependent thermal hydraulic behavior of the primary system with its individual components, and its interaction with the DHR system,
3. to generate a broad transient data basis for the analyses and identification of physical processes which should be modeled in computer codes. These verified computer codes should be able to transfer the experimental data obtained in scaled-down test facilities to full scale nuclear power plant conditions.

To address questions of an inherent safe operation of the DRC system, many experiments were carried out in test rigs of different scale and degree of detail using sodium or water as fluid [4]. The philosophy of the reactor typical tests was to start with a small geometry and a simple apparatus and to successively progress in both scale and complexity. Water instead of sodium was frequently preferred to make use of available measuring techniques and to allow the visualization of fluid motion and temperature fields.

The group of water test facilities includes the three-dimensional (3D) 1:20 scaled RAMONA test facilities and the 1:5 scaled NEPTUN apparatus. Using RAMONA numerous essentially laminar experiments were conducted under nominal and

nonnominal conditions [5]. The main parameters of steady state and transient tests were in particular: the core power, the radial power profile of the core, the geometry of the above core structure (ACS), the design and number of the operated DHXs, the complete primary side flow path blockage of the IHXs, the fluid level in the primary vessel, and the number of the DRC loops in operation. The transient investigations concerned the transition range from forced to natural convection, i.e., the postscram influence of the aforementioned parameters on the thermal hydraulics of the primary system. In addition, the coastdown characteristics of the pumps at the primary and secondary sides, the startup time of the DHXs were of interest.

Following to the transient RAMONA tests, water experiments were conducted in the 1:5 scaled 3D NEPTUN apparatus under steady state conditions [12]. The aim was to examine the effects of different design and operating parameters on the primary system thermal hydraulics such as the core power and radial core power gradient, the number of DHXs put in operation, the fluid level in the primary vessel, the design of the ACS and the complete flow path blockage of the IHXs on their primary sides.

These stationary NEPTUN tests were completed by investigations into decay heat removal during the transition range from forced to natural convection. Beside the forementioned parameters these tests also include the variation of the startup time of the DHXs and different coastdown characteristics of the primary pumps as quantities of interest.

For analyzing the combined fluid dynamics and heat transport, the computer code FLUTAN [13] has been improved, validated and applied for the 3D numerical simulation of the RAMONA investigations and several steady state NEPTUN tests. The results of the computations were compared against the measurements.

3. SIMILARITY AND MODEL DESIGN

In order to make sure that steady state and transient results gained from scaled model experiments using water instead of sodium can be transferred to practical situations, the following similaritiy criteria must be satisfied [6, 7]:

- geometrical similarity of the model to the reality,
- similarity of the governing differential equations,
- similarity of the initial and boundary conditions.

From these requirements, a model should represent the internal flow geometry of the reactor tank with all relevant components. In order to preserve similarity, the following characteristics of the scaled water test facilities and the sodium-cooled reactor must be identical:

$$\text{— Reynolds number} \quad Re = \frac{\text{inertia force}}{\text{friction force}} = \frac{u_o\, L_o}{\nu}$$

$$\text{— Richardson number} \quad Ri = \frac{\text{buoyancy force}}{\text{inertia force}} = \frac{g\, \beta\, \Delta T_{UP} \cdot L_{UP}}{u_o^2}$$

$$\text{— Peclet number} \quad Pe = \frac{\text{heat transfer by convection}}{\text{heat transfer by conduction}} = \frac{u_o\, L_o}{a}$$

$$\text{— Euler number} \quad Eu^{+} = \left(\frac{\text{pressure force}}{\text{inertia force}}\right)_{DHX} \Big/ \left(\frac{\text{pressure force}}{\text{inertia force}}\right)_{c} = \frac{\Delta p_{DHX}}{\Delta p_c} \cdot \frac{u_c^2}{u^2_{DHX}}.$$

The particular quantities are indicated in Fig. 4. The Euler number Eu* denotes the ratio of the pressure drops between the DHX and the core for the model and the reactor, respectively, and thus determines the main flow paths in the primary system. In Fig. 5, the ratios of model (M) to reactor (R) characteristics are plotted vs. the scale of the facilities:

$$Re^{*} = \frac{Re_M}{Re_R}\,;\; Ri^{*} = \frac{Ri_M}{Ri_R};\; Pe^{*} = \frac{Pe_M}{Pe_R};\quad ;\quad Eu^{*} = \frac{Eu^{+}_M}{Eu^{+}_R}$$

It can be seen that these criteria cannot be achieved altogether by the differently scaled models. From the diagram can be deduced that a 1:20 scaled water test facility results in Pe, Ri, and Eu+ numbers which are identical to those of the sodium-cooled reactor. For the Re number, however, there exists a deviation of up to 10^{-3}. This means that the RAMONA experiments were performed under laminar conditions. Therefore, the 1:5 scaled NEPTUN apparatus was built reducing the Re number deviation up to about 10^{-1} depending on the supplied heating power and consequently on the corresponding physical properties of the

fluid. A detailed derivation of the similarity laws has been described in a separate report [9].

The main purpose of these investigation was the study of the scaling between the 1:20 RAMONA-II model and the 1:5 NEPTUN model. Therefore, the parameters, the boundary and starting conditions for the transient experiments were taken from RAMONA program [5]. This procedure was limited by major variations in the technical details of NEPTUN (see chapter 6), namely:

- the power reduction before scram,
- the complexity of the core geometry,
- the design of the IHXs and PPs.

In the following report the major results achieved with regard to DHR by natural convection are summarized. The results concentrate on the thermal hydraulics behavior of the primary system of NEPTUN during the transition from forced to natural convection initiated by a scram with the unavailability of the main heat transfer route or LOSSP.

The NEPTUN and RAMONA-II models were actually initiated during the former German SNR-2 project [10]. The facilities are built up as 4 loop-systems and with geometrical similarity. Both experimental series cover the important physical effects with regard to the cooling modes in the primary system and DRC system and provide a broad data basis for the development, improvement and assessment of computer programs.

Such qualified tools are necessary to make reliable predictions with respect to uniform and non-uniform cooling modes associated with the interactions of the core, the DHXs and the upper plenum (UP) of the vessel under highly different initial and boundary conditions. A second concern is to provide a possibility to transfer results gained from water test facilities of different scale to practical situations within the EFR primary vessel, the individual components, and the total DHR system [11].

During the course of these investigations the original 4 loop SNR design was transformed in a 3-loop EFR design to spare costs and construction time. Although all results are gained with 4-loop systems, the qualitative and quantitative thermal hydraulic behaviors of the core and the UP and the reactor

vessel are valid also for the 3-loop system of the EFR. This is confirmed by thermal hydraulic investigations with a 3-loop system RAMONA-III [5], scaled 1:20 with respect to the EFR. In [5] the agreement and the systematic differences between 4- and 3-loop systems are described.

4. NEPTUN TEST FACILITY

A scheme of the NEPTUN test facility is outlined in Fig. 6. A very detailed description of the test facility and the results of the steady state investigations are given in [13]. The model is made of stainless steel and provides easy access of components. Fig. 6 shows vertical and horizontal cross-sections of NEPTUN together with the main dimensions. The vessel volume is about 30 m^3 filled with demineralized and degased water. The primary vessel is divided into the hot upper plenum (UP) and the cold lower plenum (LP), separated by the curved "redan". Both plena are interconnected through the primary side of the IHXs. The coolant is fed by simulators of the primary pumps (PPs) from the lower plenum to the high pressure plenum (HPP) underneath the core. It passes the core and reaches the UP where it circulates through the IHXs back to the LP. In the center of the upper plenum there is an above-core structure (ACS). The core is surrounded by a water filled cavity. The reference or zero level of all vertical dimensions is located at the bottom of the HPP.

NEPTUN was built in similarity to the SNR-2 [10]. This is a four loop type reactor design with 4 PPs and 8 IHXs. Four DHXs are installed pairwise in angular positions of 180 deg. The bird's-eye photo in Fig. 7 clearly shows the arrangement of 4 PPs, 8 IHXs and 4 DHXs.

The core is designed for a maximum power of 1600 kW and consists of 337 heatable fuel and storage subassemblies (SAs) arranged in 7 heating groups as well as 366 unpowered reflector and shielding elements, see Fig. 8. The core is mounted on the grid plates forming the HPP and is surrounded by a cylindrical shell of 1620 mm diameter. Its vertical measure is identical to the core height. The experiments reported in this study were carried out by heating 253 (heating group 1 to 6) or 337 (heating group 1 to 7) SAs. Heating group 1-6 represents the fuel and fissile elements below the ACS geometry, heating group 7 the additional heatable storage elements. All SAs are individually heatable in order to simulate a radial power profile.

Each heatable subassembly consists of 19 rods with 8.5 mm outer diameter, see Fig. 9. The rods are hexagonally arranged in circular wrapper tubes with an inner diameter of 50 mm. The fuel rod simulators have a heated section of 220 mm and unheated sections of 280 and 360 mm representing the lower, respectively upper fertile zones. Two grid spacers are installed upstream and downstream of the heated bundle portion to guanrantee a rather flat temperature profile across the bundle.

Downstream the 19-rod bundle, a seven pin bundle simulates the reflector zone inside the core. The circular wrapper tubes (SAs) of the core are spaced on a triangular pitch of 58 mm. At the bottom ends, the wrapper tubes are bolted to the core grid plate with an upper and lower plate. About 220 mm below the upper edge of the core, a perforated plate is inserted to simulate the pad plane which supports the SAs at the prescribed wrapper-to-wrapper pitch. In order to establish the same hydraulic behavior in the vertical direction the plate contains holes in the center of each area which is formed by the triangularly arranged wrapper tubes. This free-flow area is equal to that available between the wrapper tubes of hexagonal design.

The cylindrical above core structure of 934 mm o.d., see Fig. 10, is centrically positioned to the core, see Fig. 6. There are 2 different ACS configurations:

- a cyclindrical permeable ACS internally equipped with horizontal plates and vertical guide tubes which simulate the hydraulic behavior of the control rod drivelines and core monitoring systems. The vertical guide tubes penetrate the permeable bottom plate of the ACS. Their axial distance to the top end of the core is 28 mm. The clearance between the bottom end of the permeable ACS and the top end of the core amounts to 200 mm. A perforated shell covers the peripheral surface of the ACS characterized by a permeability of 13 %. The bottom plate has a permeability of 15 %. An additional plate bolted between the bottom plate and the lower end of the guide tubes serves as lower guiding device of these protruding vertical tubes. A permeable ACS can be passed by the fluid leaving the core.
- by covering the perforated peripheral surface with a solid sheet the socalled impermeable ACS was realized. In this case the fluid from the core is hindered to flow through the ACS.

For the four DHR-loops, straight-tube bundle-type DHXs operating on the counter flow principle have been chosen, see Fig. 11. The 180 vertically arranged tubes of 7 mm outer diameter are connected to a flow distributor at the lower end and to an annular collector at the upper end of the bundle. The bundle is installed in a shell with 20 slot-type upper inlet windows (450x15 mm) and 20 exit windows (100x15 mm). The primary upper plenum fluid enters through the inlet windows of the shell, travels down in counterflow to the secondary fluid and exits through the outlet windows in locally turbulent condition. The secondary-side coolant enters through a central tube of 30 mm diameter, travels down to the flow distributor and within the tubes up to the collector. The collector is isolated from the inlet tube to minimize heat losses. From the collector, the water is fed within the secondary cooling circuit, see Fig. 12. In each of the four circuits the mass flow rate and inlet and outlet temperatures are measured to allow a thermal balance of the heat removed from the primary vessel. The individual circuits are controlled to reach identical boundary conditions for all DHXs being in operation. The immersion depth of each DHX amounts to 1030 mm. This means that the top edge of the inlet windows at the primary side exceeds the regular water level by approximately 130 mm.

The eight intermediate heat exchangers were constructed mainly to simulate the shell side primary coolant flow. Each of them is equipped with 18 inlet and outlet windows. For the transient experiments a special device was mounted at the upper part of each IHX to guide the warm upper plenum fluid by an external pump to two external positioned heat exchangers (EHXs). The cooled fluid leaving the two EHXs is circulated back to the 8 IHXs. Suctioning and feeding of the primary fluid occurs in the region of the IHX inlet windows. Fig. 14 shows the IHX equipped with the flow guiding device. The pre- and postscram flow paths are indicated. Under prescram flow conditions the core power is totally transfered to the EHXs and from the EHXs secondary sides to a cooling tower. This forced convection procedure produces a hot upper plenum and a cold lower plenum. The transition to natural convection flow after pump coast down is realized by opening the flap in the partition flange of each IHX. This allows the warm fluid entering the IHX inlet windows to flow directly downward to the lower plenum. The external cooling circuits are put out of operation. This procedure initiates a slightly different thermal hydraulic behavior of NEPTUN with respect to the reactor: At the start of the natural convection the IHXs of NEPTUN up to the partition flange are filled with cold fluid of identical

temperature whilst the fluid in the IHXs of the reactor shows a clear temperature stratification over the total axial length.

Each of the four primary pumps is hydraulically simulated with respect to its position and hydraulic resistance. The suction side of the pump dummy communicates via inlet slots with the lower plenum, whilst the outlet side is connected via pipework with the HPP (Fig. 15). During these experiments the primary pumps are represented by one external pump installed in the external coolant circuits having similar flow characteristics as the model pumps of RAMONA-II. Under forced convection operation the pump outlet pressure exists in the lower plenum, the pump simulators and in the IHXs.

5. INSTRUMENTATION AND DATA ACQUISTION

The measuring and control systems of the NEPTUN facility can be subdivided into systems for the adjustment, surveillance and safe operation of the plant, and those devices necessary for the real measurements. Beside the primary system all secondary and tertiary circuits are mainly equipped with temperature and flow sensors. Additionally pressure and fluid level detectors are installed, together with the power supply monitors.

NEPTUN serves to study the transition from forced to natural convection. Therefore stationary and movable temperature and flow measuring devices are available. Because of the dimensions and complexity of the test set-up the number of measuring position is high. Within the vessel, about 1200 thermocouples (TCs) are mounted at various locations of interest. These are isolated NiCr-Ni-thermocouples of an outer diameter of 1.5 mm with measuring tips of 30 to 300 mm length and 0.5 mm o.d. Calibration tests show that the uncertainties of the measurements are less than $\pm$ 0.2 K in the temperature range of $20°C < T < 60°C$.

The stationary temperature measuring devices are installed at various locations of interest within the core, the ACS, the IHXs, the DHXs, the HPP, the "redan", and the lower plenum. Thermocouples on movable supporting systems are installed in the upper plenum and allow temperature measurements at nearly each position of the upper plenum.

5.1 Stationary Measuring Devices

The instrumentation of the core comprises the measuring positions in the HPP, inside the SAs, and in the interwrapper spaces. The layouts of Figs. 9, 16 and 17 illustrate the measuring positions. The temperatures of the coolant entering the SAs are recorded in the HPP along two diagonals (see lower part of Fig. 16). Each radial position is equipped with one TC at the axial level of 158 mm. There are eight SAs (see upper part of Fig. 16, closed markers) which are instrumented at four axial levels (see Fig. 9). At the axial levels of 234 and 851 mm, six TCs are arranged to register the coolant temperatures upstream and downstream of the 19 heater rods. Three TCs are located at the axial level of 926 mm.For the measurement of the coolant temperatures at the outlet side of the SAs, the heads of the same SAs are provided with four TCs fixed at the axial level of 1,037 mm. In addition, there are 39 core element positions with one TC placed in the SA head (see upper part of Fig. 16, open markers). The instrumentation of the interwrapper spaces consists of two groups. The first group comprises ten measuring positions along a diagonal (see upper part of Fig. 17). Each radial position is equipped with five TCs located at different axial levels (see axial layout of Fig. 17). A second group of measuring devices is at 60° intervals along the perphery of the core (see lower part of Fig. 17). The TCs are located at four axial levels.

The instrumentation of the ACS can be subdivided in three groups (Fig. 10). The first group (A) consists of 44 TCs which are situated all together at the axial level of 1,248 mm. The second group (B) concerns five radial positions which are uniformly equipped with 14 TCs in axial direction. Between the axial levels of 1,129 and 1,285 mm, the TCs are installed at 12 mm intervals. The third group (C) comprises two radial positions which have the same instrumentation in axial direction. The measuring traverses are located at the centerline and at a radial distance of 201 mm from it. The axial levels of 16 TCs are shown in Fig. 10.

The simulators of the PPS are instrumented at their lower ends of the inlet slots. At the outside of each simulator, three TCs are located on pitch circle diameters of 249 mm at angular intervals of 120°. Details are shown in Fig. 15.

The inlet and outlet windows of two opposed IHXs (No. 2 at 69° and No. 6 at 249°) are equipped with TCs as shown in Fig. 13. The measuring devices are located

within the IHX housing on a common pitch circle diameter of 394 mm. Each axial position is provided with eight TCs at angular intervals of 45°. There are three axial TC positions at the inlet and the outlet windows. The remaining six IHXs are less extensively instrumented with three TCs uniformly distributed over the periphery with an angular interval of 120°. The TCs are fixed at one axial level at the inlet side (z = 1,832 mm) and three levels at the outlet side.

The inlet and outlet windows of three DHXs (No. 1 at 84°, No. 3 at 264°, and No. 4 at 276°) are equipped with TCs as shown in Fig. 11. The temperatures are measured within the DHX housings on a common pitch circle diameter of 178 mm. Each of the six different axial levels includes eight TCs in circumferential direction. For control purposes, 25 TCs are installed at DHX No. 2 at 96°.

In addition the fluid temperatures at the inlet and at the outlet of the secondary sides of the DHXs as well as of the external heat exchangers (simulating the IHXs) are also registered.

The mass flow rates of the core are measured by four flow meters installed in the suction side of the primary pumps dummies. These are calibrated turbine flow meters. They are calibrated in the range of mass flow rates between 10.0 and 800.0 g/s with an accuracy of $\leq \pm 5$ %. In addition some experiments were carried out with small turbine type flow meters mounted at the top end of individual subassemblies. Thereby the mass flow rate for each heating group can be determined. The mass flow rates of the secondary side of the DHXs are also measured as well as the flow rates of the primary side of the IHXs during forced convection operation. In this case magneto inductive flow meters were used calibrated in the range between 50.0 and 500.0 g/s with an accuracy of $< \pm 3$ %.

5.2 Movable Measuring Devices

In order to record the temperature profiles within the upper plenum, two special appliances were developed which enable a controlled selection of the measuring points within the cylindrical coordinate system.

In general, one support system is equipped with a single measuring lance (MEL) provided with up to 15 TCs having a vertical distance of 120 mm from each other. They are movable in radial, azimuthal and vertical direction. All positions of the

upper plenum can be reached using special formed MELs. Fig. 18 shows the actual TC positions of MEL in the upper plenum of the NEPTUN test facility.

A second support is equipped with a measuring rake (MER) consisting of a parallel arrangement of three vertical lances. These lances are different with respect to their length and to the axial intervals between the individual TCs. The lances are fixed with radial distances of 602 mm, 867 mm, and 1,227 mm from the NEPTUN centerline. The movement of MER around the centerline of the test facility allows temperature measurements for each azimuthal position within the upper plenum. Fig.. 19 shows a summarization of the radial and axial TC positions of the MER system.

5.3 Data Acquisition and Control System

Data acquisition takes place within an S-Net serial data transfer system using Isolated Measurement Pods (IMPs) and a VAX computer system of the type MicroVAX 3400. A schematic of the data acquisition and test control system is shown in Fig. 20. It registers and stores all temperature readings, flow rates and powers. In addition, 20 digital input/output signals are recorded and stored for controlling external units and for counting of events.

The data are handled by a multi-user operating system in conjunction with graphics and specifically written software. The S-Net is a decentralized configuration of the acquisition units and the signal transfer by a simple shielded twisted wire ring circuit of a maximum length of 1,000 m. Hence the system can be operated at its maximum data transfer rate of 163 kbits/s at any time. Q-bus interface cards serve as link between the IMPs and the computer. Each Q-bus can transfer a maximum of 50 IMPs = 1,000 data channels to the central VAX computer. All measured values are taken within a time interval of < 800 ms, even if the effective transfer rate would be reduced by a software overhead.

Due to the required accuracy of < 0.2 K for the temperature measurements, a comparative reference temperature for the TC measurements is required. Therefore, the terminal temperature is determined utilizing a 1/10-DIN PT100 measuring gauge mounted in the center of the isothermal screw connections of the TCs. The resistance of the PT100 is determined by a comparative measurement at a 100 Ω precision resistor. By the common power source, errors of the voltage measurements are compensated. The total error of the measuring

section is < 0.177 K at an ambient temperature of 20 to 40 °C. To obtain a more homogeneous temperature distribution in the connection field, a copper sheet is installed there. Conversion of the TC voltages is carried out by a user specified program.

Following the start by the central computer, the state of the experiment can be recorded, printed, or plotted (transfer rate of up to 38.400 bits/s) in real time or background mode in tables or charts via three screens using the graphic software. For the measured values and the user software, a main memory of 20 MB and two Winchester disk drives with 778 MB gross capacity are available in the system. The current experimental data are stored and filed on a magnetic tape drive TK50 (50 MB). Via an Ethernet link and the LAN, the current measuring data calculated by the user program are transferred to the central computer (IBM 9021-640) of the Research Center Karlsruhe for evaluation and documentation of the experiments. Together with the RAMONA data and the computed FLUTAN data, this central computer allows the analysis, the comparison and graphical re-presentation of all data of this project.

6. EXPERIMENTAL PROCEDURE

A typical experiment consists of a warm-up phase, a stationary phase, the scram and the transient after-scram phase. The warm-up phase and the stationary phase constitute the pre-scram-phase. During the entire experiment, important primary- and secondary-system flow rates and temperatures are registered by chart writers. This information is used in the pre-scram phase to adjust the model to standard steady-state temperature and flow conditions.

To reach these stationary conditions, the core heats up the water volume ($\simeq$30 m^3) of the NEPTUN facility using the test specific power. The water temperatures in the upper and lower plena as well as in the core are controlled.The external primary pump is running and the external heat exchangers are put in operation as soon as a set temperature level of about 50°C is reached in the upper plenum. The DHX circuits are also operating at a very low level, so called "stand by operation conditions". This procedure assures the formation of the proper steady-state flow and temperature distributions before scram. For the same purpose, additional externally positioned low-flow pumps are used during the warm-up phase to stir the fluid in the cold plenum and to circulate fluid into the cavity. These pumps are turned off at least 10 min before scram. After 2 h to 4 h

of warm-up, stationary flow and temperature conditions are reached. The scram is performed by reducing automatically the set core power to zero followed by a manual increase to the post-scram value. The controlled primary pump coast down decreases the forced primary fluid flow. Within a few seconds after scram the flaps within the IHXs simulators are opened manually. This initiates the natural convection flow within the vessel and stops the external flow via the EHXs and the external primary pump. This procedure was studied in preexperiments to minimize the influence of the active actions on the transient course of the post scram thermal-hydraulics. To simulate the transition phase from forced to natural circulation, the experiments are continued for a period of about 5 h after scram. After that time period, conditions are reached which are identical to the steady state situation known from proceeding tests [12].

7. PARAMETERS OF THE INVESTIGATIONS

From the RAMONA transient tests [5] the main magnitudes of interest are well known. Therefore the tests are concentrated on the study of the following parameters:

- Core power: Under forced convection conditions the core power is varied in the range of 800 kW $\leq$ P $\leq$ 1600 kW and for natural post scram conditions in the range of 133 kW $\leq$P $\leq$ 155 kW.

- Radial core power profile: Two radial core power profiles were investigated. The first profile is realized by heating all rod bundles belonging to the radial heating groups 1 to 6. The second profile results from the operation of all heatable rod bundles (groups 1 to 7). Hence in this case the power release by the storage elements is simulated.

- Delayed start of the DHXs: The DHXs are put in operation 240 s after scram and reach full power with 25 s. To simulate a failure in the start up of the DHXs on demand, experiments were performed with a 3000 s delayed operation of all DHXs.

- Complete failure of 2 out of 4 DHR circuits: The number of DHXs being in operation causes symmetrical and asymmetrical cooling modes, respectively. An asymmetrical cooling mode is realized when two DHXs located side by side are turned off without any reduction in core power.

Consequently, the power generated must be removed through the immersion coolers still in operation. However, as these are run at constant secondary mass flows with constant inlet temperatures, the UP temperature is bound to rise.

- Blockage of all flow paths via IHXs from UP to lower plenum (primary flow path): Experiments were carried out closing the flow paths between the upper plenum and the lower plenum. In these cases, no fluid reaches the HPP and the core must be cooled from the UP alone.

- The ACs design: Impermeable and permeable ACSs are investigated. In both cases the axial gap height between the top end of the core and the bottom end of the ACS is 200 mm.

- Primary pump coast down: In these investigations the primary flow rate was reduced by the rundown of the external primary pump with the pump stops after 25 s, respectively 240 s after scram.

The transient NEPTUN tests are conducted following the preceding transient RAMONA experiments. On the basis of a similarity consideration, the time depending data are defined for the different components installed in the primary vessel. For the so called baseline test, (see Table 1: Test No. 9) the following transient functions are defined:

- Reduction of the core power at scram from 1450 to 133 kW within 40 secondes with a radial power distribution over the core.

- Reduction of the core mass flow rate from 27.8 kg/s in accordance with a PP coastdown characteristic of 10 s half-time; PP stop at 25 s after scram.

- Change of the primary fluid in the IHXs from external to internal flow conditions within 5 s. This procedure starts at 18 s after scram.

- 240 s delayed startup at the DHXs secondary sides, linear increase of the total mass flow rate from standby conditions to 8.3 kg/s within a period of 25 s. The inlet temperature is 15 °C.

For this baseline test the core is heated by six heatable groups. Outside of this heated range the remaining core elements (heating group seven: storage elements, all reflector and shielding elements) do not have any hydraulic connection to the UP. All DHXs are serviceable. The ACS is an impermeable design.

The main parameters being under consideration are given for the 20 experiments in Tab. 1. The influence of the main parameters are described in this report for 9 out of these 20 tests. The number of heated subassemblies and the electrical power of each heating group of the core are given in Table 2 for the various core powers investigated.

For all these cases the temperatures and mass flow rates were registered over a time of about 5 h after scram. With this knowledge the thermohydraulic behavior of the primary system during the transition from forced to natural convection can be described. Usually each test will be characterized by a sequence of four plots namely the time dependent courses of:

- the core mass flow rate,
- the core inlet and outlet temperatures,
- the DHX inlet and outlet temperatures, and
- the behavior of a vertical temperature distribution in the UP.

The thermalhydraulic experimental results are compared with calculations as far as available. Due to time restrictions only steady state calculations have been performed using the 3D thermal hydraulic computer code FLUTAN [13]. These results describe the steady state situations under forced (pre-scram) and pure natural convection (post scram) conditions. The capability of the FLUTAN code for transient calculations can be taken from references [5, 14, 15].

8. NUMERICAL SIMULATION OF THE EXPERIMENTS

The fully vectorized thermal-hydraulic computer code FLUTAN is utilized for the numerical simulation of the NEPTUN experiments. The FLUTAN computer code is a tool to analyze the combined fluid dynamics and heat transport for 3D, laminar and turbulent, steady-state and transient problems. The selection of either rectangular Cartesian or cylindrical coordinates is provided. The program includes physical models for volume porosity, surface permeability, surface heat flux,

volumentric heat source, thermal interaction between the immersed structure and surrounding fluid, and turbulence. Two temperature-dependent fluid property packages are presently implemented, i.e., for water and sodium. Apart from the vectorization, an essential feature of FLUTAN is the self-optimizing algorithm CRESOR [16] for solving the Poisson equations for pressure, energy, and turbulence using a finite-difference numerical technique.

For the simulation of the NEPTUN experiments, a 90° sector is modeled by using a three-dimensional noding scheme with about 20,000 volume cells. Figure 21 illustrates the nodalization of the test facility with r-ϕ and r-z cross-sections. The number of the chosen mesh cells depends on the degree of detail required to resolve the fluid field, the phenomena to be modeled, and practical restrictions such as computing time and computer storage limitations. To capture the dominant physical phenomena, the following approach is chosen:

- For the multi-dimensional simulation of the core, an unequal mesh spacing is selected according to different requirements. In vertical direction, a different node length has to be provided to fit the axial regions of the heated rod bundles, the pad plane, and the horizontal ACs plate installed close to the upper end of the core. In addition, the axial noding scheme has to coincide with selected measurement locations. In the angular direction, the positions of PPs, IHXs, and DHXs govern the nodalization. In the radial direction, the arrangement of the fuel, storage, reflector, and shielding elements (see Fig. 8) together with the power profile (Table 2) determine the modelling. The flow area between the wrapper tubes is characterized by the radial length increment of the mesh. The chosen network, however, does not allow the simulation of the interstitial flow in the angular direction. The volume cells of the SAs are described by porosities and permeabilities and by taking into account the space-dependent heat capacities of the SAs in conformity with the actual radial power profile. Heat transport between the SA regions and the interwrapper spaces is taken into consideration by so-called "slab-type thermal structures". Heat transfer between the interwrapper space and the high-pressure plenum below the core is modelled. In addition, the modelling includes local pressure losses due to the design of the SA inlet and outlet sections, orifice plates, grid spacers, pad elements, and other obstructions along the coolant as well as such caused by friction forces.

This information is based on pretests carried out to determine the thermal-hydraulic characteristics of the NEPTUN core and its SAs [17].

- In the case of a permeable ACS, the perforated shell of the ACS is approximated by solid walls and holes in such a manner that the resulting permeability amounts to 15 %. At the peripheral surface, the simulated distributions and sizes of the holes are defined in accordance with the ACS design installed in NEPTUN. The same procedure is applied to simulate the bottom plate of the ACS having a permeability of 13 %. The impermeable ACS version requires a modification of the data input to fit the fluid cell boundaries with reference to the actual design of the ACS surfaces.

- The data input for the PPs and IHXs concentrates essentially on information about the free flow areas which are the same as in the NEPTUN test facility and about the pressure losses in the vertical flow direction caused by the presence of internal installations and friction forces. Additional specifications for the IHX are required for forced convection conditions and blocked primary flow path of the IHX. For forced convection conditions a primary pump simulation is modelled with inlet and outlet boundary conditions. In case of a primary flow blockage of the IHXs the cross-sections are closed by permeabilities.

- Identical free flow and heat transfer areas are attributed to the DHXs in the computer simulations as in the test facility. The conditions at the secondary sides of the components are calculated by the FLUTAN heat exchanger model [18] with inlet mass flow and inlet temperature and by taking into account the heat capacities of the solid material and the fluid which correspond to the reality of the experimental units. The thermal-hydraulic characteristics of the DHXs are specified for the data input by making use of pretest measurements carried out with the original components [19, 20].

- The actual contour of the "redan" is approximated by a graded net.

Except for the core, adiabatic and slip boundary conditions are supposed at the solid surfaces. Friction losses and drag coefficients are modelled for all

components and plena. Free slip is taken into consideration for the free water surface.

All computations are based on essentially laminar conditions. Locally turbulent flows are taken into account. Initially, uniform pressure, velocity, and temperature values are specified for all fluid cells at the beginning of a computer run. The initial values of the temperatures are specified following the measurements of the individual experiments. The computation is solved in time and continued until a steady-state solution is reached, i.e., when the energy generated in the core corresponds to the energy transferred to the DHXs as well as the values of the variables stop varying with the time and prescribed convergence criterion parameters ($\varepsilon \leq 1 \cdot 10^{-5}$) are met for pressure, velocity, and enthalpy.

9. DISCUSSION OF THE EXPERIMENTAL RESULTS

In the following the most decisive results are described on the basis of the 9 marked tests from Table 1. They have been performed with maximum core powers of up to 1600 kW to study and reveal the crucial parameters influencing the transient thermalhydraulics behavior of the primary system. The test results of the additional 11 experiments which are not described in detail will be given as plots in Appendix A.

9.1 Comparison of NEPTUN baseline test with RAMONA reference case [5]

Both experiments have been carried out in a comparable experimental procedure and under similar boundary conditions. In both tests the IHX secondary side flow rate is linearly reduced to zero within 15 s and the DHXs are put in operation 240 s after scram. The power reduction at scram is about three times higher in RAMONA in comparison to NEPTUN. This, however, is of minor influence on the physical system characteristics. On the left hand side the results of RAMONA and on the right hand side those of NEPTUN baseline test 9 (Table 1) are shown.The average core mass flow rates are indicated in Fig. 22a. At time zero, the flow rates start to decrease continuously, drop down to a minimum value at ~ 0.5 h after scram, then recover again, and reach an approximately constant value at ~ 1.5 h after scram.

The core mass flow reduction of the RAMONA test, indicates a sharp depression at the time point where the primary pumps stop. In contrast to this the transient profile of the core mass flow rate of the NEPTUN test is very homogeneous. This can be explained by the higher downward pressure in the IHXs of NEPTUN, as they are filled with cold water up to the inlet windows as well as by the reduced power ramp at scram. The pronounced flow reductions at 0.5 h after scram for both tests are attributed to the following facts:

- the IHXs are warmed up with hot fluid of the upper plenum temperature and the cold fluid of the IHXs producing descending forces is consumed subsequently.
- Starting with the DHXs operation 240 s after scram the cold fluid filled up the cavity and generated cold fluid layers (temperature stratification) above the cores. These stratifications lead to a downward pressure gradient within the cores. To compensate both effects, stronger buoyancy forces have to be established within the cores. This is achieved by increasing the temperature differences within the cores. This thermal behavior continues up to ~ 0.5 h after scram as demonstrated by the data plotted in Fig. 22b. The graphs show typical transient temperatures measured at the inlet and outlet sides of core elements placed within heating group No. 4 for the NEPTUN test and as averaged temperatures of the RAMONA core.

The transient temperature profiles recorded at the core outlet sides exhibit considerable temperature drops immediately after scram followed by sharp rising temperatures. These temperature depressions are due to the reduction of the core power and the still operating PPs feeding large fluid masses through the core. After the PPs stop the core temperature differences increase again producing the necessary upward buoyancy forces.

The inlet temperatures of the cores increase due to the fact, that the cold water in the lower plenas is mixed up with warm water coming from the upper plenas. About 1 hour after scram, these temperature differences reach approximately constant values. From an energy balance it results that the core powers and the decay heat removed by the DHXs are about equal at 4 h after scram.

The thermal behavior of the UPs is reflected by the transient variations given in Fig. 22c. At scram point the upper plenas of RAMONA and NEPTUN are at

identical temperatures of about 45 °C. Immediately after scram cold fluid from the cores enters the lowest regions in the UPs (cavities) due to the reduction in core power and the still running PPs. The formation of temperature differences in the UPs starts. Cold fluid reaches the cavities and at the highest point of the UPs the prescram temperatures can still be registered. After start of the DHXs operation cooling is increased considerably in the lower parts of the UPs. These cooling effects reach the highest points of the UPs at about 0.5 h after scram and initiate its temperature reduction. About 2 h after scram constant UP temperature differences are obtained, but the temperature level still decreases. 4 h after scram the UP temperatures reach steady-state conditions.

The transient thermal behavior of the UPs is illustrated in Fig. 22d. The data represent the development in time of vertical temperature profiles recorded along a measuring travers. Starting with forced convection at the time of 0 s, uniform temperature profiles are registered. After scram, first of all the lowest parts of the UPs are affected by cold water flowing out from the cores during the steep temperature drop immediately after scram. After start of the DHXs operation, the cooling effects are increased considerably in the UPs region below the bottom end of the ACSs. The top end of the UPs, however, remains warm during the first 1,500 s after scram. With increasing time after scram, higher-level positions begin to be cooled down to a greater extent reaching constant temperature differences between the top end and bottom end of the UPs at a time of 8,000 s after scram. A temperature stratification is formed which takes place in the region between the bottom end of the ACSs and the outlet windows of the DHXs. The temperature gradient amounts to about 5 K in the NEPTUN test and to 3 K in the RAMONA test.

The vertical temperature profiles remain unchanged by far. As can be observed by these sequences of characteristic results of NEPTUN and RAMONA transient tests, there exist similar experiments for different scaled reactor geometries. In both experiments the Richardson and Euler Numbers are the same, the Peclet and Reynolds numbers differ by 1.5 decade. This means that also in the NEPTUN test facility there exist only local turbulent flow conditions during the transient tests.

9.2 Comparison of different core powers

The influence of different core powers on the thermal hydraulic behavior of the UP and the core is shown in Fig. 23. On the left hand side the core power amount

to 800 kW and on the right hand side to 1450 kW.The only difference in these two experiments is the core power before scram under forced convection conditions, i.e. temperature rise in the core and hence the UP temperature are the higher the core power is as the core mass flow rate and the inlet temperatures are kept constant.

The total measured core mass flow rates are shown in Fig. 23a. Right after scram in both cases the mass flow rates decrease continuously to minima at ~ 0,5. In test No. 1 (left hand side) the minimum measured core mass flow rate is 1,2 kg/s and in test No. 9 (right hand side) 0,7 kg/s. This difference results from the 5 K higher temperature level before scram in test No. 9 compared to test No. 1 (see Fig. 23b). The higher temperature level in the UP reduces the downward pressure in the IHXs, consequently the core needs higher buoyant forces, which is indicated in Fig. 23b by a slightly higher core temperature rise.

The measured DHX inlet and outlet temperatures are plotted for both cases in Fig. 23c. After the start of the DHXs, the outlet temperatures in both cases decrease immediately. The temperature drop from inlet to outlet reaches about 0.5 h after scram 9 K and 12 K for the 800 kW and 1450 kW power cases respectively though the core power after scram is identical in both cases. This is because the accumulated heat in test No. 9 is higher than in test No. 1. Hence the DHXs have to remove more power until they reach equilibrium conditions where the heat production is equal to the heat removal. This state is reached about 4 h after scram and for both tests the DHXs temperature differences amount to about 8 K. The temperature fluctuations at the outlet windows of the DHXs can be explained by the flow pattern provoked by the cold fluid leaving the DHXs and penetrating into the warm fluid of the UP. The vertical temperature distributions in the UP are represented in Fig. 23d. The comparison shows that the qualitative temperature distributions in both cases are similar. There exists only a small difference in the temperature distribution at 2000 s after scram where in the case with higher core power (right hand side) already mixed fluid of the UP enters the IHX windows whilst in the case of lower core power the temperatures in this region are still at the initial level. This is due to the fact, that in the lower power case the UP temperatures after scram are in the range of those for the thermal equilibrium conditions. After 4 h after scram identical temperatures of 38°C in the upper part of the UP are reached for both tests.

9.3 Comparison of different delayed DHX startup times

Fig. 24 shows on the left hand side again the results of the NEPTUN baseline test No. 9 and on the right hand side those of the test No. 10 with delayed operation of the DHXs. The only difference between both experiments is the startup time of the DHXs. In the baseline test they are put in operation 240 s after scram. A delayed operation of the DHXs is realized with 3000 s after initiation of scram in test 10.

The total measured core mass flow rates are shown in Fig. 24a. Right after scram, the flow rate of the experiment with delayed operation of DHXs decreases continuously to a first minimum at ~ 0.15 h. This minimum results from the warm fluid in the UP entering the IHXs during the heatup phase. Immediately afterwards, the effectiveness of the buoyancy forces becomes evident that causes a recovery of the flow rate. 3,000 s after scram, the DHXs start to operate which leads to a second flow reduction due to the effect of the cold fluid layer established above the core which counteracts against the buoyancy forces of the core. The turnaround point is reached at ~ 1.2 h after scram.

In contrast to the transient core mass flow rate and also to the measured core inlet and outlet temperatures plotted on the left hand side for the baseline test the effect of the 3000 s delayed startup time of the DHXs becomes clearly visible. The core temperatures (see Fig. 24b) increase in this case up to a time of ~ 1.2 h. This results from the increasing UP temperatures during the time when the DHXs are out of operation. The onset of DHX operation is not visible in the course of the outlet temperature of the core, but with a delay of about 15 min. the increasing core inlet temperature became constant. This results from the strong reduction of the core mass flow rate.

At 1.2 h after scram, the temperature difference within the core is high enough to increase the buoyancy forces strongly and hence the core mass flow rate. With the onset of this flow augmentation, the maximum core temperatures start to decrease. At ~ 2 h after scram the core temperature rise is established and held constant. In comparison to the baseline test there exists a delay in this development of the core temperature rise of about 1 h.

The measured DHX inlet and outlet temperatures are plotted in Fig. 24c. The delayed start of the DHXs can be easily identified from the characteristic drop of the outlet temperature in the figure on the right hand side. After the start of the DHX, the outlet temperature drops immediately by about 9 K, which is about the same temperature decrease for the baseline test. The temperature difference between inlet and outlet temperature is slightly reduced in time. The fluctuations of the outlet temperatures can be explained by the flow pattern of the cold fluid leaving the DHXs and the warm water accumulated in the UP.
The vertical temperature distributions in the UP are represented in Fig. 24d. From these profiles in the figure on the right hand side, the delayed startup time of the DHXs becomes clearly visible, too. After 3,000 s, the temperatures of the upper part are increased by about 2 K. Below the top end of the core, however, the region is colder due to the occurring "cold shock" after scram. This is the temperature difference depression slight after scram due to the power reduction with still running pumps (Fig. 24b) A comparison of these data with corresponding values represented in the figure on the left hand side allows the conclusion that profiles are basically similar in view of a time shift of 3,000 s. Again, the delayed DHX startup time can be easily identified. Furthermore, it should be noted that the temperature level is still about 2 K higher at 18,000 s compared to the baseline test.

9.4 Comparison of 4 and 2 DHXs in operation

The test No. 11 shown on the right hand side of Fig. 25 differs from the baseline test only by the number of operable DHXs circuits. That means that the same amount of decay heat has to be removed by two DHXs only since all other test parameters as well as initial and boundary conditions were kept constant. To remove a twice as high power per component, an increase of the driving temperature differences and of the mass flow rate at the primary side of the serviceable DHXs is necessary. Since the DHX inlet temperatures on the secondary side are the same for both cases, consequently a higher driving temperature is visible by a higher UP temperature.

Figure 25a shows the cooling effect of the DHXs on the core mass flow rate. Compared to the baseline test (left hand side), the transient exhibits a flatter minimum and in general a slightly increased mass flow rate. This is due to the fact that the mixed temperature of the cooled DHX flow which is laying on top of the core is higher and, hence, the natural-convection pressure head above the core is

lower compared to the baseline test. This reduces the temperature rise within the core slightly (Fig. 25b). The temperature course, however, differs and the temperature level is about 6 K higher at 4 h after scram. The inlet temperature increases over a long time up to 2 h after scram. This increase is the consequence of the warm fluid in the UP. The temperatures measured at the inlet and outlet windows of the DHXs (Fig. 25c) are nearly constant during the transient whereas the comparable data on the left hand side decrease with increasing time after scram. The constancy of the temperatures registered at the inlet windows of the DHXs is an indication of the steady-state thermal behavior of the UP. This is confirmed by Fig. 25d on the examples of the vertical temperature profiles. The set of time-dependent curves is close together and the most important cooling effects occur in the lower part of the UP.

9.5 Comparison of impermeable and permeable ACSs

The influence of the permeable ACS on the thermohydraulics of the UP will not be compared to the baseline test, but to test No. 13. The experiment with the permeable ACS is test No. 17. Both experiments are characterized by the following parameters, which are different from the baseline test:

- the core power is 1600 kW,
- the core mass flow rate before scram is 38.1 kg/s,
- the core power of the decay heat is 150 kW,
- the storage elements are heated also (heating groups 1 to 7),
- reflector and shielding elements have hydraulic connection to the upper plenum.

The results of both experiments are shown in Fig. 26. For the average core mass flow rates only the plots in Fig. 26a) can be given. During normal operation under forced conditions the average core mass flow rate is 38.1 kg/s. At scram time the flow rates decrease continuously and drop down to zero at ~ 15 min. after scram, but only one flowmeter out of four shows a fluctuational mass flow rate. This is due to the fact that the reflector elements connect directly the UP with the high-pressure plenum and consequently with the flow inlet of the core elements.

One larger part of the necessary core flow rate enters the high-pressure plenum directly via the reflector elements and only a small part (~ 1/4) via the IHXs and primary pumps. Since for each heating group one element is installed at the top

with a turbine flowmeter, a rough core mass flow rate can be deduced. By 337 elements the calculation for the total core mass flow rate for tests No.13 and No. 17 results in 1.7 kg/s. This agrees very well with the measured core flow rate in test No. 9 for the steady-state core mass flow rate 4 h after scram. The conclusion can be drawn that in tests No. 13 and 17 the buoyancy-driven cores work in the same mode as in test No. 9.

The inlet and outlet core temperatures are shown in Fig. 26b. The core temperature rise for the test with permeable ACS (right hand side) is slightly higher (~ 1 K) than that with impermeable ACS. This effect can be explained as an influence of the permeable ACS on the thermohydraulics of the UP. The permeable ACS allows the hot core flow to pass through. It leaves the ACS at the top. Therefore, the whole UP temperature is stratified, that means, the temperature increases slightly by about 2 K with increasing UP height, which can be seen in Fig. 26d. By this effect the downward pressure on the core is slightly higher by the colder fluid layer in comparison to the impermeable case (left hand side). This higher downward pressure must be compensated by higher buoyant forces in the core elements and this implies a higher temperature rise.

These facts explain also the small differences in the thermohydraulic behavior of the DHXs, as seen in Fig. 26c. The differences between inlet and outlet temperatures of the permeable to impermeable case are about 2 K, that means in the case of permeable ACS the DHX temperature difference is higher by this value. This is due to the necessary higher downward pressure inside the DHXs, since the inlet temperature is higher than for the impermeable case. Fig. 26d demonstrates the influence of the permeable ACS on the thermohydraulics of the UP. From the beginning of the transient at 0 sec. up to 4 h after scram the upper part of the UP is stratified.

9.6 Comparison of different primary-pump coast downs

The influence of different primary-pump coast downs is demonstrated by tests No. 17 and 20 in Fig. 27. These experiments run with 7 heating groups and permeable ACSs. On the left hand side of Fig. 27 the primary pumps are stopped at 25 s and on the right hand side at 240 s after scram. The average mass flow rates cannot be determined for the same reasons as described in the previous chapter.

The core inlet and outlet temperatures are shown in Fig. 27b. A rapid and steep depression in the outlet temperature is detected right after scram for both cases. But the recovery of this is faster in the case where the pumps are stopped 25 s after scram. When the primary pumps are stopped at 240 s after scram (right hand side) the cooling time of the core is longer and hence the effect of the "cold shock". The increase of this temperature takes more time. The rapid temperature increase results from the low core mass flow right after the pump stop. The increasing temperature differences in the core initiate the onset of natural circulation. The inlet temperatures of the core of both cases are practically identical during this time. This is also the case for the inlet and outlet temperatures of the DHXs primary sides, Fig. 27c.

A more pronounced effect of the longer primary-pump coast down on the UP thermal hydraulics can be seen in Fig. 27d. The vertical temperature distributions registered at 250 s after scram demonstrate the difference of the stronger cooling effect by the primary-pump coast down of 240 s. Compared with the 25 s coast down of the primary pumps, the fluid temperatures from the bottom of the cavity up to the bottom of the ACS shell are colder by 2 K. This is due to the cold fluid which passes the core, penetrates inside the cavity. After about 1000 s the influence of the different primary pump coast downs on the thermohydraulics of the UP is negligible.

9.7 Comparison of unblocked and blocked IHX flow paths

The objective of test No. 12 shown in Fig. 28 on the right hand side is to simulate the thermal hydraulic behavior following a possible break of the hot leg piping system in the top entry loop-type reactor [21]. For that purpose the inlet windows at the IHX primary sides are closed in order to block the flow paths between the UP, the lower plenum, and the coolant inlet side of the core. This means that the core is only coolable from the UP by fluid flowing into the SAs and interwrapper spaces, respectively. The remaining test conditions are identical with those of test No. 9 (left hand side of Fig. 28). The core mass flow rate cannot be measured in this case because the main flow paths are blocked.

Figure 28b shows temperature transients recorded at the inlet and outlet sides of the core. It can be seen that the maximum temperature rise appears ~ 0.25 h after scram and amounts to 20 K. In test No. 9, the corresponding value is 16 K. At a time of 4 h after scram, the comparable differences come to 15 K and 10 K,

respectively. This increased temperature rise can be explained by the fact that the core elements are cooled by the thermosiphon effect. In each element there is a cold downward and a warm upward flow circulation. It is obvious that this effect produces a higher pressure loss than the normal flow path via IHXs and primary pumps. This higher pressure loss results in an increased overall core temperature difference.

A second cooling effect is caused by the interstitial flow. Cold fluid passes the interwrapper spaces and contributes remarkably to the decay heat removal. The cooling effect of the interstitial flow will be described in detail in the next chapter. At the DHX inlet and outlet sides (Fig. 28c), the transient thermal behavior corresponds to a great extent to that observed during test No. 9. A comparison of the data plotted in Fig. 28d on the right hand side with those represented on the left hand side indicates that the vertical temperature profiles measured in the UP are very similar at the corresponding points of time. That means that the installation of DHXs in the upper plenum above the core work very effective even in the case where the fluid is hindered to pass the IHX/PP flow paths.

9.8 The influence of the interstitial flow and its calculation with the FLUTAN code

A significant advantage of the NEPTUN test facility is the real simulation of the interstitial flow, its cooling effects on the core elements and core grid plate and also the thermal hydraulic interaction with the UP. To demonstrate the important cooling part of the interstitial flow Fig. 29a illustrates the fields of isotherms on the basis of measured data for the unblocked (test No. 9 left hand side) and blocked (test No. 12 right hand side) flow paths between the UP and the lower plena.

The isotherms (interval of 1 K) of the blocked case are tighter and indicate a higher temperature gradient for the interwrapper space compared to the baseline test No. 9. The maximum temperature of the interstitial flow is increased by about 4 K and the cold fluid which penetrates from the cavity into the interstitial space cools the fluid there more effectively than in the baseline test. Besides, the isotherm lines take a horizontal course in the region of the heated core zone which indicates a large and equal heating up of interstitial flow. But the influence of the interstitial flow on the thermal hydraulics of the UP is of

minor effect as the higher temperature of the interstitial outlet flow is intensively mixed with the cold flow of the DHXs. From this the core coolability from above seems to be feasible. In comparison, Fig. 29b shows the calculated results of the same cross-section of the interstitial space performed with FLUTAN code. The overall isotherm fields are very similar to those from the experimental data and are also tighter in the core region for the blocked case, which is an indication of a higher temperature gradient. The temperature of the interstitial flow increases also by 4 K for the blocked flow path, but the absolute temperature level differs there from the experimental data by up to 4 K. The explanation can be given by the very sophisticated modeling of heat transfer and pressure losses in the interwrapper space. The calculated isotherms in the high-pressure plenum for the blocked case indicate a backflow in the outer heating groups. Hot stagnant fluid can be observed in the high-pressure plenum.

The backflow effect is clearly seen by the calculated velocity fields for the blocked case (right hand side) in Fig. 30b, representing a cross-section through the core and DHX. In the outer region of the core the downward velocity can be observed.

An explanation of the higher temperature gradient in the interstitial space for the blocked flow paths can be given also in the computed velocity fields in Fig. 30a. The velocity vectors indicate a stronger clockwise flow circulation in the interstitial space than for the unblocked case (left hand side). This is due to higher heating of the interstitial flow by the core elements via the wrapper tubes. As seen before in Fig. 29a and b the cavity flow temperature which penetrates in the interstitial space conducts in both cases to the same temperature. The vector plots in Fig. 30a and b indicate also only a minor influence of the blockage on the hydraulic behavior of the UP.

But as mentioned before the vector plot in Fig. 30b informs about a backflow in the outer region of the core elements (heating groups 3,4,5 and 6). This large backflow exists only in the cross section of the DHX, where the coldest fluid enters the core region, but for core elements positioned 90 degree far from the DHX the calculation shows backflow only in the heating group No. 6. In contrast to this calculation, the experimental data show no backflow effect at any region of the core. The core elements must be cooled then by a thermosiphon effect in each element and by higher cooling effects via the wrapper tubes.

The thermal hydraulic behavior of the core elements and of the interstitial flow can be represented very well by a comparison of measured and computed radial temperature profiles at the outlet sides of the SAs (Fig. 31a) and at the upper end of the interwrapper space (Fig. 31b). The comparison is given again for the unblocked case (test No. 9, left hand side) and the blocked case (test No. 12, right hand side). The temperature distributions for the forced convection condition are indicated with 0 s. For both tests No. 9 and 12 exist the same flat temperature distribution at the outlet of the SAs and at the upper end of the interwrapper space for the forced convection condition. The agreement of the calculated temperatures with the experimental data are quite good for the interstitial flow and deviate slightly for the SAs temperatures. At the scram time nearly identical temperature distributions are registered.

At 18.000 s after scram, a time at which the steady state of natural convection is almost reached, the temperature distributions are governed by the cooling effects of the DHXs and the buoyancy forces acting inside the core. The corresponding temperature profiles are highly altered. At the periphery of the core region, temperatures of 33°C and 38°C are measured for the interstitial flow and the SAs flow, respectively. In the central part of the core region exist for the SAs and the interstitial flow higher temperatures than at the core periphery. In test No.12 the center SAs outlet temperatures reach even 10 K higher temperatures after 18000 s in comparison to the prescram conditions. The maximum temperatures of the interstitial and of the SAs flows differ from each other in both experiments. Compared to test No. 9, the maximum interwrapper and SA temperatures are 4 K higher in test No. 12.

With FLUTAN, calculated temperatures at the outer region of the core and the interstitial space differ only slightly from the measured data. The calculation of the maximum temperatures in the interstitial space and for the SAs results only in about 3 K higher temperatures comparing both tests. As mentioned earlier, these higher temperatures in the SAs are caused by higher pressure losses arising for the experimental data by a thermosiphon effect in the SAs and for the calculated data by the backflow effect via the core elements placed at the core periphery. Since the interstitial flow is coupled by the heat transfer to the core elements, the temperature of the interstitial flow is increased too. This temperature rise leads to an enhanced cooling effect of the interstitial flow in test No. 12 compared to test No. 9. Mass flow rates locally measured in each heating group indicate that

about 60% of the core power is removed by the interstitial flow in test No. 12 and approximately 50 % in test No. 9.

In Fig. 32 a comparison of the computed vertical temperature distributions in the UP with measured data is given. These data are compared for the unblocked case (a) and the blocked case (b) for the time before scram (forced convection) and for 18000 s after scram (natural convection). The agreement of the computed data with the measurements is good, small deviations in the cavity region - higher calculated cold temperatures - can be explained by numerical diffusion.

10. SUMMARY AND CONCLUSIONS

Experimental and theoretical investigations on the transition from forced to natural convection in the primary system of a fast reactor model have been carried out using the three-dimensional NEPTUN facility scaled 1:5 with water as the simulant fluid.

Under forced convection condition (prescram phase) the upper plenum reveals identical temperatures. This is also due for the colder temperatures of the lower plenum. The heat production in the core results in about identical temperatures across the core diameter. After scram the upper plenum becomes stratified by the cold fluid fed by the IHXs and DHXs. This temperature stratification is maintained during the post scram phase. The start of the natural convection is mainly influenced by two effects, namely, the temperature increase on the IHXs primary sides as a result of which the downward pressure within these components are reduced, and the start up of the DHXs which leads to a decrease of the buoyancy forces in the core.

The influences of the core power before and after scram, its radial distribution across the core, the interwrapper cooling, the primary-pump coastdown, the DHXs startup delay time and their availability, the ACS geometry, and the blockage of the primary flow paths of the IHXs on the thermal hydraulic behavior through the primary system has been studied.

- With increasing core power the system temperature increases for identical DHX secondary side conditions. Strong radial core power gradients, however, result in the outer region of the core in strong gradients of the average outlet temperatures.

- The interwrapper flow contributes remarkably to the cooling of the core elements. Up to 60 % of the core power is transfered by this effect during the transition phase up to the steady-state condition.

- The primary-pump coastdown influences the primary-vessel thermal hydraulics only during the first 1000 s after scram. For long-term behavior of the primary-vessel thermal hydraulics no remarkable influence of the pump coastdowns can be observed.

- A delayed startup of the DHXs results in an additional temperature rise in the core elements and in the upper plenum. These slight temperature increases do not lead to uncoolability of the core and UP and can be mastered by an optimized startup time of the DHXs.

- An asymmetrical cooling mode due to a complete failure of two neighboring DHX circuits causes a remarkably higher final steady-state temperature level of the UP but does not alter the overall temperature distribution.

- A permeable ACS produces a temperature stratification along the whole UP, and therefore a lower temperature gradient in the region between core outlet and lower edge of the ACS, whereas the impermeable ACS generates a strong temperature gradient in this region with uniform temperatures in the upper and lower parts of the UP.

- A complete flow path blockage of the IHXs primary fluid flow leads to an enhanced cooling effect of the interstitial flow and gives rise to a thermosiphon effect inside the core elements or backflow effect by the computation, respectively. The core outlet temperatures increase slightly, but the core coolability from above is feasible without any difficulty.

- The experimental thermal hydraulic behavior of NEPTUN in comparison to that of RAMONA is similar, even the quantitative results are comparable. The assumption for this comparability is to restrain practically the adequate inlet and boundary conditions.

- One deduction of the above statement means that most of the physical problems are described in the results of RAMONA and NEPTUN investigations. When all these physical effects can be calculated using the FLUTAN code the code becomes the transferability tool to the real reactor.

- The FLUTAN code is now improved by a turbulence model which is valid from low to high Reynolds numbers and also for mixed convection flow with buoyant forces. The transferability to fluids with small Prandtl numbers (sodium) needs additional expenditure.

ACKNOWLEDGEMENT

The authors would like to express their gratitude to Messrs. M. Daubner, J. Harbauer, A. Hinz, H. Krause, L. Pawlak, and K. Thomauske for their very valuable and effective technical support.

11. REFERENCES

[1] EFR Associates (eds.): European Fast Reactor, concept design specification and justification. EFR Associates, 10 rue Juliette Récamir, BP 3087, F-69398 Lyon, Cedex 03, France, EFR A000/0/0333A, June 1993.

[2] C. Essig, M. Düweke, V. Ruland, V. Ertel, and M. Kiera: Consistent thermal hydraulic approach of EFR decay removal by natural convection. Proc. of the 5th Internat. Topical Meeting on Nuclear Reactor Thermal Hydraulics (NURETH-5), Salt Lake City, UT, USA, Vol. I, pp. 135-142, Sept. 1992.

[3] W. Gyr, G. Friederl, H.J. Friedrich, H. Pamme, G. Firth and P. Lauret: EFR Decay Heat Removal System, Design and Safety Studies, 1990 Internat. Fast Reactor Safety Meeting, Snowbird, UT, USA., August 1990, Vol. III, pp. 543-552.

[4] H. Hoffmann, P. Sardin, and R. Webster: The European R & D program on natural convection decay heat removal of the EFR. Proc. of the Internat. Conference on Fast Reactors and Related Fuel Cycles, Kyoto, Japan, Vol. II, pp. 13.5/1-5/9, Nov. 1991.

[5] H. Hoffmann, K. Marten, D. Weinberg, H.H. Frey, K. Rust, Y. Ieda, H. Kamide, H. Ohshima, and H. Ohira: Summary report of RAMONA investigations into passive decay heat removal. Wissenschaftliche Berichte, FZKA 5592, July 1995.

[6] D. Weinberg, H. Hoffmann, H. Tschöke, and H.H. Frey: unpublished internal report, Sept. 1985.

[7] D. Weinberg, H. Hoffmann, K. Hain, and M. Düweke: Experimental and theoretical program to study the natural convection decay heat removal system of the SNR 2. Proc. of the Internat. Conf. on Science and Technology of Fast Reactor Safety, St. Peter Port, Guernsey, GB, Vol. 1, pp. 289-294, May 1986.

[8] J.U. Knebel, D. Weinberg, and U. Müller: Scaling of natural circulation decay heat removal from coolant pools. Y.A. Hassan and R.M. Singer (eds.): Thermal hydraulics of advanced nuclear reactors. Papers presented at the Winter Annual Meeting of the American Society of Mechanical Engineers, Chicago, IL, USA, HTD-Vol. 294, pp. 31-38, Nov. 1994.

[9] D. Weinberg, H. Hoffmann, K. Rust: Overview Report of RAMONA-NEPTUN Program on Passive Decay Heat Removal. Wissenschaftliche Berichte, FZKA 5667, 1995.

[10] SNR 2 - Abschlußbericht der SNR-2-Pool-Vorplanung (Phase 1c), Kraftwerk Union AG, Interatom, Bensberg, F.R. Germany, No. 41.07117, Dec. 1983.

[11] D. Weinberg, D. Suckow, U. Müller, and H. Hoffmann: The transferability to reactor conditions of thermal hydraulics model investigations of decay heat removal. Proc. of the 1990 Internat. Fast Reactor Safety Meeting, Snowbird, UT, USA, Vol. II, pp. 341-350, August 1990.

[12] K. Rust, D. Weinberg, H. Hoffmann, H.H. Frey, W. Baumann, K. Hain, W. Leiling, H. Hayafune, H. Ohira: Summary report of NEPTUN investigations into the steady state thermal hydraulics of the passive decay heat removal. Wissenschaftliche Berichte, FZKA 5665, 1995.

[13] H. Borgwaldt, W. Baumann, and G. Willerding: FLUTAN input specifications. KfK 5010, Kernforschungszentrum Karlsruhe, May 1992.

[14] D. Weinberg, K. Rust, H. Hoffmann, H. Hayafune, and H.H. Frey: Comparison of code predictions against natural convection experiments, Proc. of the ASME Winter Annual Meeting, Chicago, IL, USA, HTD-Vol. 281 (1994), pp. 11-21.

[15] D. Weinberg, H.H. Frey, H. Tschöke, and K. Rust: Comparison of transient 3D calculations with RAMONA model experiments, Proc. of the 5th Internat. Topical Meeting on Nuclear Reactor Thermal Hydraulics (NURETH-5), Salt Lake City, UT, USA, Vol. II (1992), pp. 571-579.

[16] H. Borgwaldt: CRESOR - A robust vectorized Poisson solver implemented in the thermal hydraulic code COMMIX-2 (V). Proc. of the First Internat. Conference on Supercomputing in Nuclear Applications, Mito City, Japan, pp. 346-351, March 1990.

[17] J. Krapp, W. Leiling, M. Prüßmann, and F. Schloß: unpublished internal report, Oct. 1987.

[18] A. Class: unpublished internal report, January 1990.

[19] V. Brems, H. Tschöke, and H. Hoffmann: unpublished internal report, July 1988.

[20] H. Hoffmann, D. Weinberg, W. Baumann, K. Hain, W. Leiling, K. Marten, H. Ohira, G. Schnetgöke, K. Thomauske: Scaled Models Studies of Decay Heat Removal by Natural Convection for the European Fast Reactor, Proc. of the 6th Int. Topical Meeting on Nuclear Reactor Thermal Hydraulics (NURETH-6), Grenoble, France, Vol. 1, pp. 54-62, October 1993.

[21] T. Koga, H. Takeda, S. Moriya, T. Funada, K. Yamamoto, Y. Eguchi, K. Sasaki, H. Kajiwara, O. Watanabe, and I. Maekawa: Natural circulation water tests for top-entry loop-type LMFBR. M. Courtaud and J.M. Delhaye (eds.): Proc. of the 6th Internat. Topical Meeting on Nuclear Reactor Thermal Hydraulics (NURETH-6), Grenoble, France, Vol. 2, pp. 1302-1308, October 1993.

12. NOMENCLATURE

a	thermal diffusivity, m^2/s
Eu	Euler number (pressure/inertia), dimensionless
g	acceleration of gravity, m/s^2
L	characteristic length, m
p	pressure, N/m^2
Pe	Péclet number (conduction/convection), dimensionless
Re	Reynolds number (inertia/friction) dimensionles
Ri	Richardson number (buoyancy/inertia), dimensionless
t	time, s
T	temperature, °C
u	characteristic velocity, m/s
z	height, mm
β	coefficient of thermal expansion, 1/K
Δp	pressure drop, N/m^2
ΔT	temperature difference, K
$\Delta\phi$	angle difference, deg
ε	convergence criterion parameter, dimensionless
ν	kinematic viscosity, m^2/s
ϕ	angle, deg
τ	time period

Subscripts

c	core
M	model
R	reactor
th	thermal

Abbreviations

ACS	above core structure
AHX	sodium/air heat exchanger
DHR	decay heat removal
DHX	decay heat exchanger
DRC	direct reactor cooling
EFR	European fast reactor

EHX	External heat exchanger
HPP	high pressure plenum (diagrid)
IHX	intermediate heat exchanger
IP	intermediate plenum
LOSSP	loss-of-station service power
LP	lower or cold plenum
MEL	measuring lance
MER	measuring rake
o.d.	outer diameter
PP	primary pump
SA	subassembly
SNR	German abbreviation for sodium cooled fast reactor
TC	thermocouple
UP	upper or hot plenum
2D	two-dimensional
3D	three-dimensional

TABLES AND FIGURES

Transient test number	Total core power before scram [kW]	Core power after scram [kW]	No. of heated groups	No. of operated DHXs	Start time of DHX after scram [s]	Impermeable or permeable ACS	Primary flow path	PP coast down [s]
1*	800	133	6	4	240	impermeable	unblocked	15
2	800	133	6	4	300	impermeable	unblocked	15
3	800	133	6	2	240	impermeable	unblocked	15
4	800	133	6	4	240	impermeable	blocked	15
5*	1100	133	6	4	240	impermeable	unblocked	15
6	1100	133	6	4	3000	impermeable	unblocked	15
7	1100	133	6	2	240	impermeable	unblocked	15
8	1100	133	6	4	240	impermeable	blocked	15
9*	1450	133	6	4	240	impermeable	unblocked	15
10*	1450	133	6	4	3000	impermeable	unblocked	15
11*	1450	133	6	2	240	impermeable	unblocked	15
12*	1450	133	6	4	240	impermeable	blocked	15
13*	1600	150	7	4	240	impermeable	unblocked	15
14	1600	150	7	4	3000	impermeable	unblocked	15
15	1600	150	7	2	240	impermeable	unblocked	15
16	1600	150	7	4	240	impermeable	blocked	15
17*	1600	150	7	4	240	permeable	unblocked	15
18	1600	150	7	2	240	permeable	unblocked	15
19	1600	150	7	4	240	permeable	blocked	15
20*	1600	150	7	4	240	permeable	unblocked	240

Table 1: Main parameters of transient NEPTUN experiments
* Tests are described in detail.

Heating Group No.	1	2	3	4	5	6	7
No. of SA	37	36	36	42	48	54	84
Core Power	Heating Group, kW						
800	158	150	139	153	158	39	-
1100	222	206	191	221	199	49	-
1450	296	274	254	296	265	65	-
1600	296	274	254	296	265	65	175
133	24	22	20	24	25	20	-
150	24	22	20	24	25	19	16

Table 2: Power of heating groups of NEPTUN core

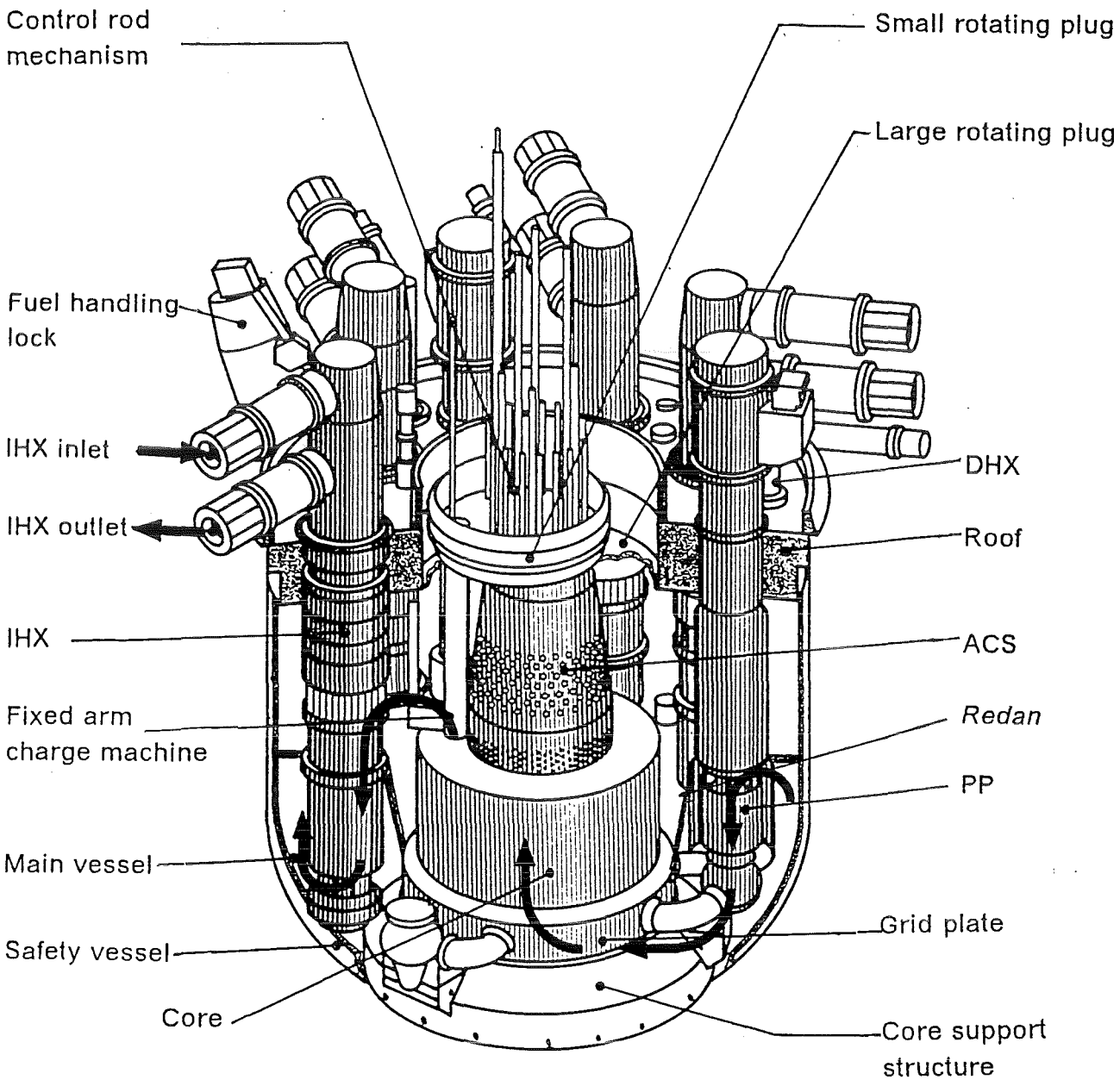

Fig. 1 EFR-Primary system - Overall view

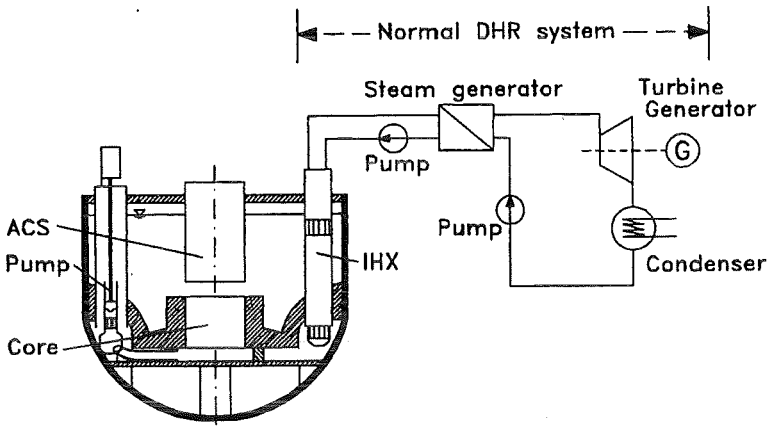

Fig. 2 Normal decay heat removal system

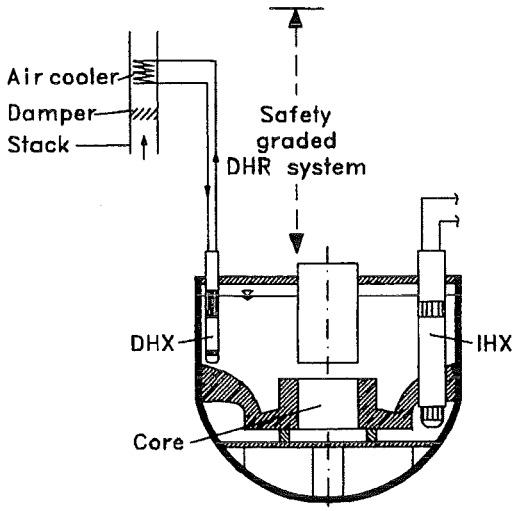

Fig. 3 Safety-graded decay heat removal system

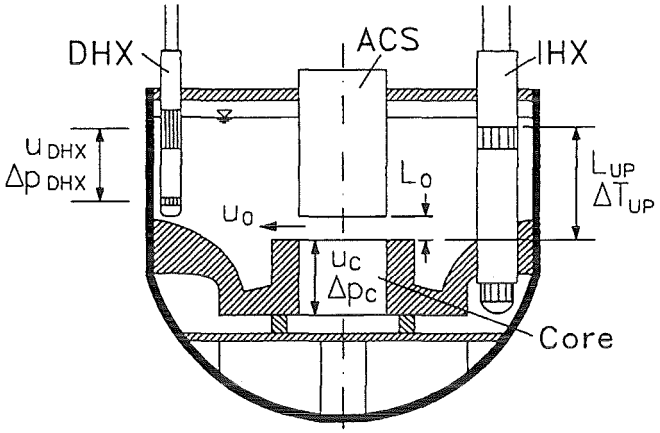

$$Ri = g \cdot \beta \, \Delta T_{UP} \cdot L_{UP} / U_o^2$$

$$Re = U_o \cdot L_o / \nu$$

$$Pe = U_o \cdot L_o / a$$

$$Eu^+ = \Delta p_{DHX} \, U_C^2 / \Delta p_C \, U_{DHX}^2$$

Fig. 4 Definition of the characteristic numbers

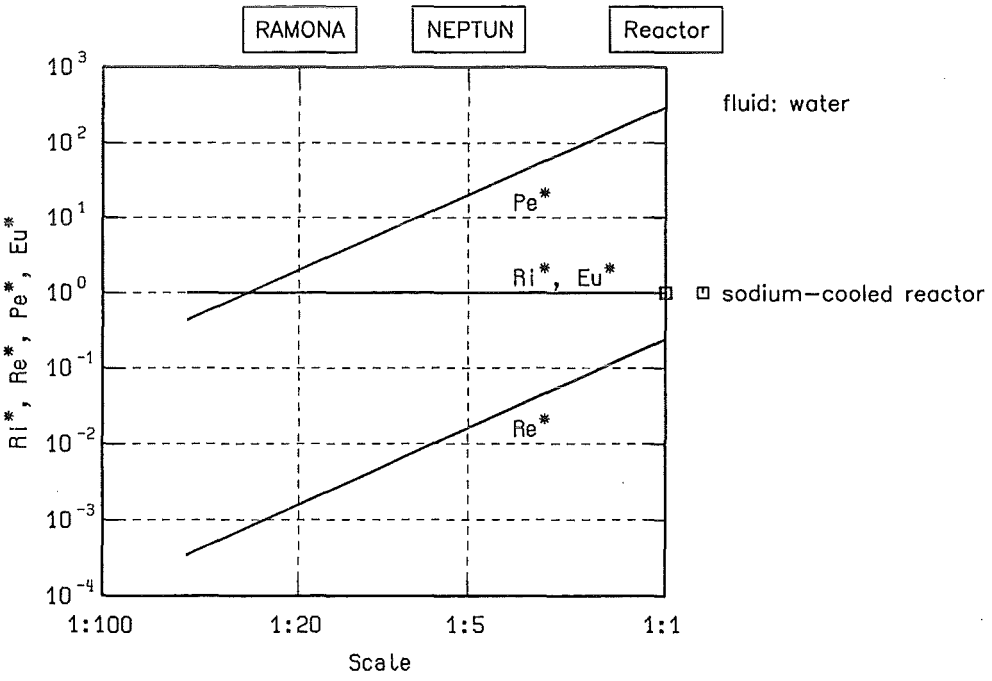

Fig. 5 Characteristic numbers as a function of the model scale

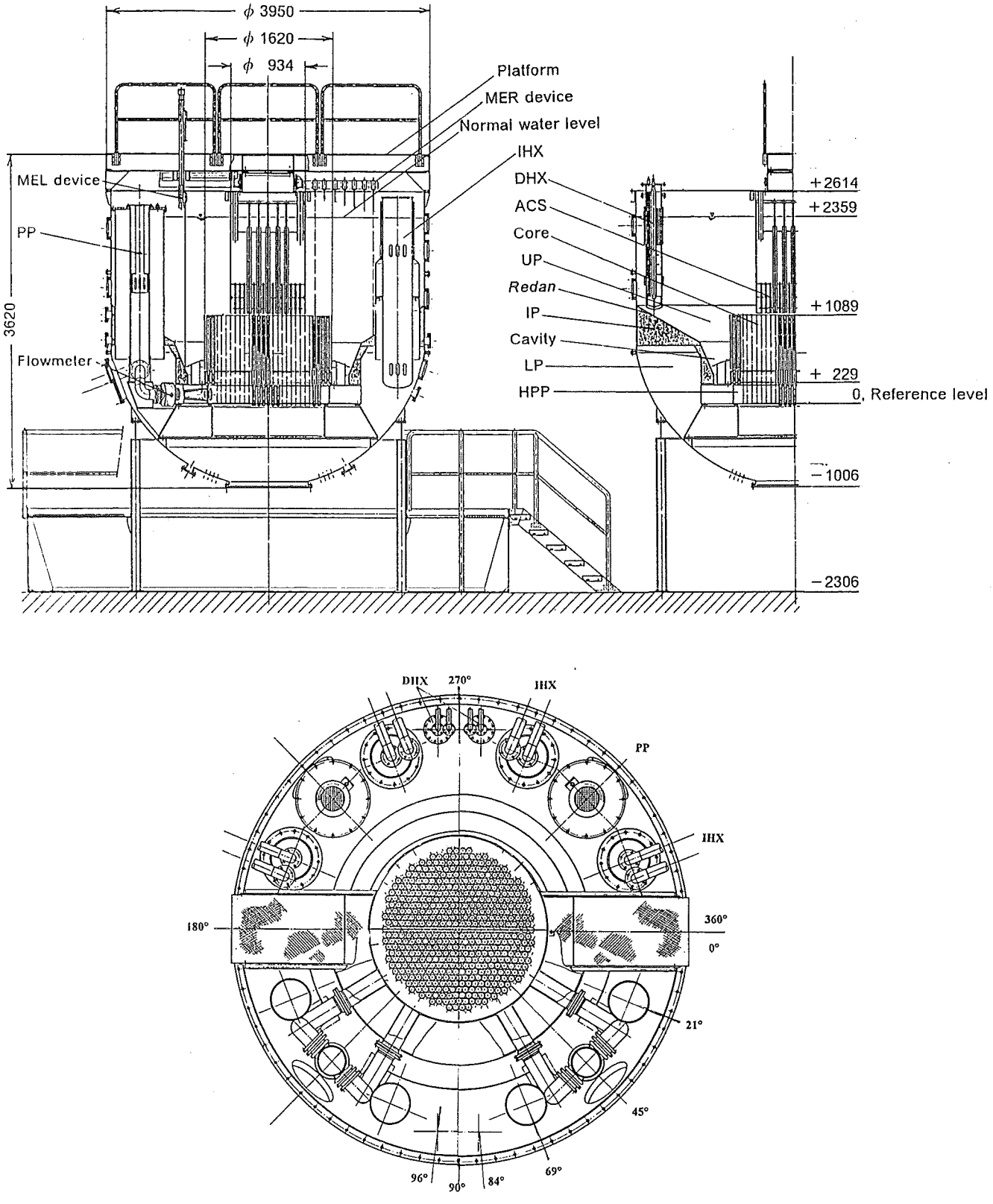

Fig. 6 Vertical and horizontal cross-sections of the NEPTUN test facility

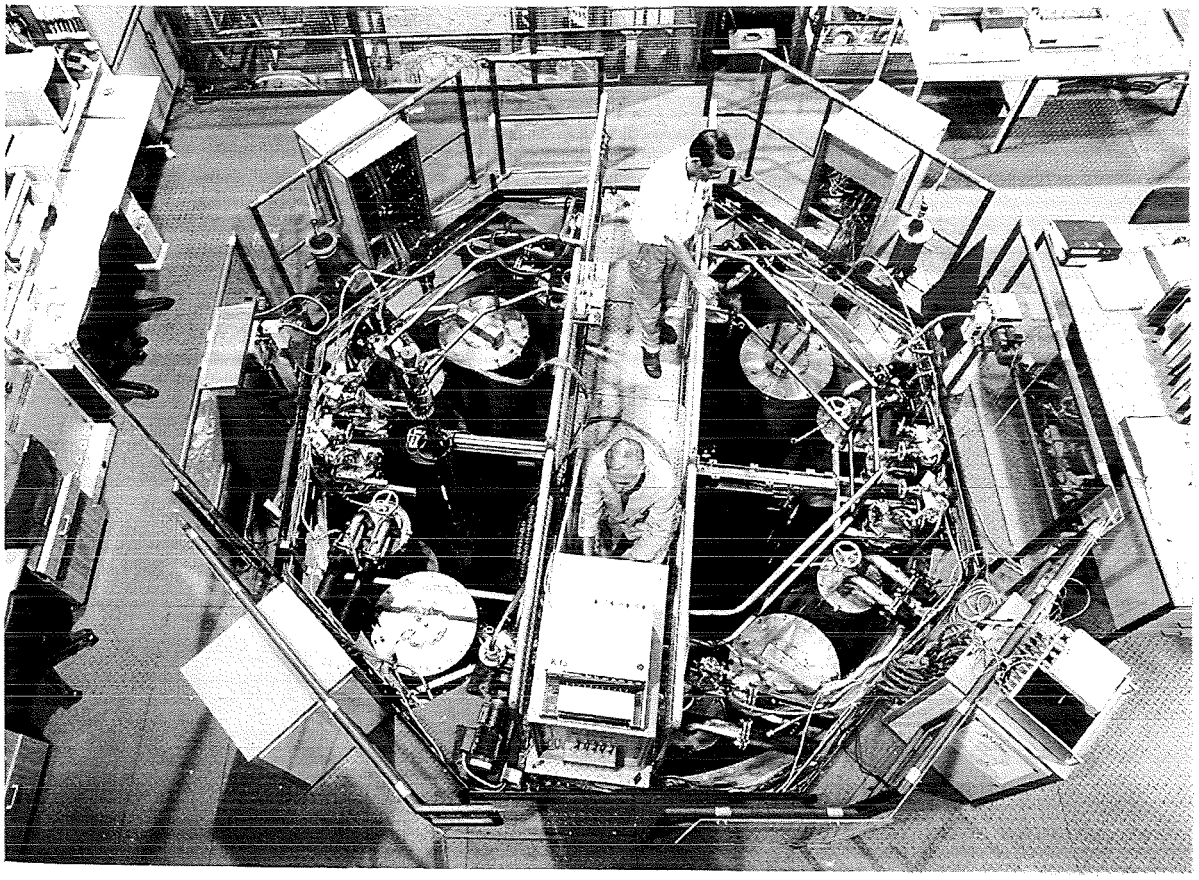

Fig. 7 Overall view of the NEPTUN test facility with transient test equipment

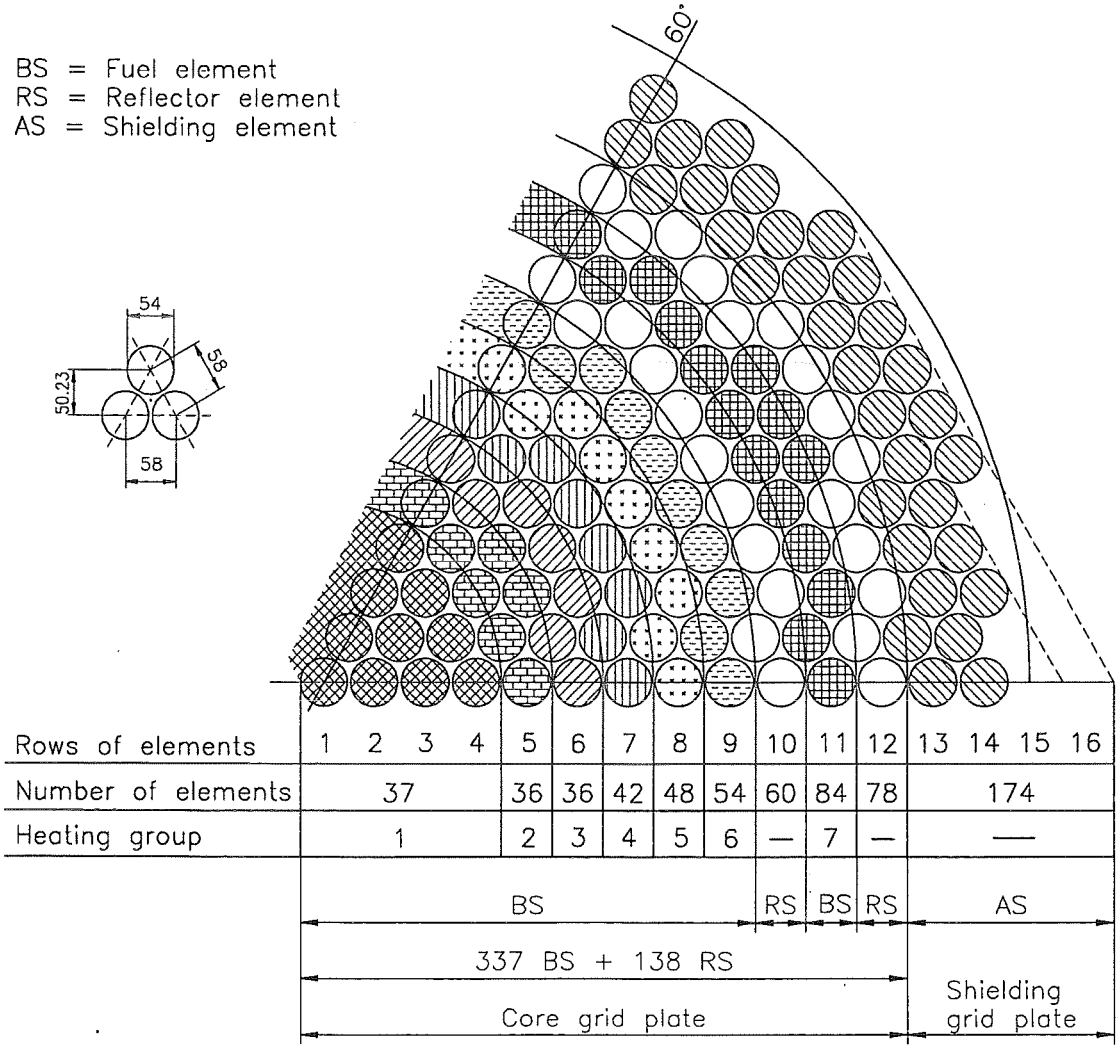

Fig. 8 Subassembly arrangement of the NEPTUN core

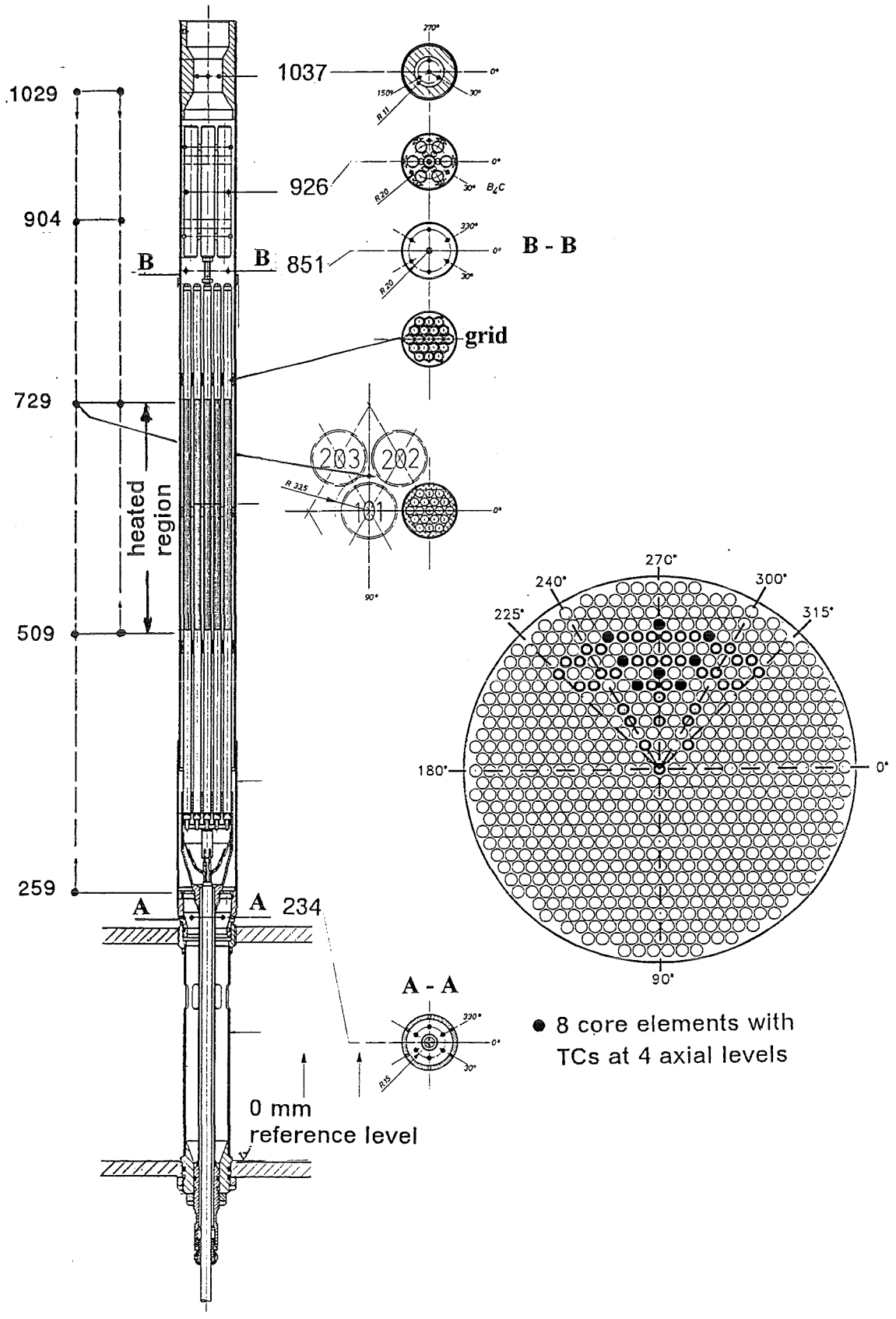

Fig. 9 Fuel element simulator of the NEPTUN core and its instrumentation

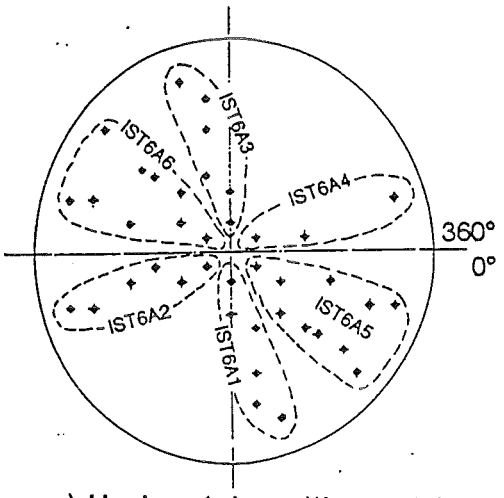

a) Horizontal positions at (A)

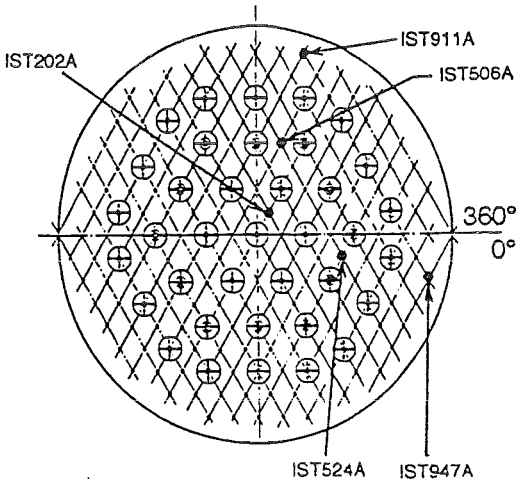

b) Axial positions at (B)

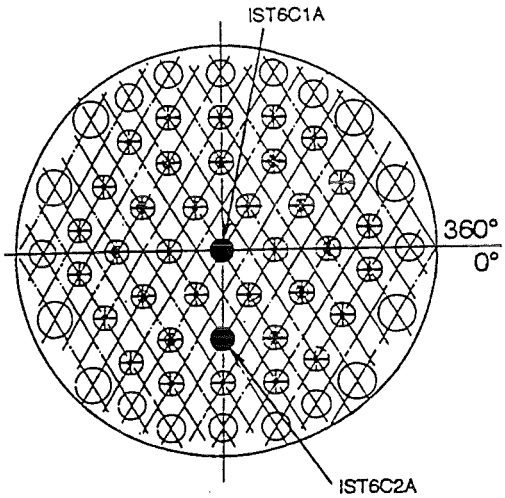

c) Axial positions at (C)

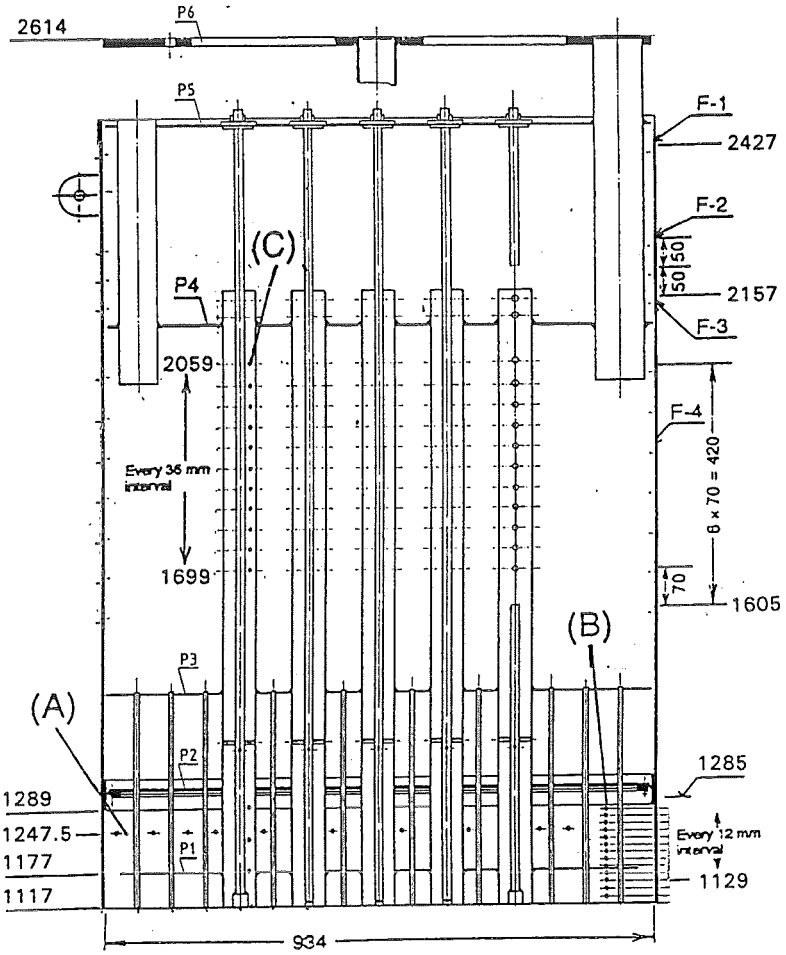

Flow routes

F-1: 12 holes of Ø 30 mm
F-2: 30 holes of Ø 40 mm
F-3: 36 holes of Ø 40 mm, 2 rows
F-4: 36 holes of Ø 40 mm, 7 rows

Fig. 10 The above core structure and its instrumentation

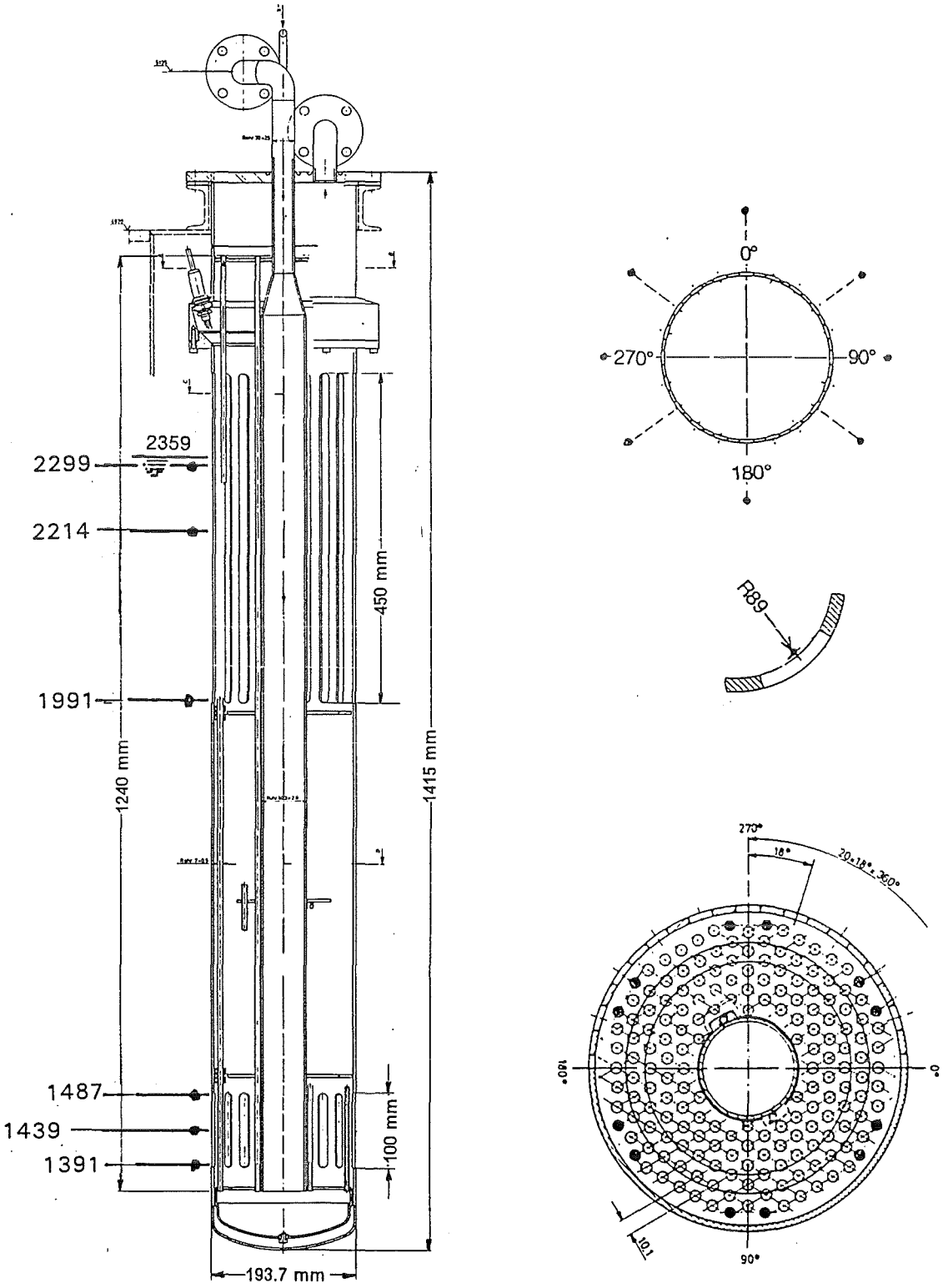

Fig. 11 Cross section of decay heat exchanger and its instrumentation

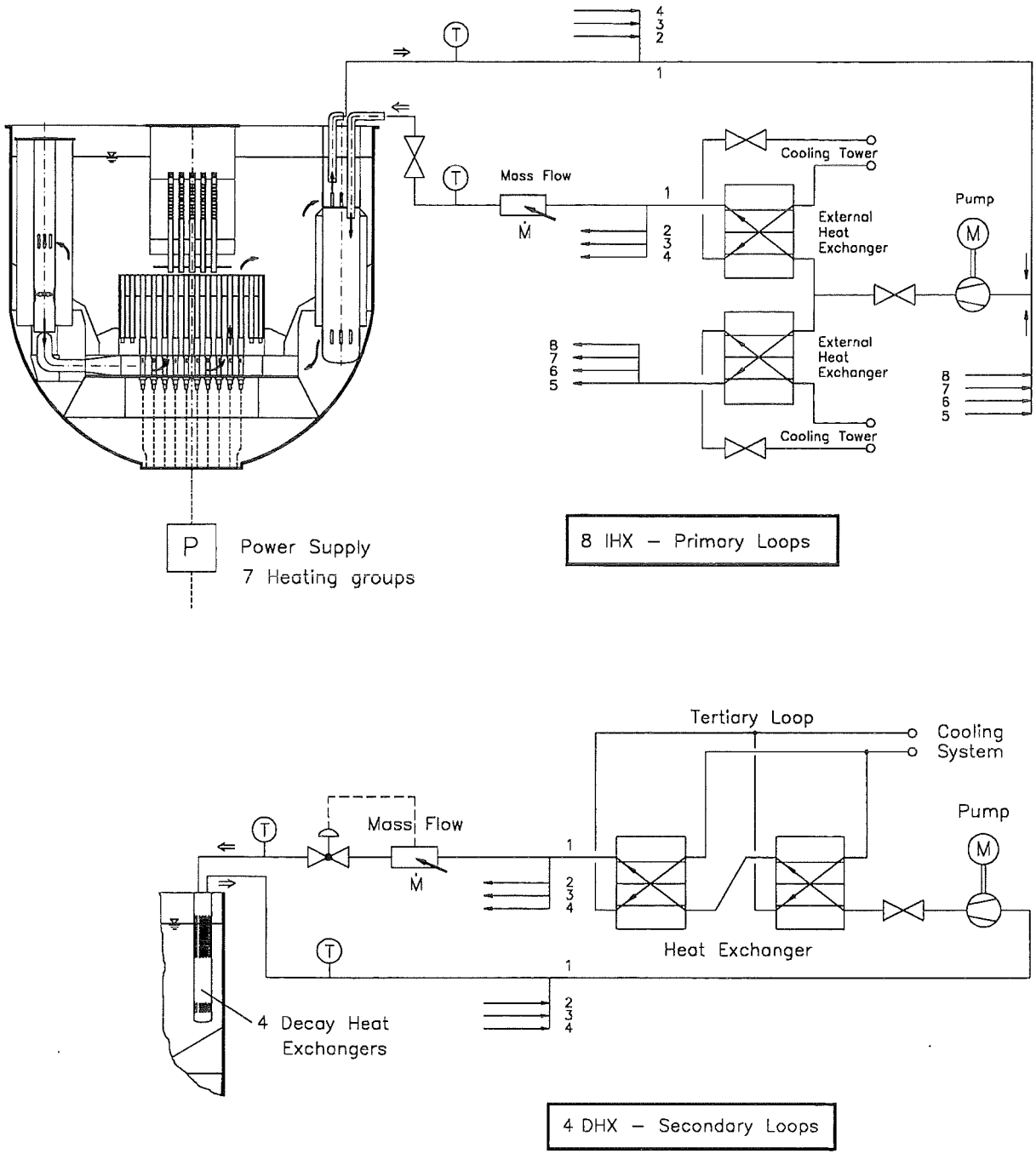

Fig. 12 Secondary heat transport circuits and their instrumentation

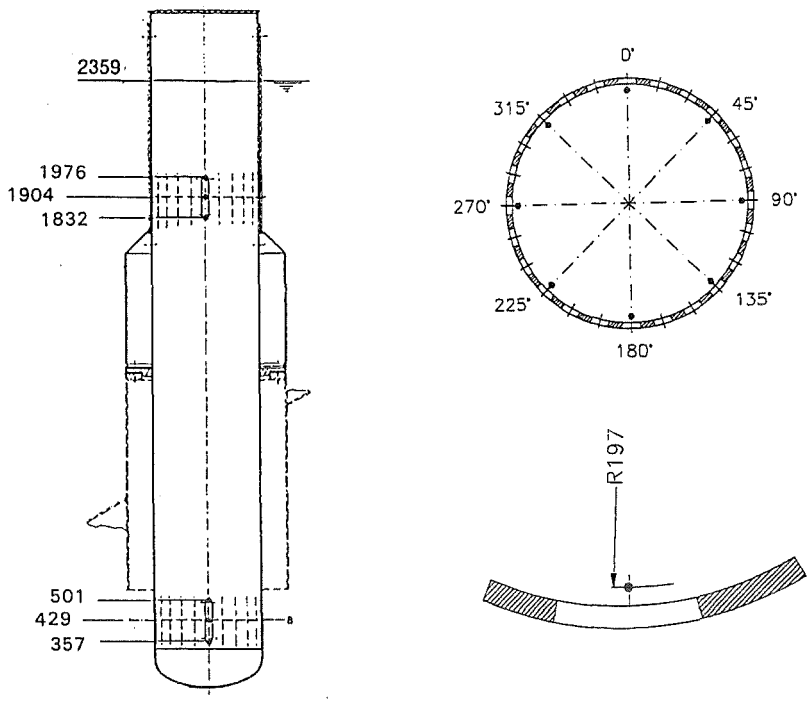

Fig. 13 Instrumentation of the intermediate heat exchanger simulator

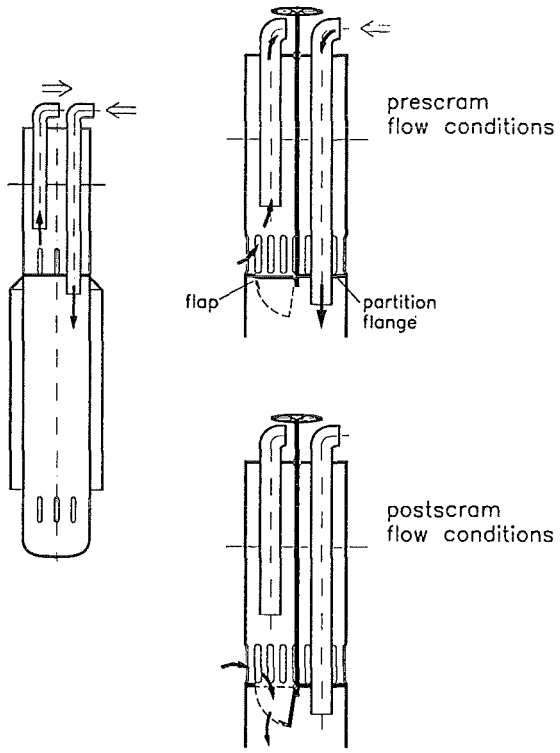

Fig. 14 Change-over mechanism of the IHXs for transient NEPTUN tests

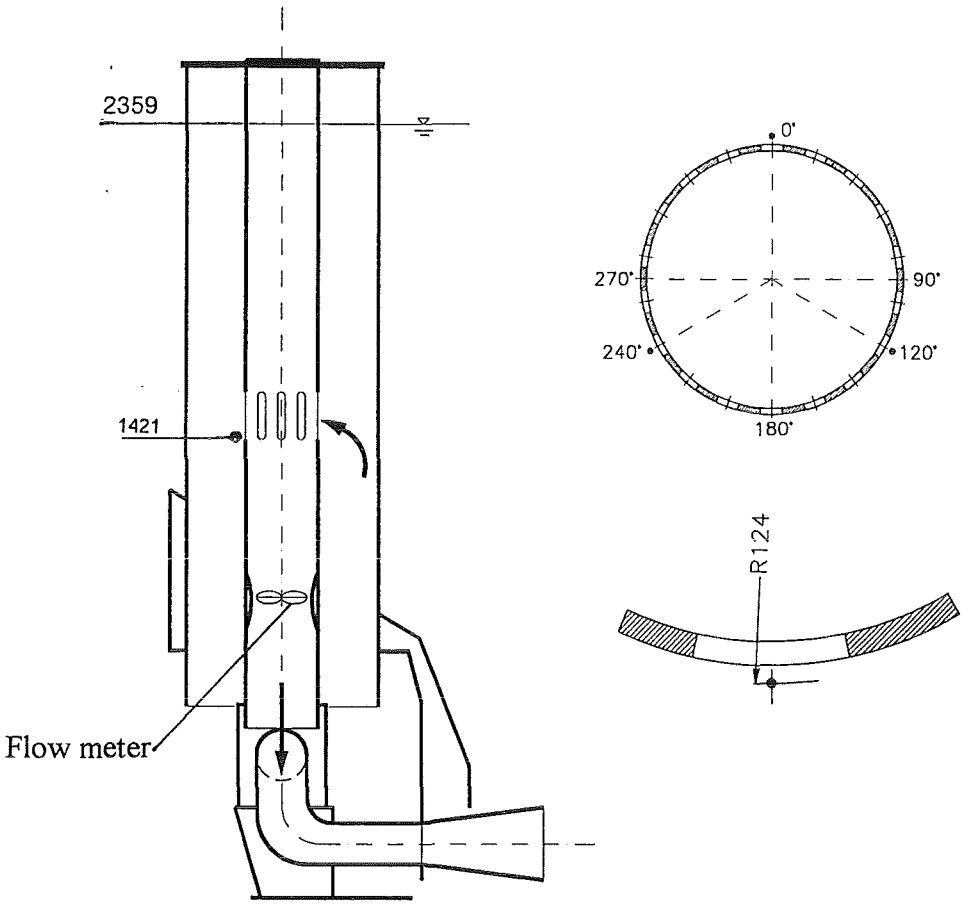

Fig. 15 Instrumentation of the primary pump simulators

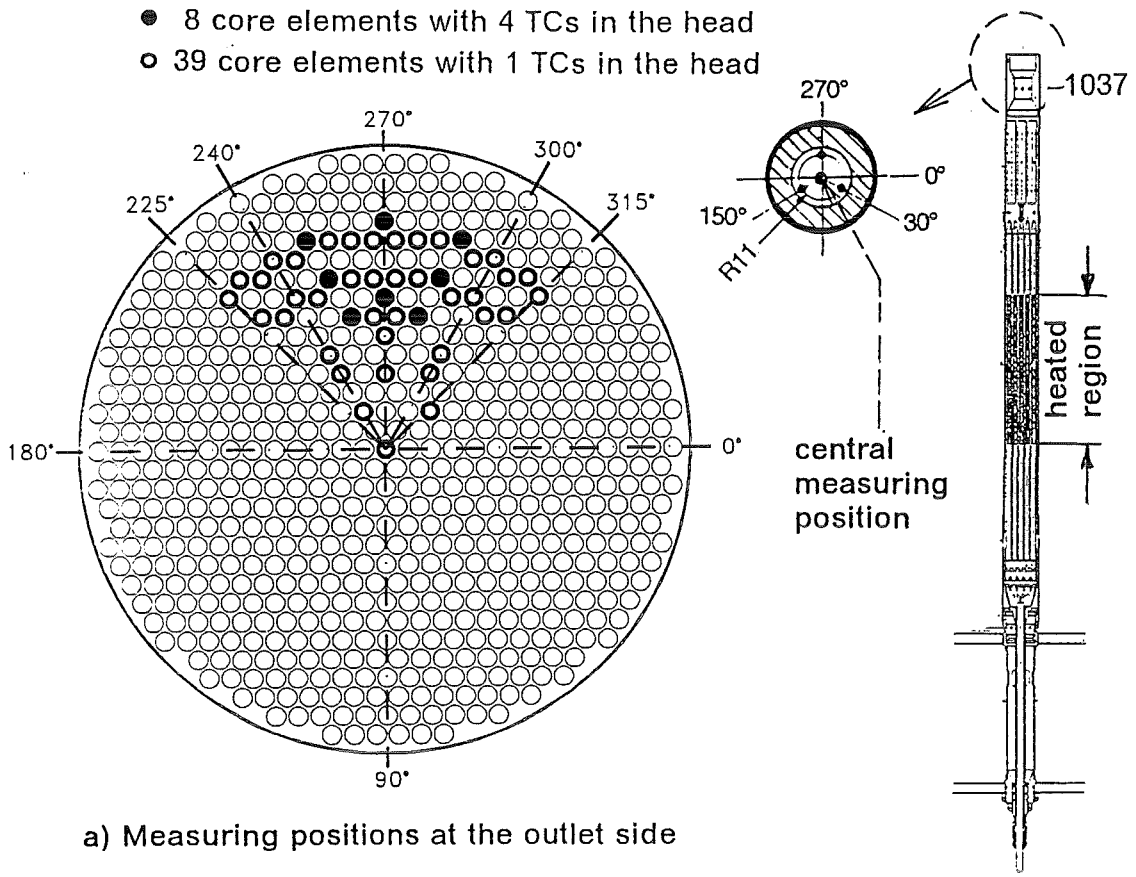

a) Measuring positions at the outlet side

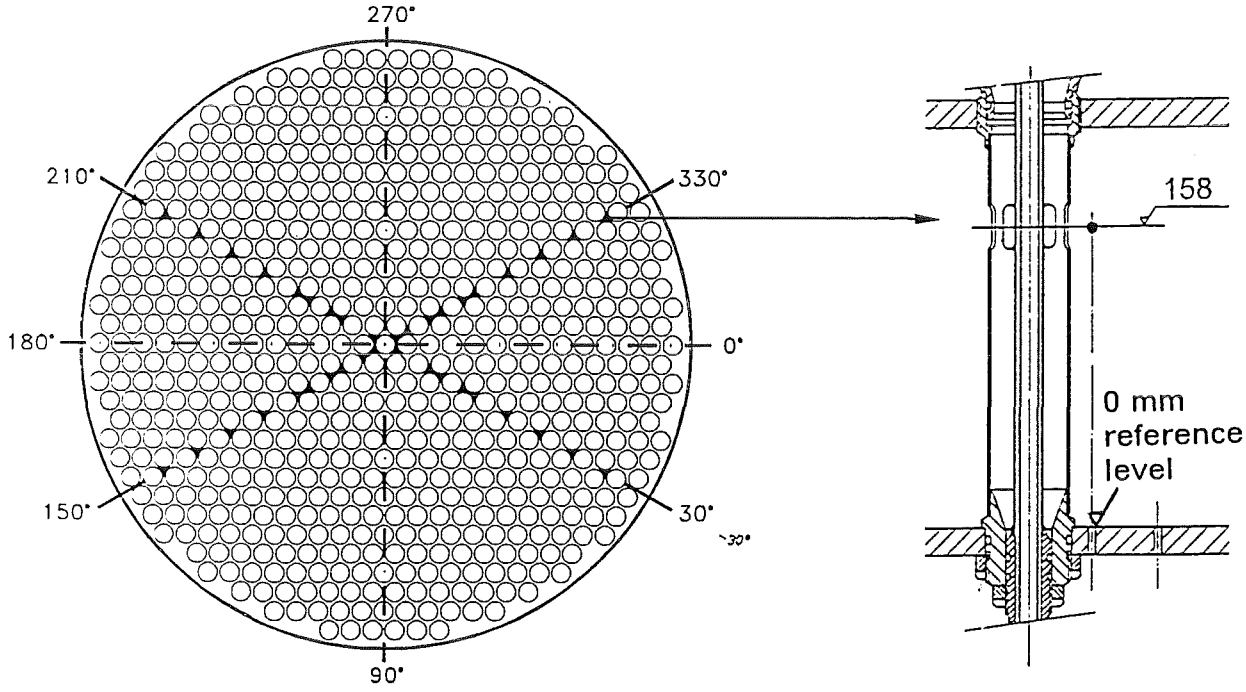

b) Measuring positions at the inlet side

Fig. 16 Instrumentation of the inlet and outlet sides of the NEPTUN core

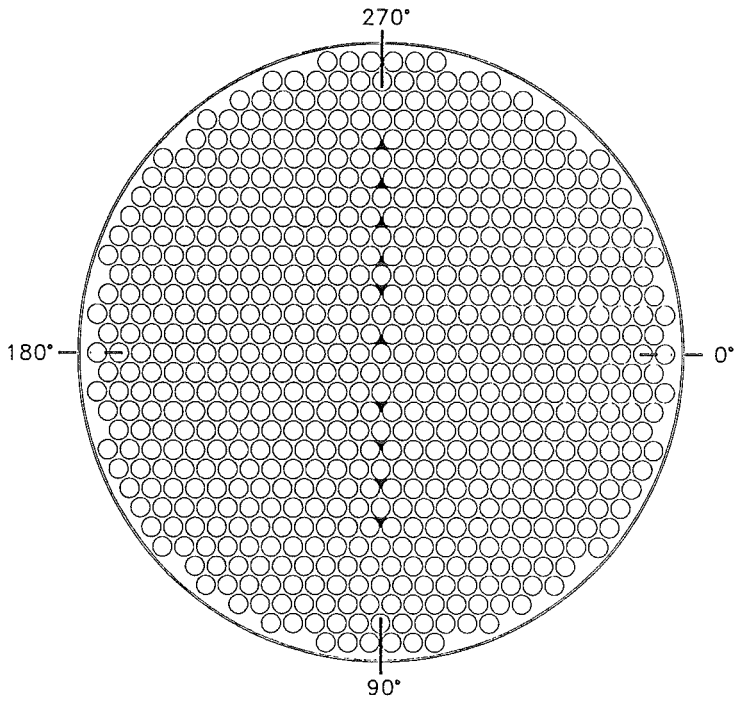

a) Radial positions

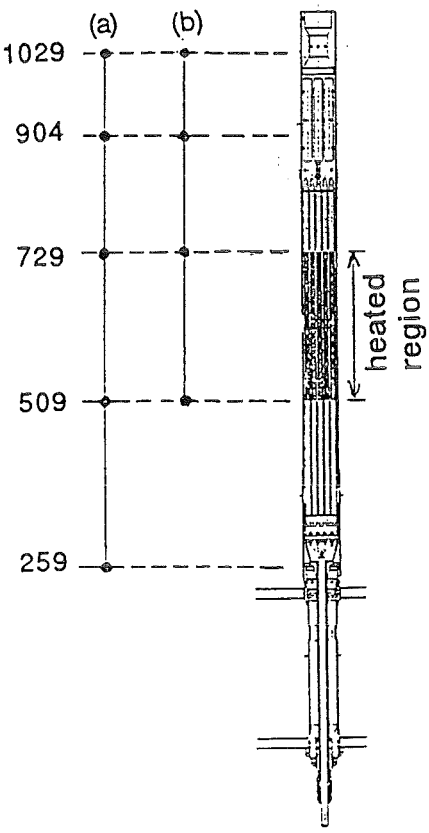

c) Axial positions

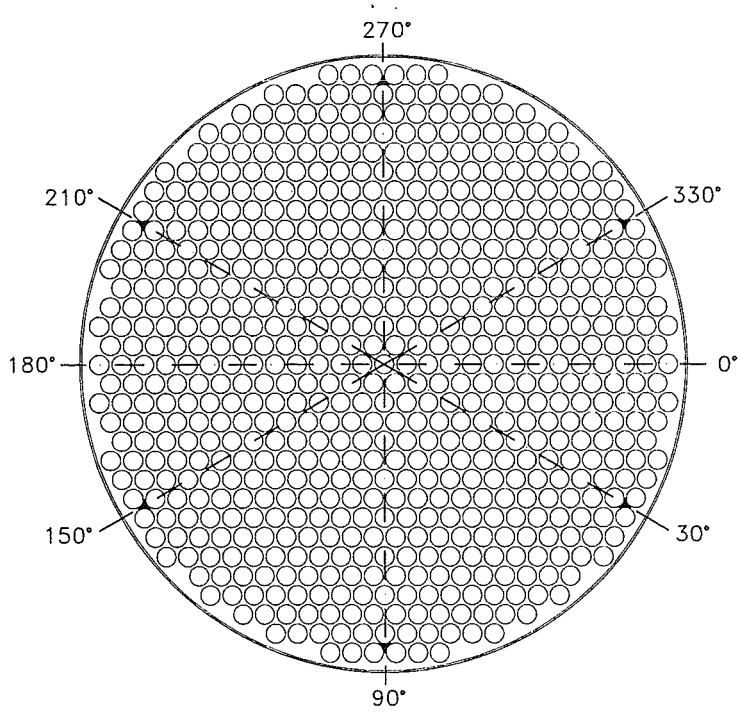

b) Positions at the periphery of the core

Fig. 17 Instrumentation of the interwrapper space

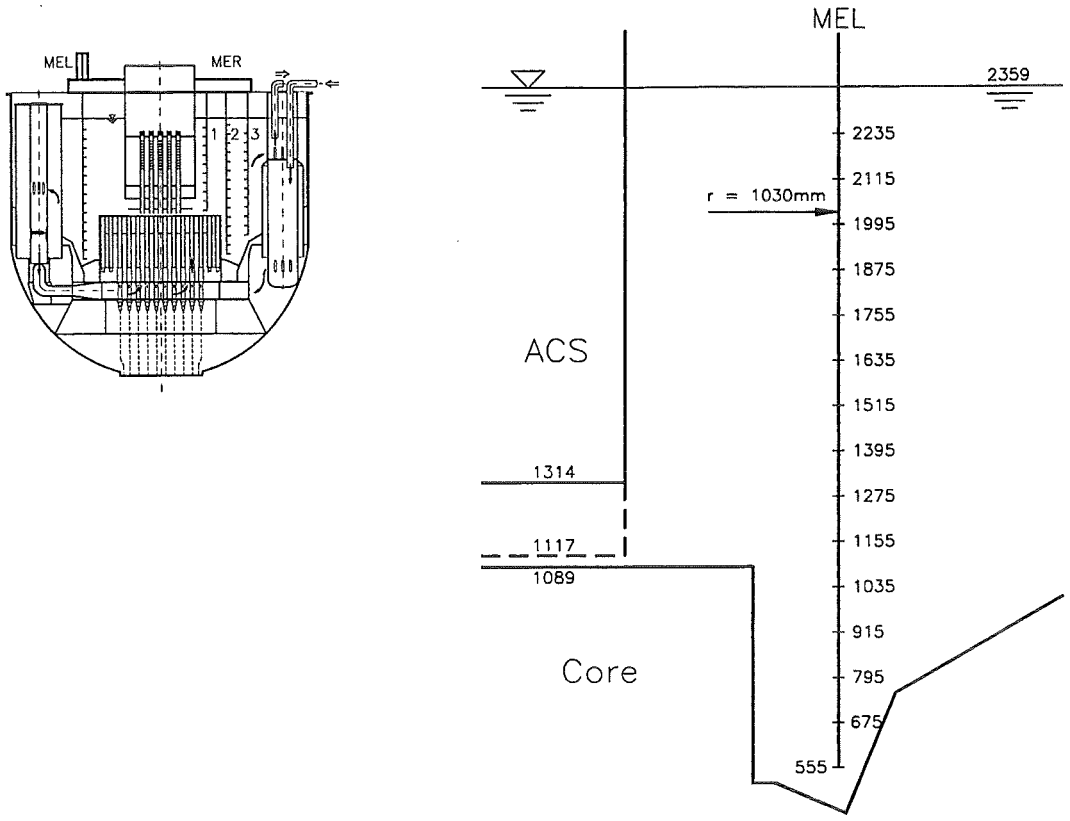

Fig. 18 Instrumentation of upper plenum, MEL divice

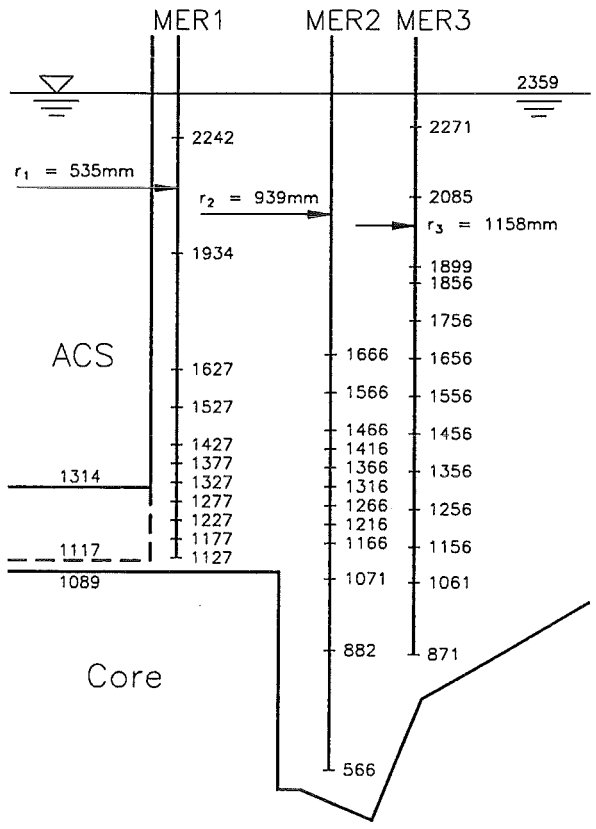

Fig. 19 Instrumentation of upper plenum, MER divice

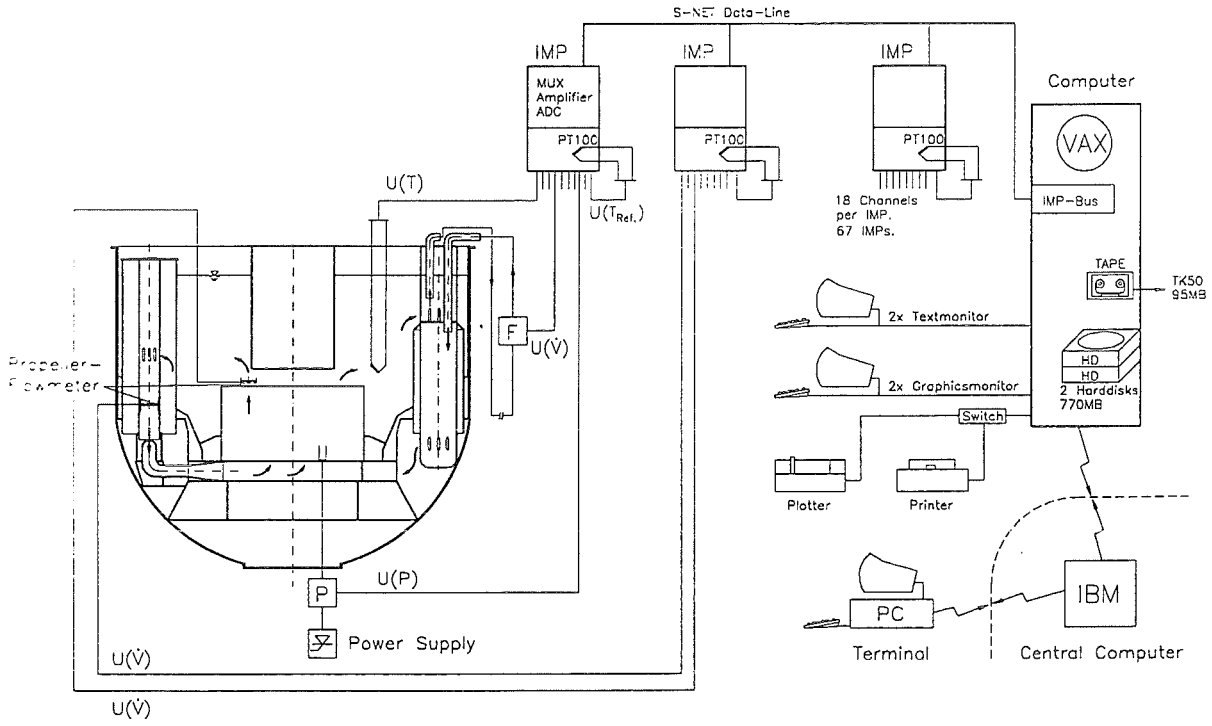

Fig. 20 Data acquisition and control system of NEPTUN test facility

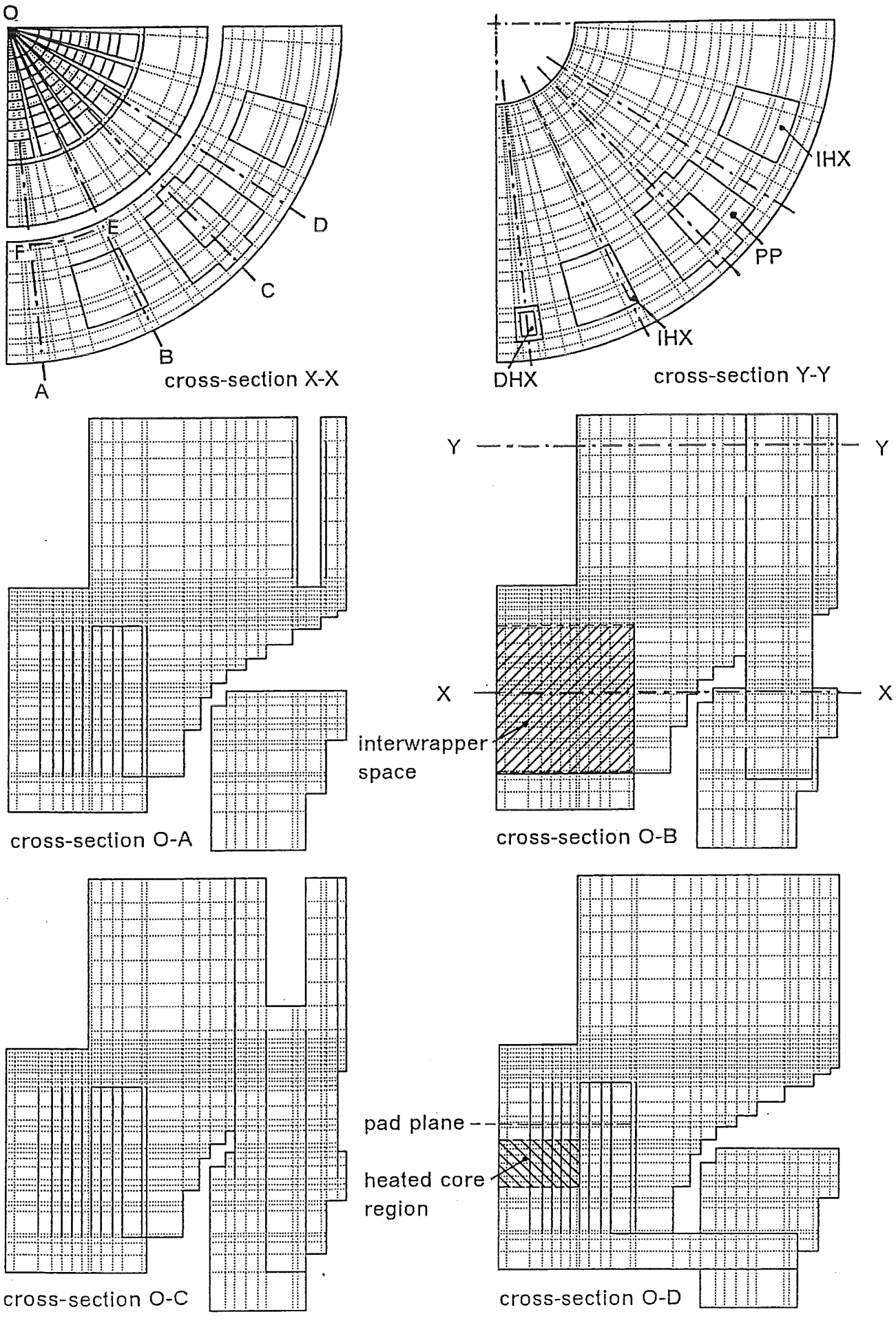

Fig. 21 Nodalization of the NEPTUN geometry

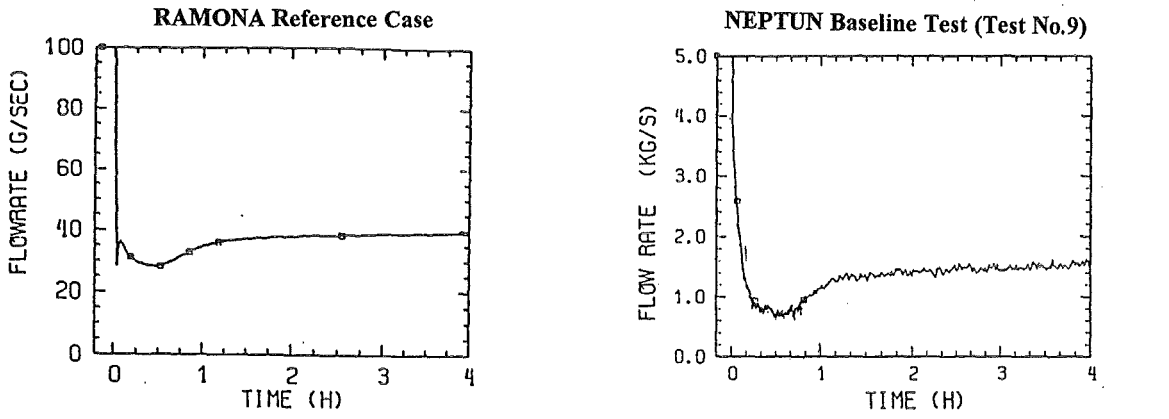

a) core mass flow rate

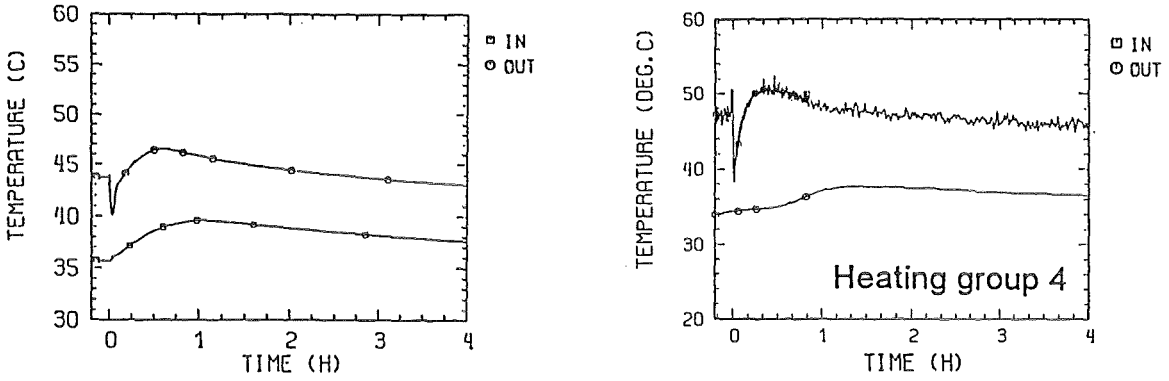

b) core inlet and outlet temperatures

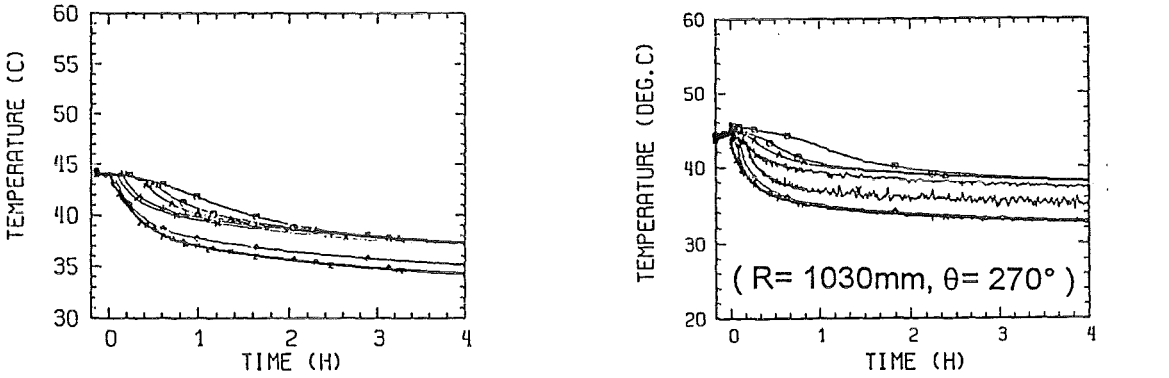

c) upper plenum temperatures

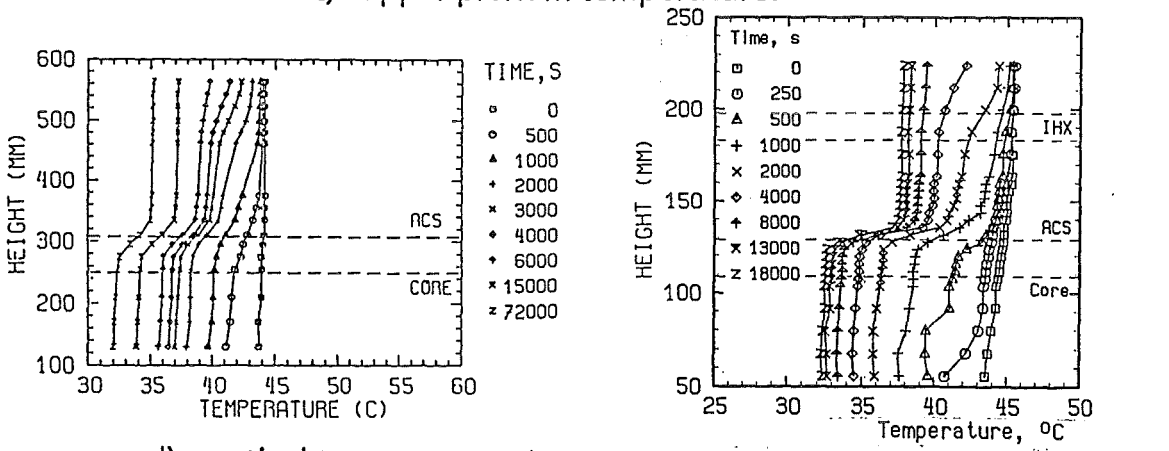

d) vertical temperature distributions in the upper plenum

Fig. 22 Comparison of RAMONA Reference cas with NEPTUN Baseline Test (30→1 kW, 1450→133 kW; $\tau_{IHX} \approx$ 15s, τ_{DHX} 240 s)

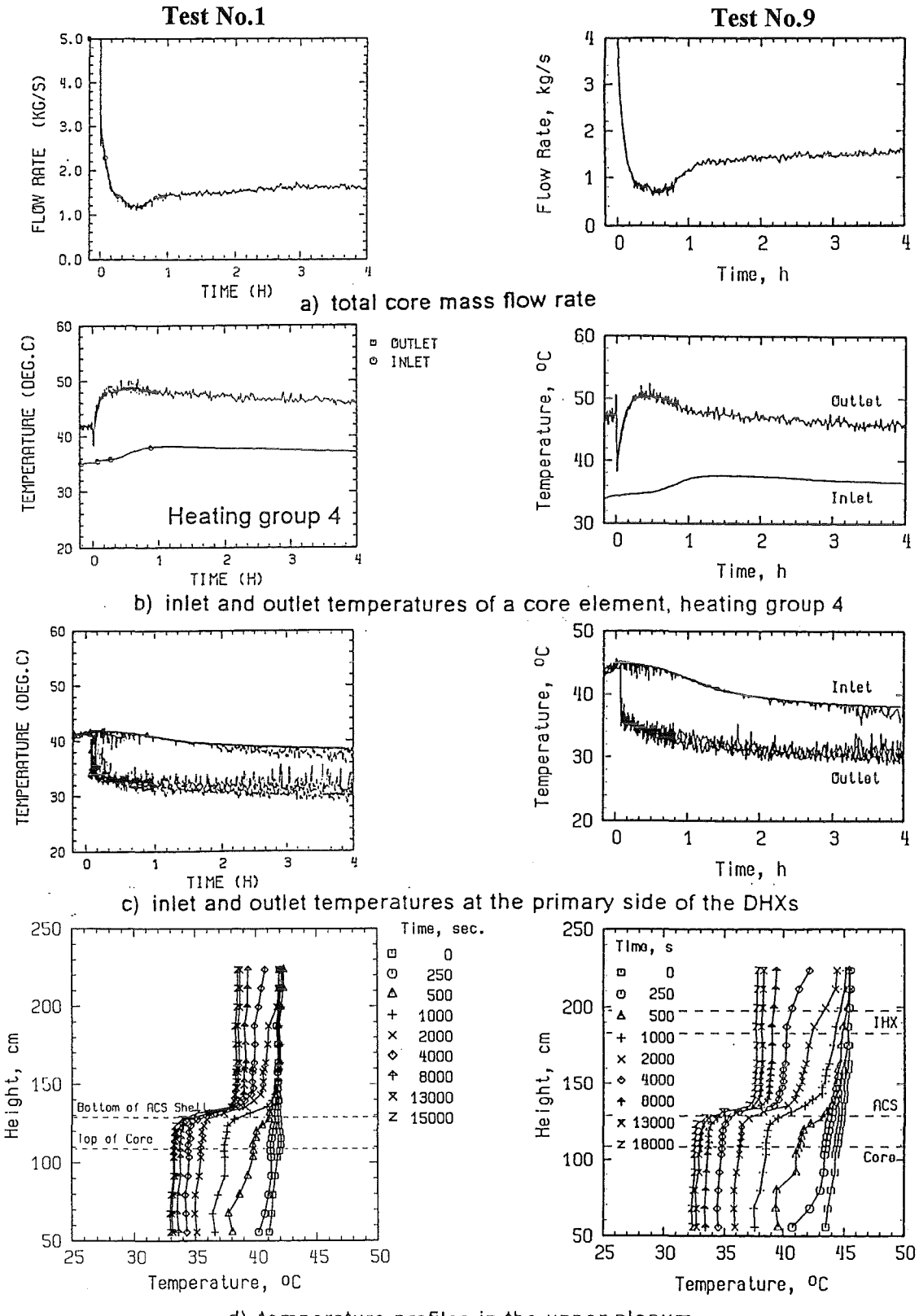

Fig. 23 Influence of different core powers on the thermal hydraulics of NEPTUN
(800→133 kW; 1450→133 kW)

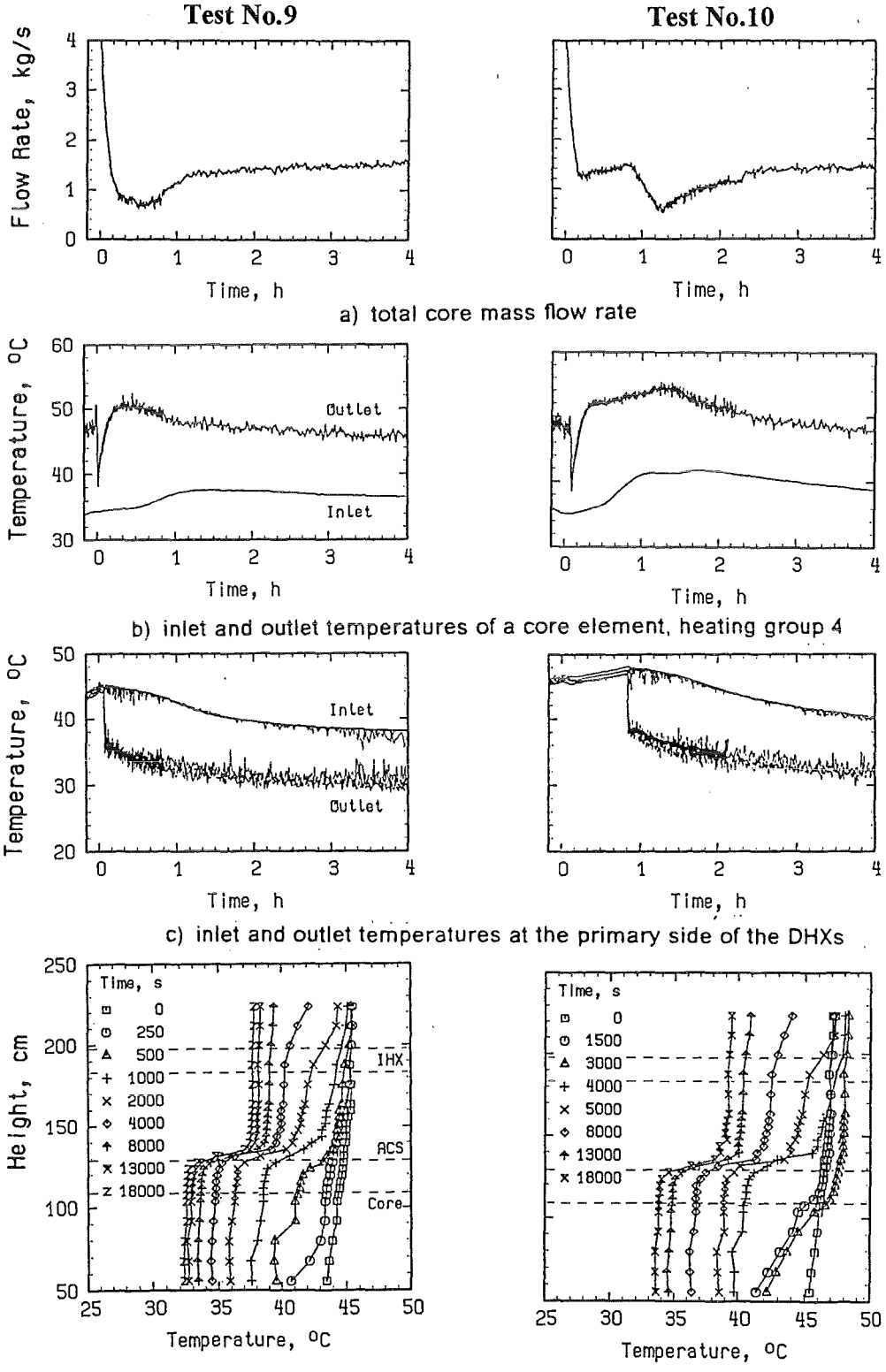

Fig. 24 Comparison of different delayed DHX startup times (τ_{DHX} = 240 s, τ_{DHX} = 3000 s)

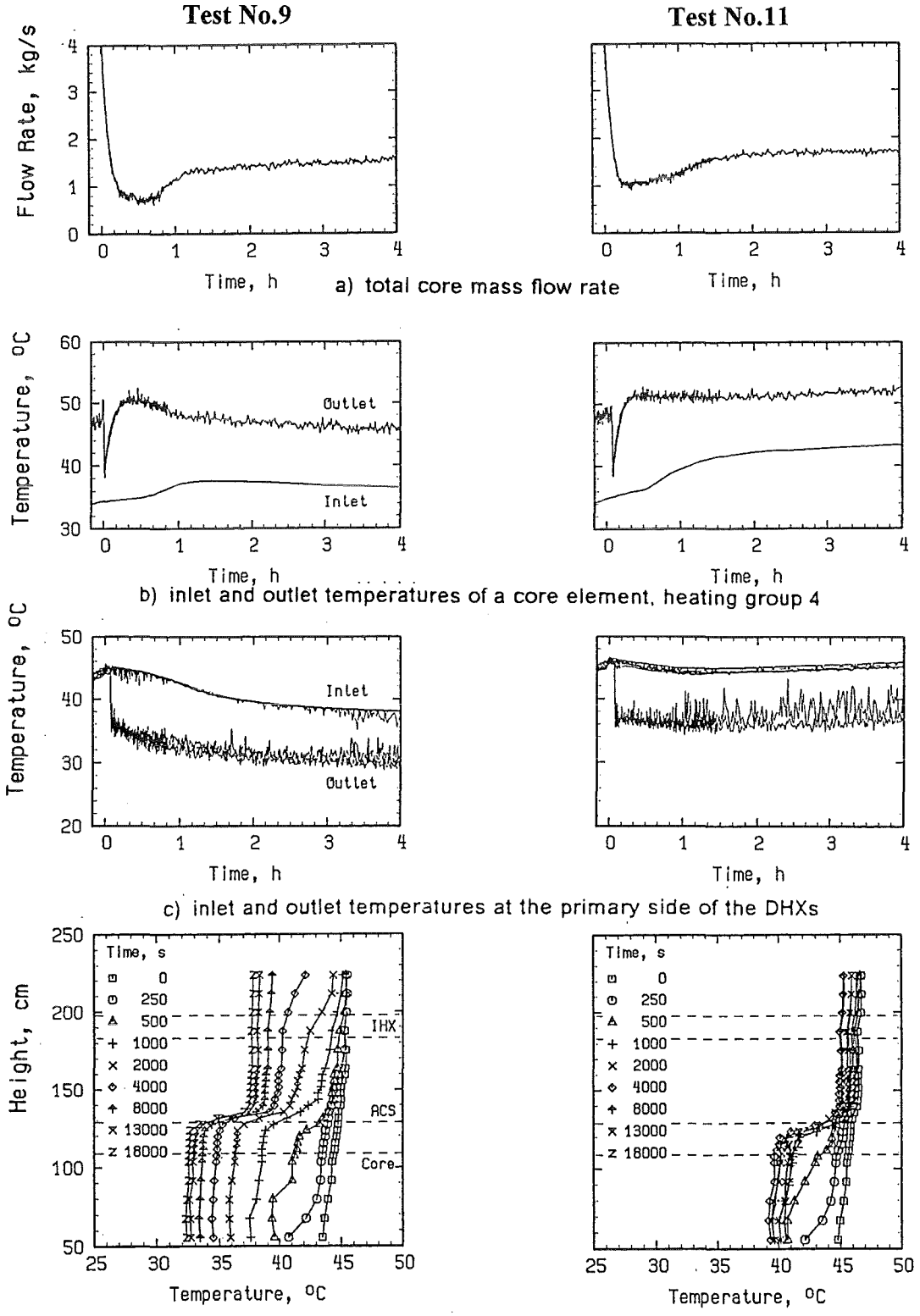

Fig. 25 Comparison of 4 and 2 DHXs in operation and their influence on the NEPTUN thermal hydraulics (τ_{DHX} = 240 s)

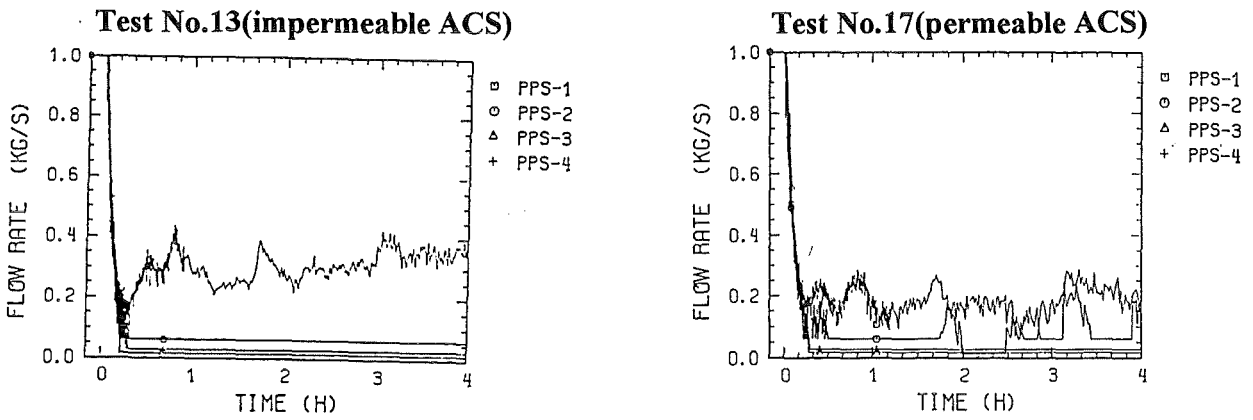

a) total core mass flow rate

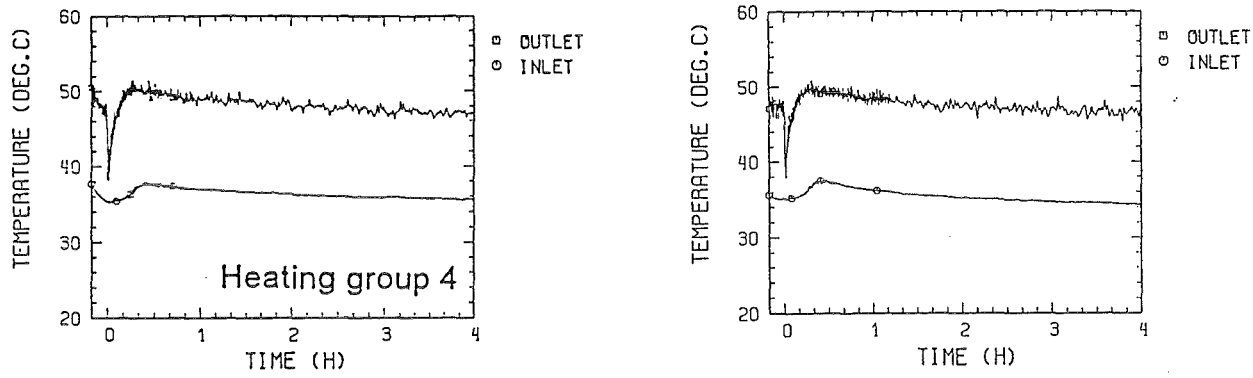

b) inlet and outlet temperatures of a core element, heating group 4

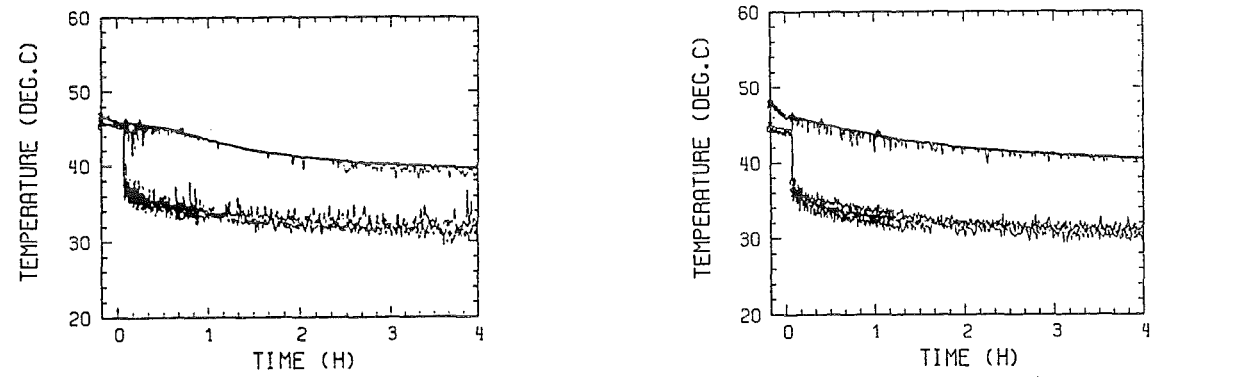

c) inlet and outlet temperatures at the primary side of the DHXs

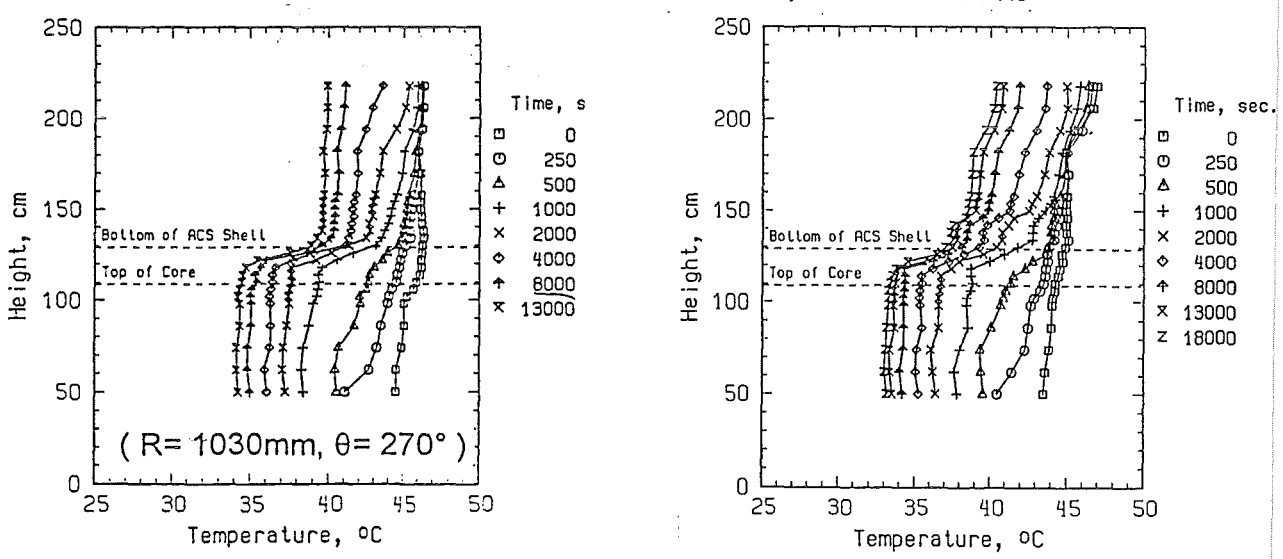

d) temperature profiles in the upper plenum

Fig. 26 Comparison of the influence of impermeable and permeable ACS

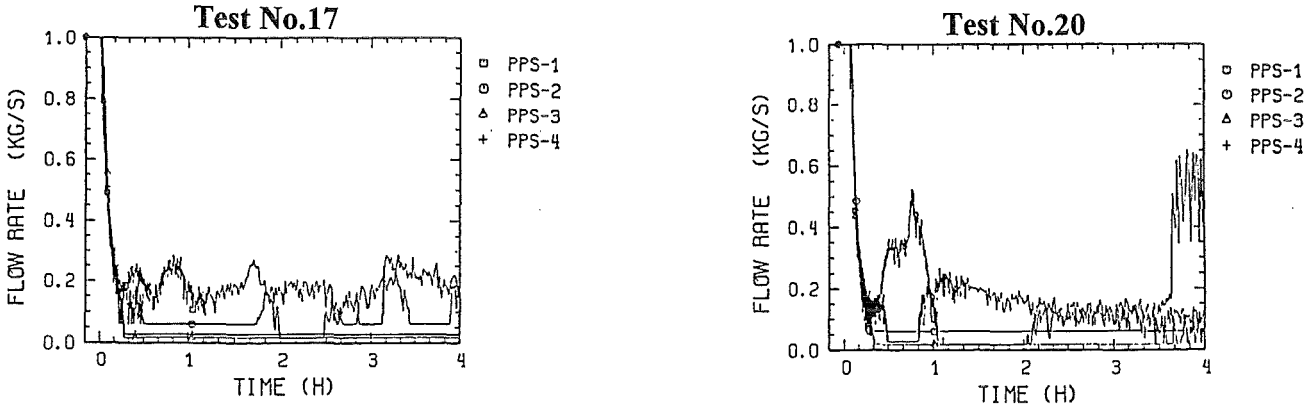

a) total core mass flow rate

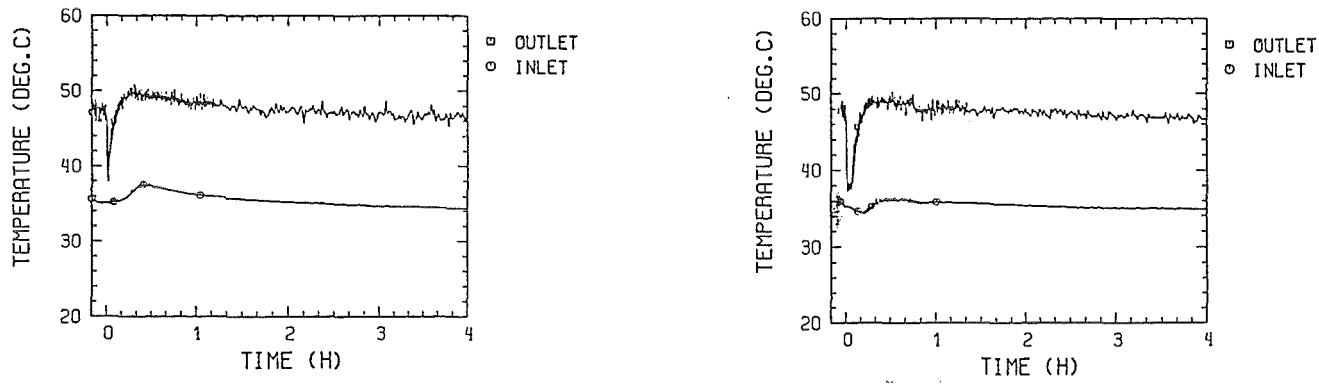

b) inlet and outlet temperatures of a core element, heating group 4

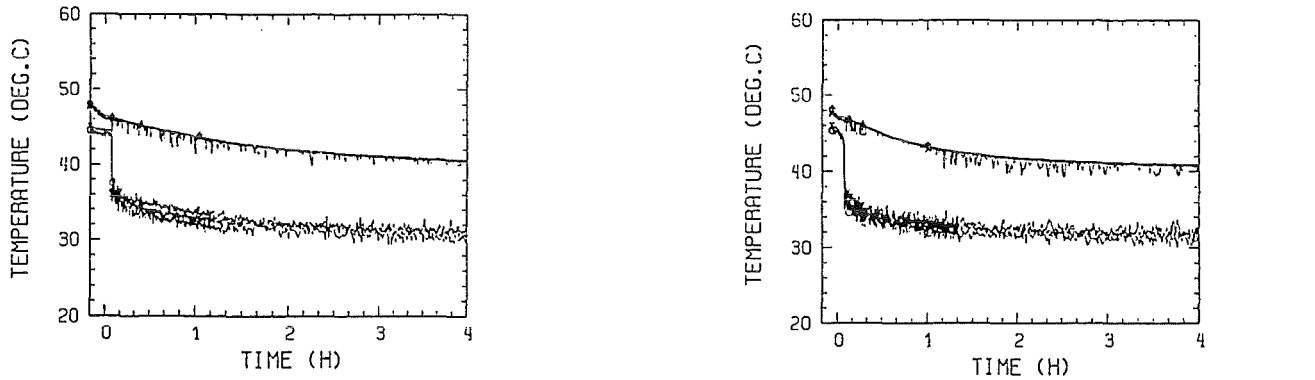

c) inlet and outlet temperatures at the primary side of the DHXs

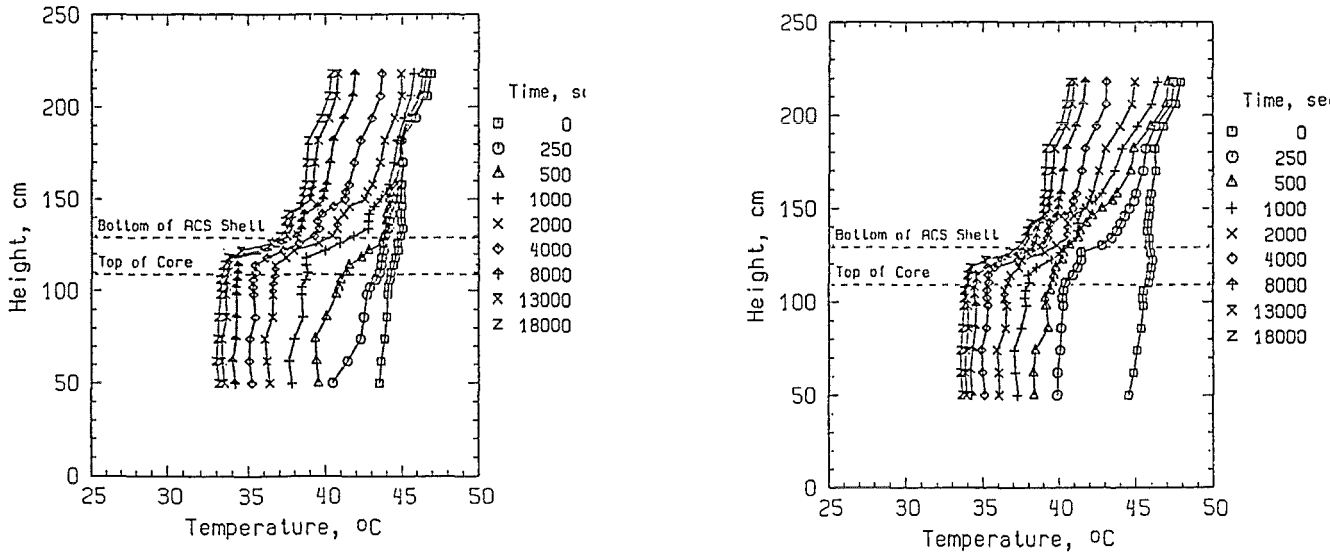

d) temperature profiles in the upper plenum

Fig. 27 Comparison of different primary pump coast downs
(τ_{PP} = 25 s; τ_{PP} = 240 s)

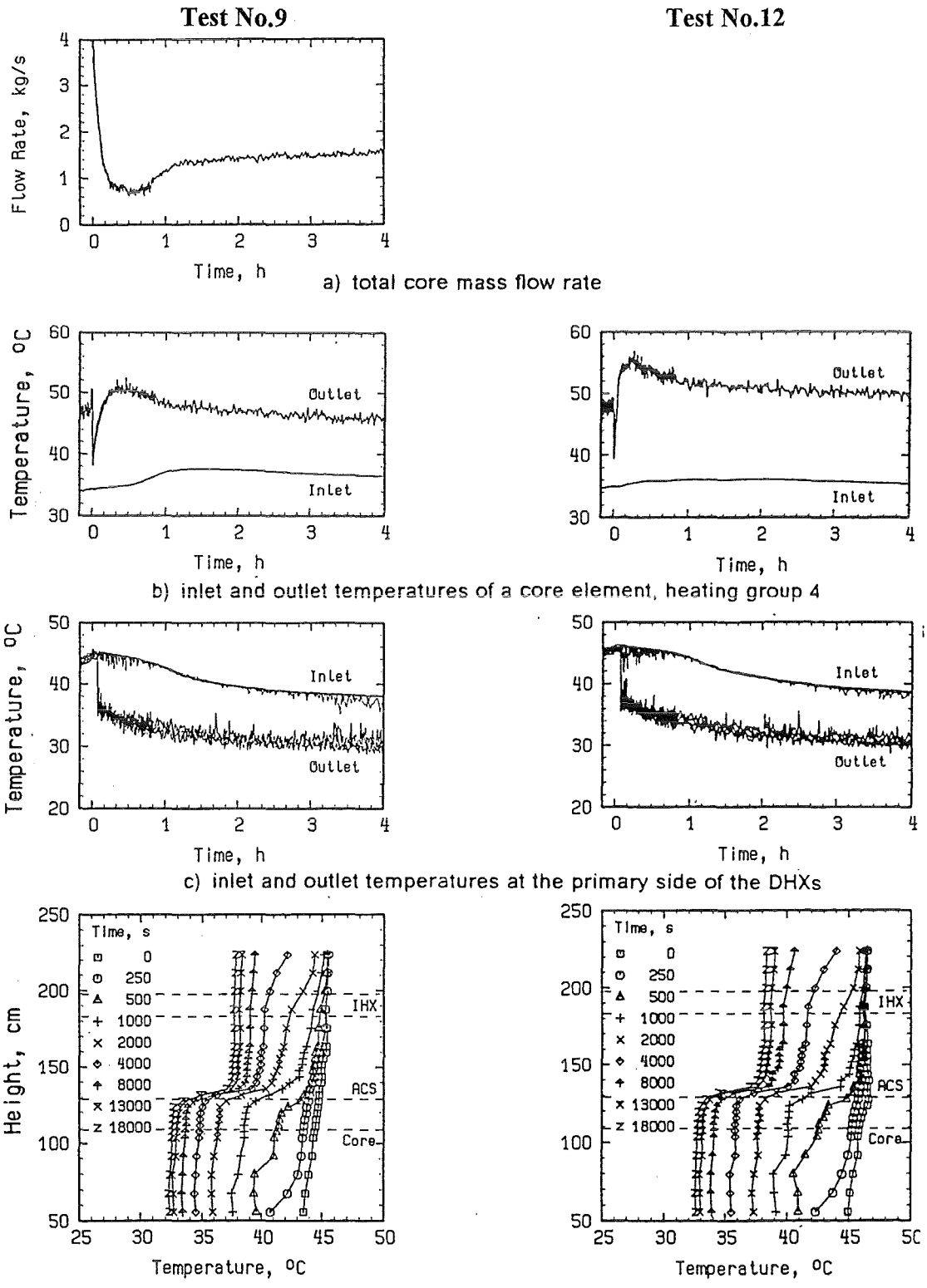

Fig. 28 Comparison of unblocked and blocked primary flow paths of the IHXs

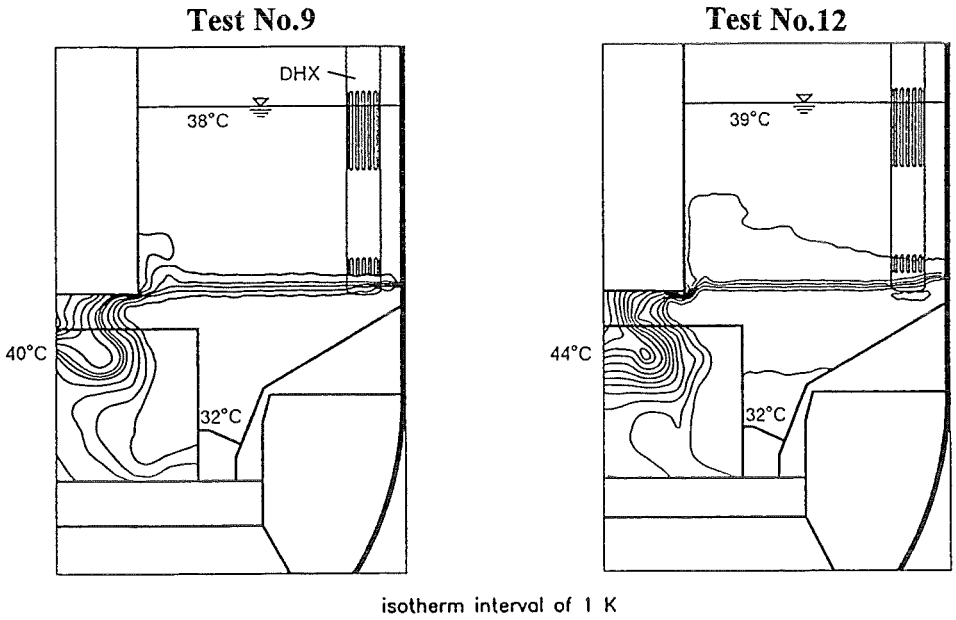

Fig. 29a Influence of blocked primary flow paths of IHXs on the temperature fields at 18000 s after scram. Measured data

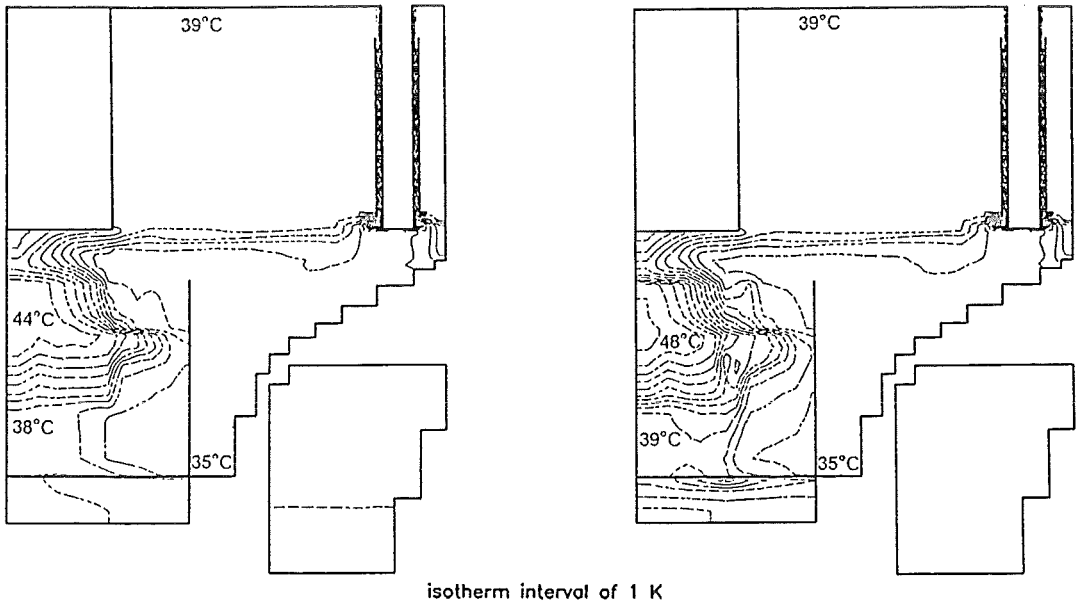

Fig. 29b Influence of blocked primary flow paths of IHXs on the temperature fields at 18000s after scram. Calculated data.

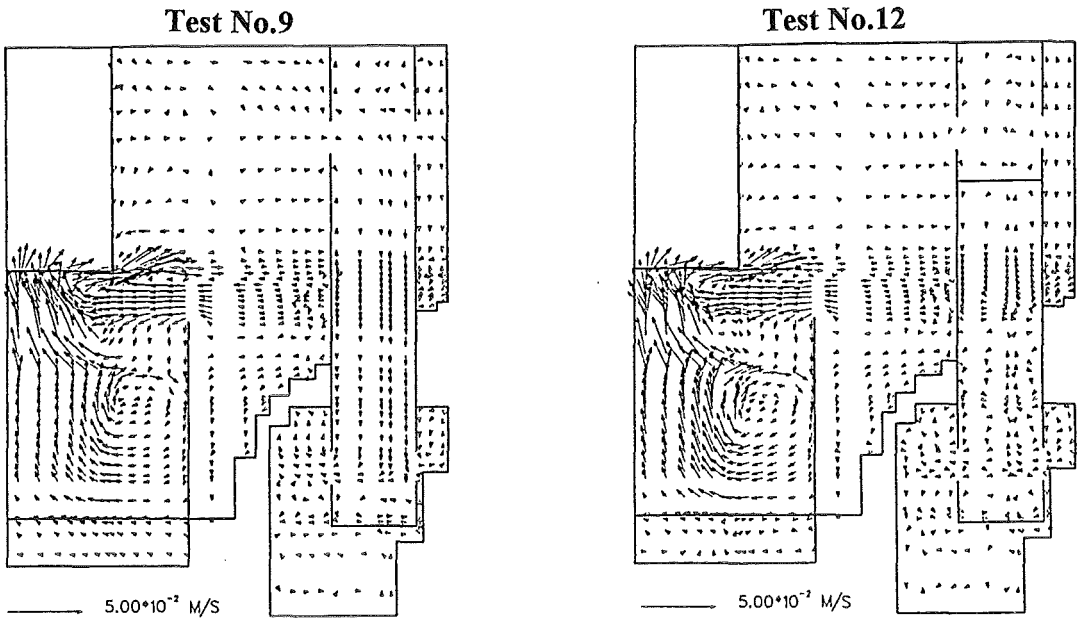

Fig. 30a Influence of blocked primary flow paths of IHXs on velocity fields at 18000 s after scram. Calculated data in a cross section with interstitial flow.

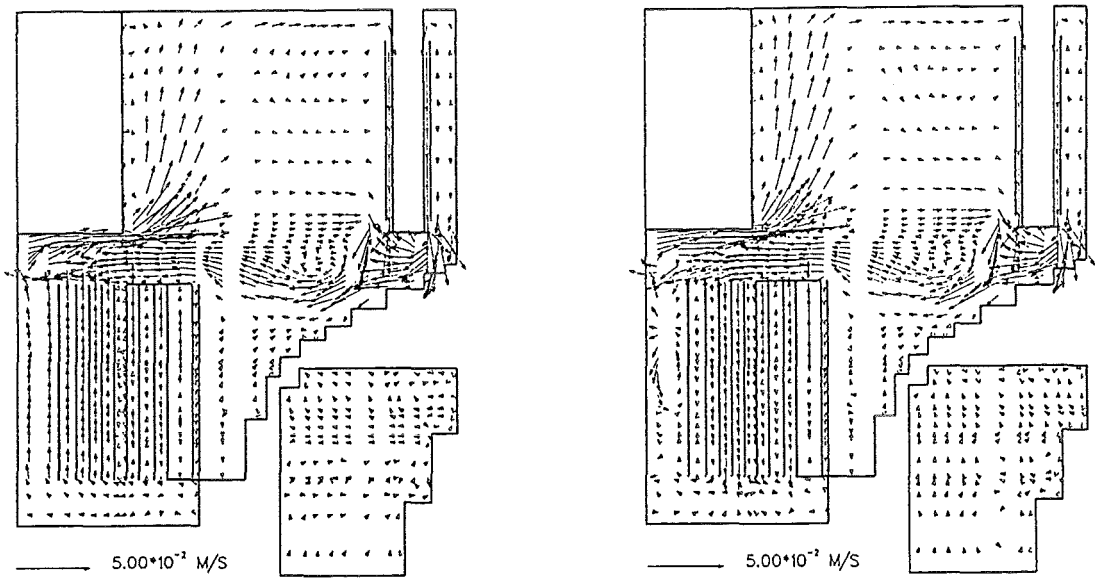

Fig. 30b Influence of blocked primary flow paths of IHXs on velocity fields at 18000 s after scram. Calculated data in a cross section with core elements

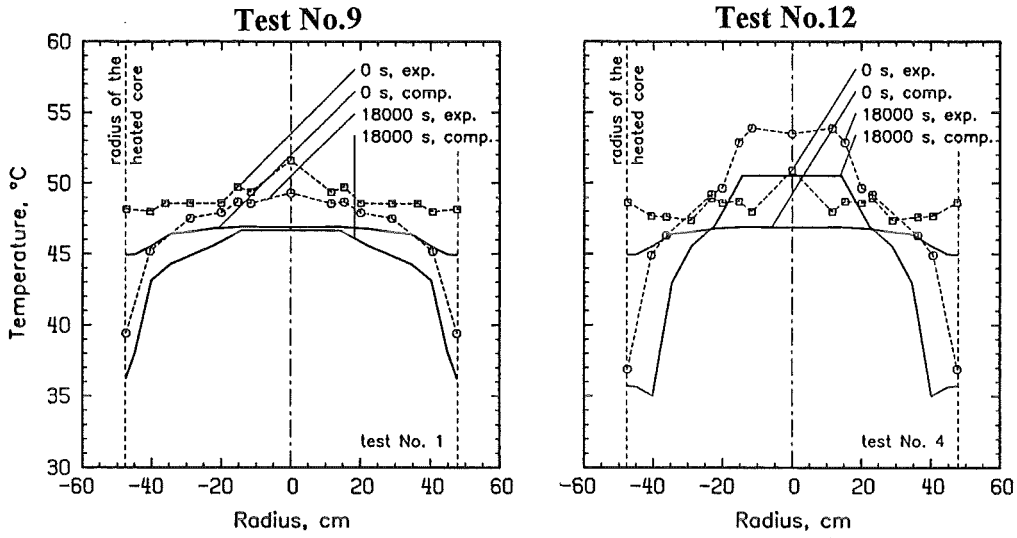

Fig. 31a Comparison of measured and computed radial temperature profiles at the outlet of SAs. Influence of blocked primary flow paths of IHXs.

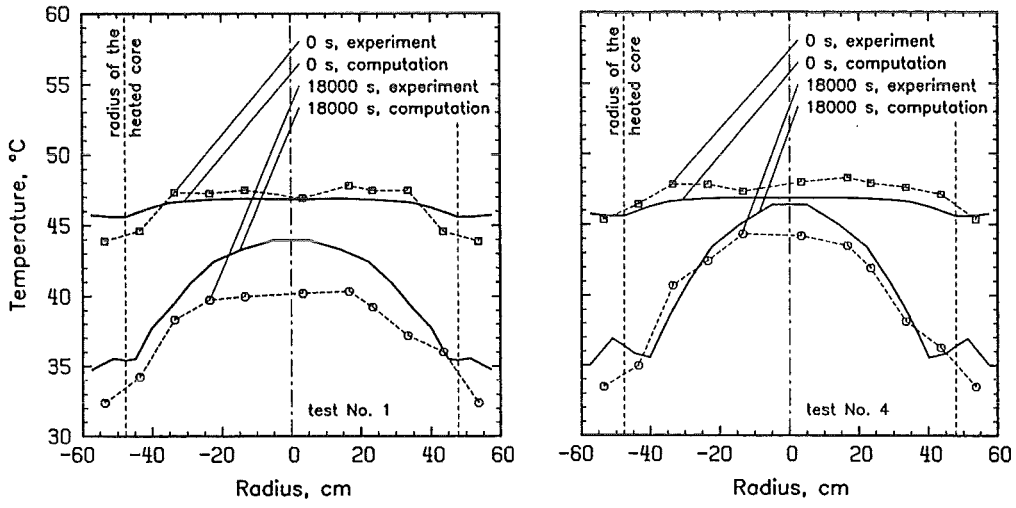

Fig. 31b Comparison of measured and computed radial temperature profiles at the upper end of the interstitial space. Influence of blocked primary flow paths of IHXs.

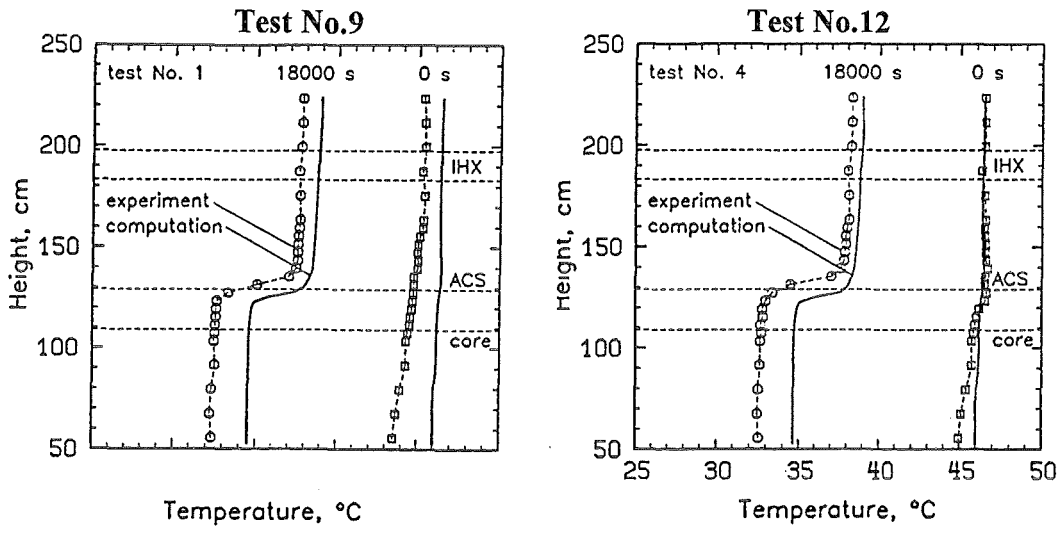

Fig. 32 Comparison of measured and computed axial temperature profiles in the UP. Influence of blocked primary flow paths of IHXs.

APPENDIX

Test No.2

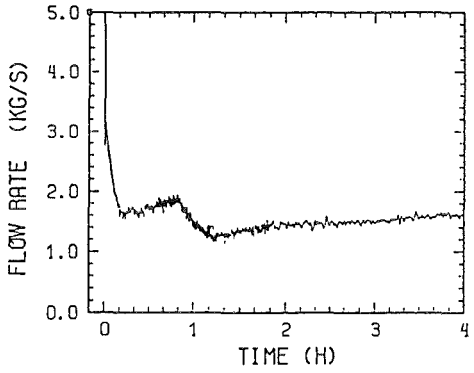

a) total core mass flow rate

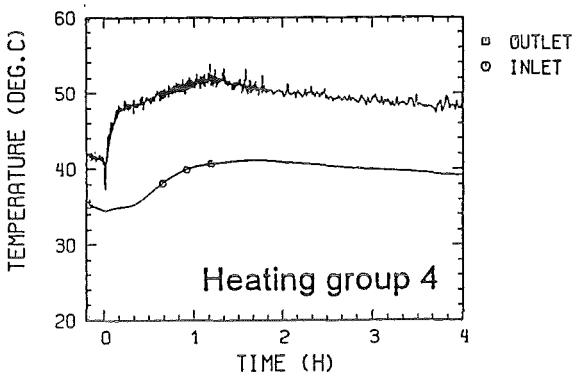

b) inlet and outlet temperatures of a core element, heating group 4

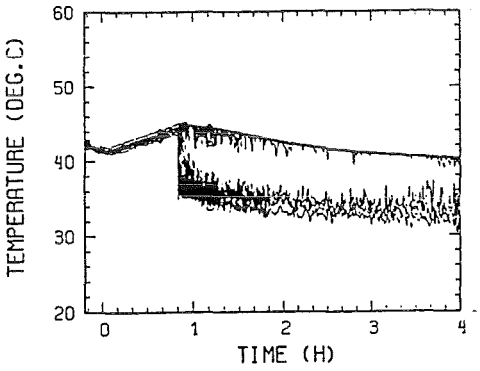

c) inlet and outlet temperatures at the primary side of the DHXs

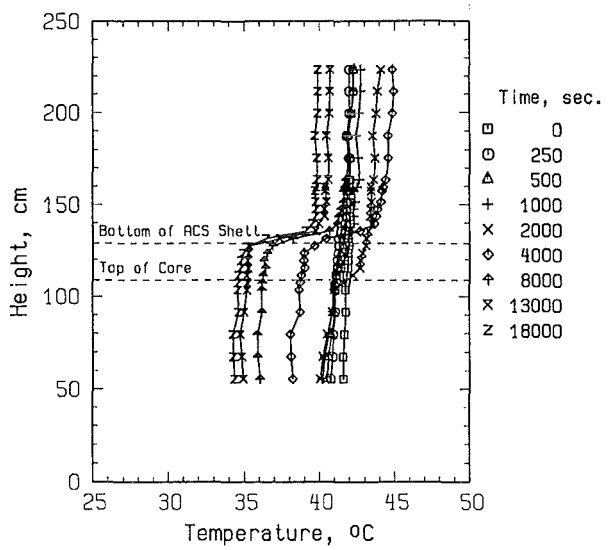

d) temperature profiles in the upper plenum

Fig.1-A Influence of the DHX startup delay time of 3000s on the transition from forced to natural convection (P =800 kW)

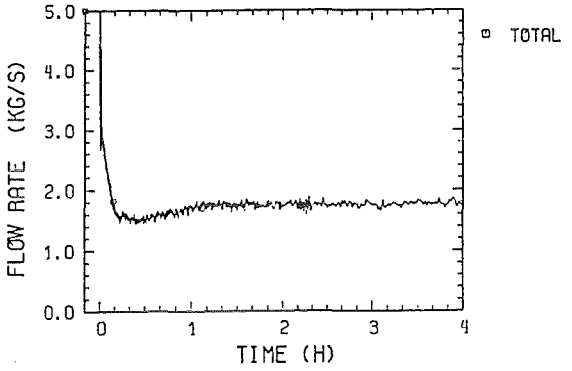

Test No.3

a) total core mass flow rate

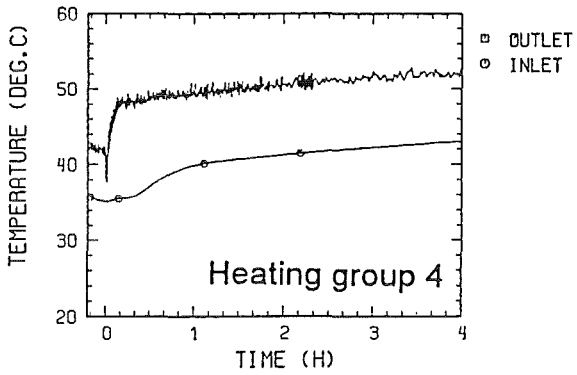

b) inlet and outlet temperatures of a core element, heating group 4

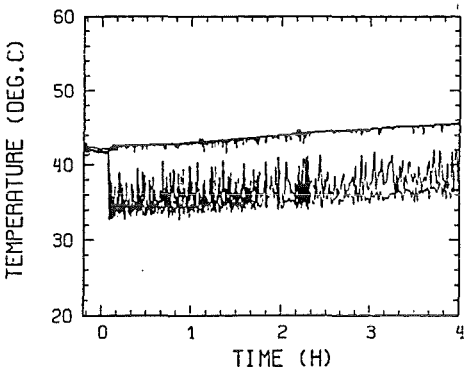

c) inlet and outlet temperatures at the primary side of the DHXs

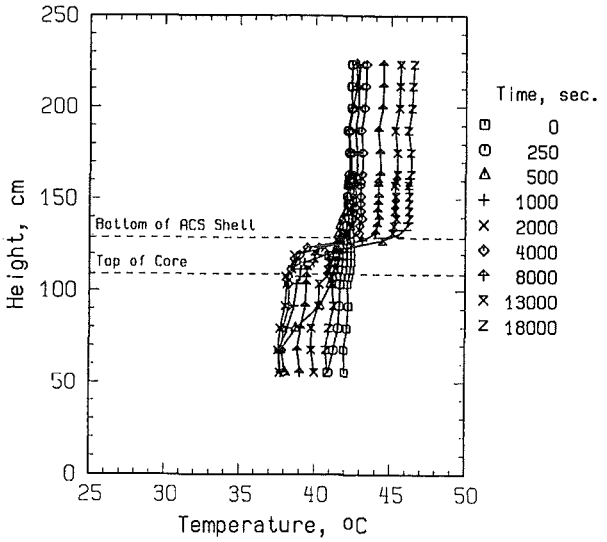

d) temperature profiles in the upper plenum

Fig.2-A Influence of asymmetric cooling mode on the transition from forced to natural convection (P =800 kW)

Test No.4

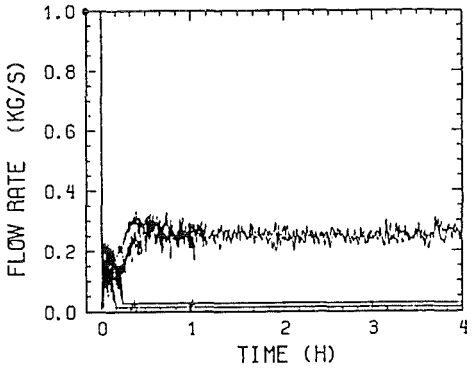

a) total core mass flow rate

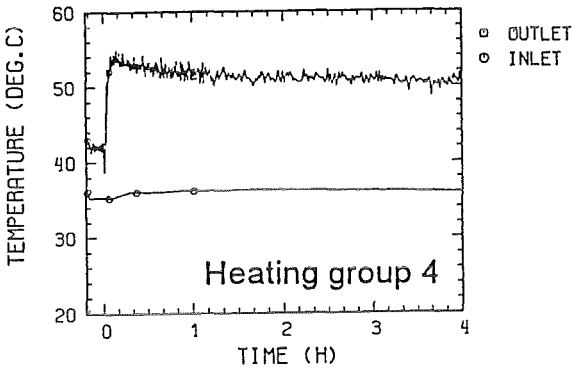

b) inlet and outlet temperatures of a core element, heating group 4

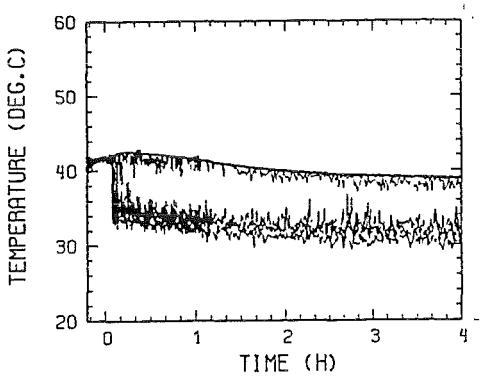

c) inlet and outlet temperatures at the primary side of the DHXs

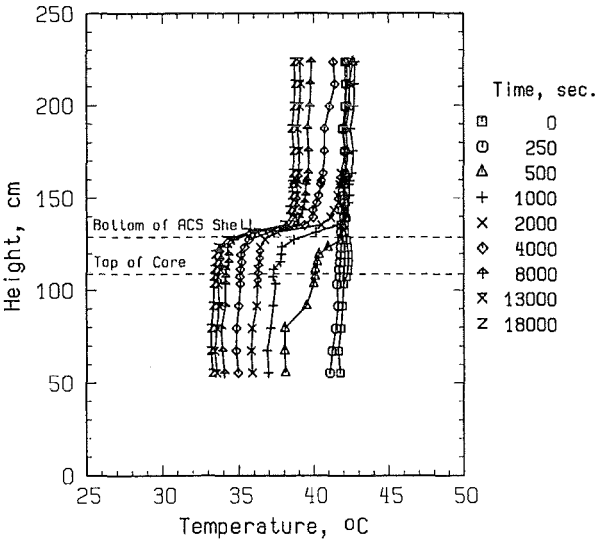

d) temperature profiles in the upper plenum

Fig.3-A Influence of the blocked primary flow paths of the IHXs on the transition from forced to natural convection (P =800 kW)

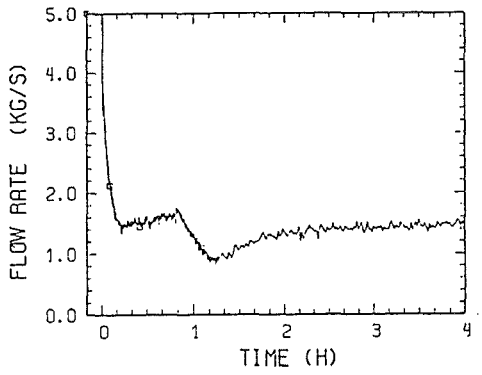

Test No.6

a) total core mass flow rate

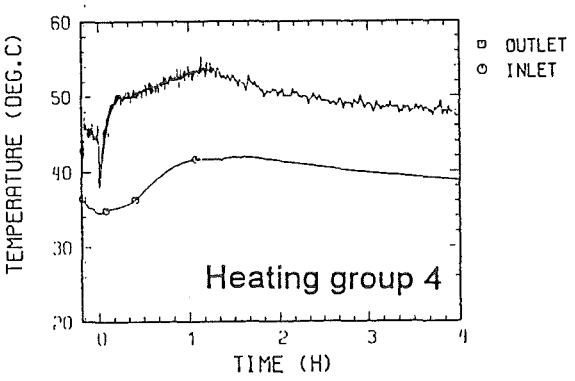

b) inlet and outlet temperatures of a core element, heating group 4

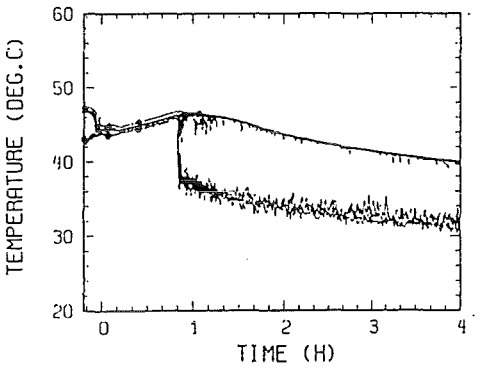

c) inlet and outlet temperatures at the primary side of the DHXs

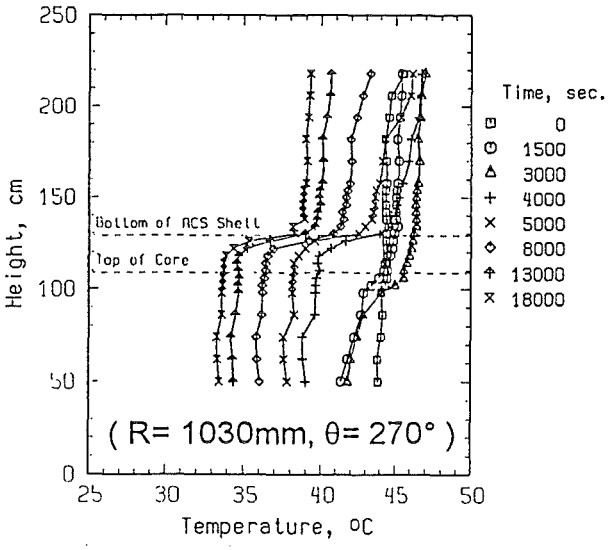

d) temperature profiles in the upper plenum

Fig.4-A Influence of the DHX startup delay time of 3000s on the transition from forced to natural convection (P =1100 kW)

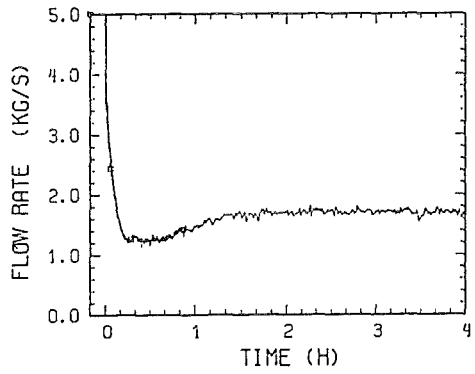

Test No.7

a) total core mass flow rate

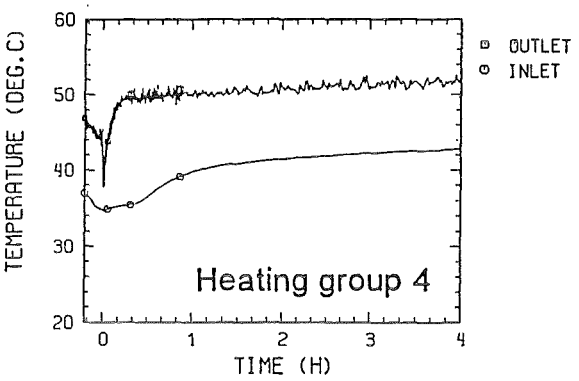

b) inlet and outlet temperatures of a core element, heating group 4

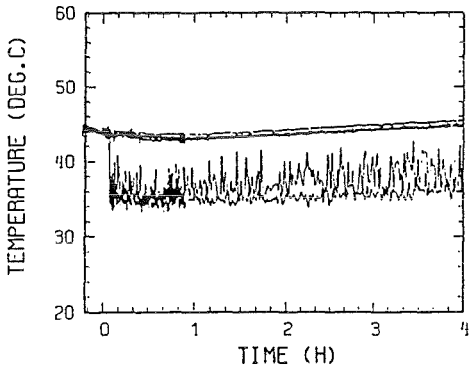

c) inlet and outlet temperatures at the primary side of the DHXs

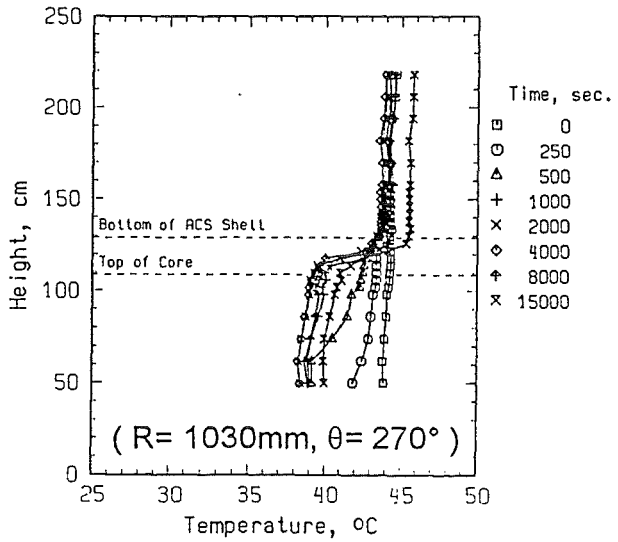

d) temperature profiles in the upper plenum

Fig.5-A Influence of asymmetric cooling mode on the transition from forced to natural convection (P =1100 kW)

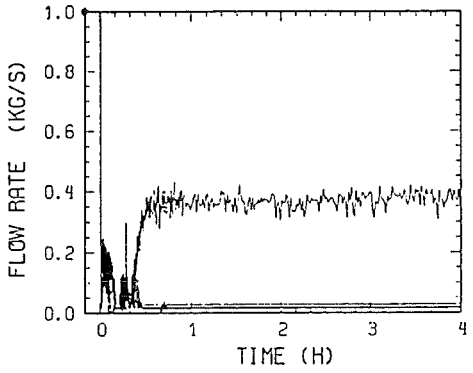

Test No.8

a) total core mass flow rate

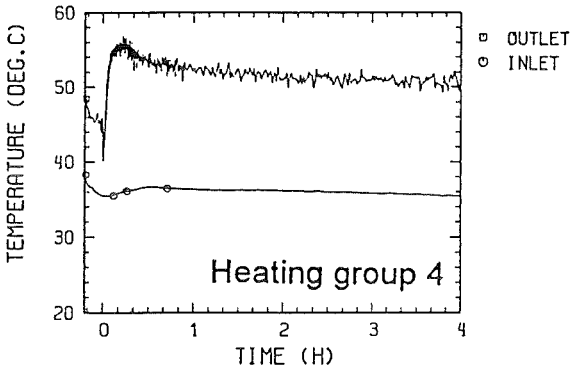

b) inlet and outlet temperatures of a core element, heating group 4

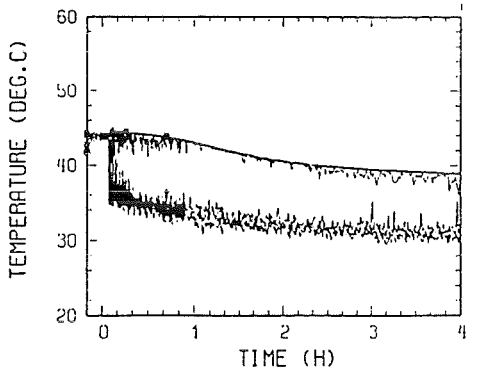

c) inlet and outlet temperatures at the primary side of the DHXs

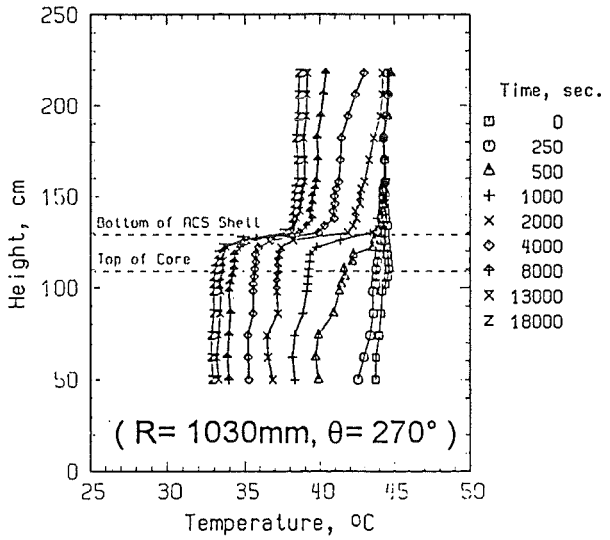

d) temperature profiles in the upper plenum

Fig.6-A Influence of the blocked primary flow paths of the IHXs on the transition from forced to natural convection (P =1100 kW)

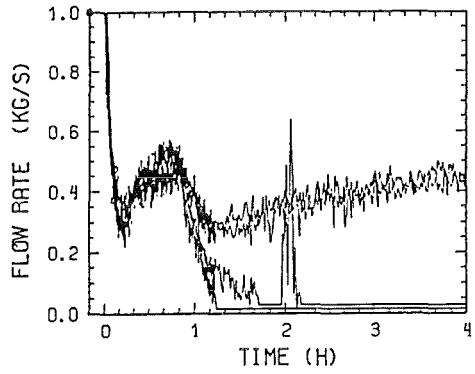

Test No.14

a) total core mass flow rate

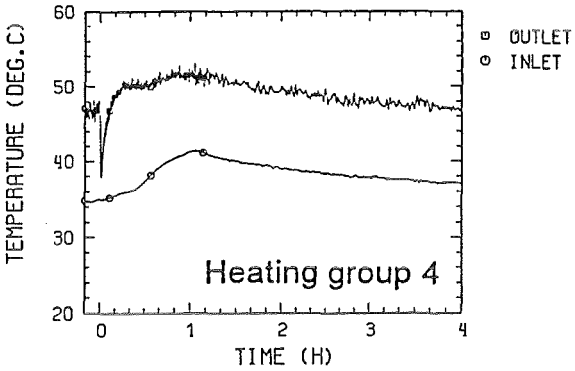

b) inlet and outlet temperatures of a core element, heating group 4

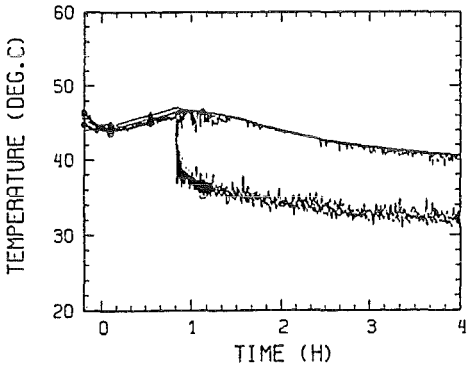

c) inlet and outlet temperatures at the primary side of the DHXs

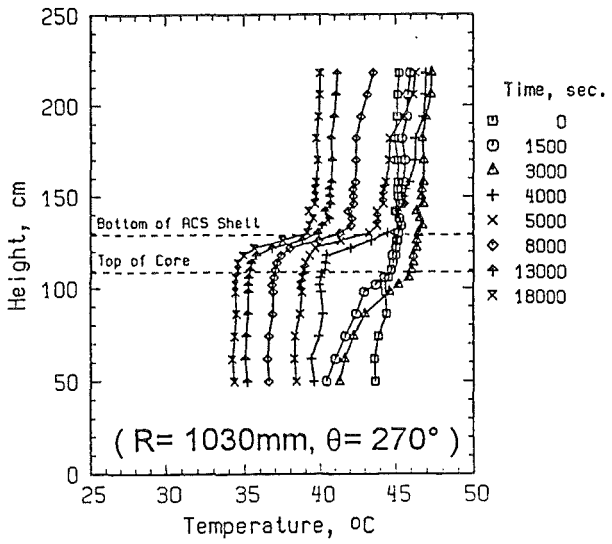

d) temperature profiles in the upper plenum

Fig.7-A Influence of the DHX startup delay time of 3000s on the transition from forced to natural convection (P =1600 kW)

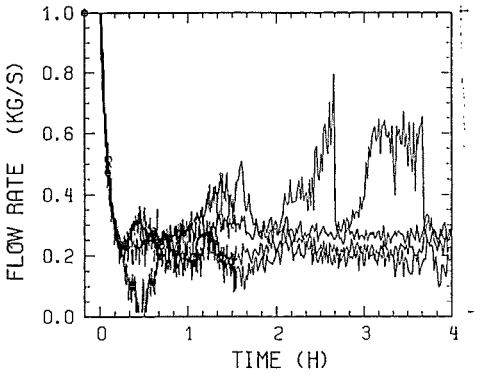

Test No.15

a) total core mass flow rate

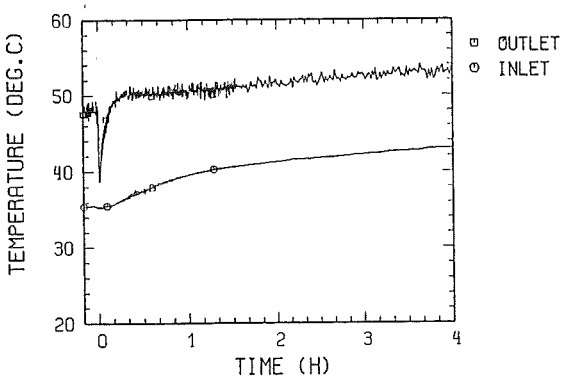

b) inlet and outlet temperatures of a core element, heating group 4

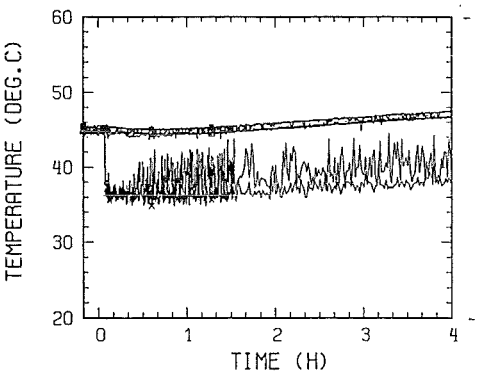

c) inlet and outlet temperatures at the primary side of the DHXs

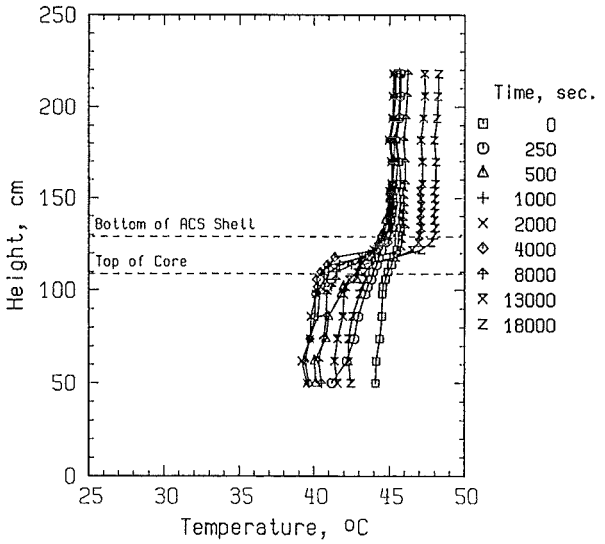

d) temperature profiles in the upper plenum

Fig.8-A Influence of asymmetric cooling mode on the transition from forced to natural convection (P =1600 kW,ACS impermeable)

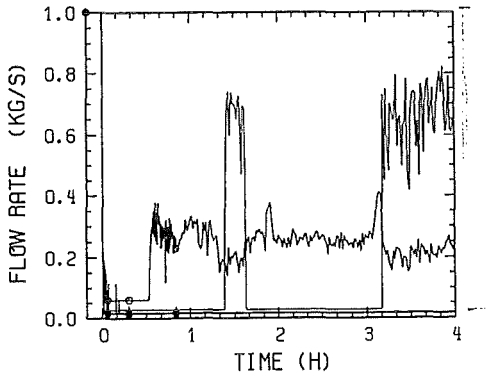

Test No.16

a) total core mass flow rate

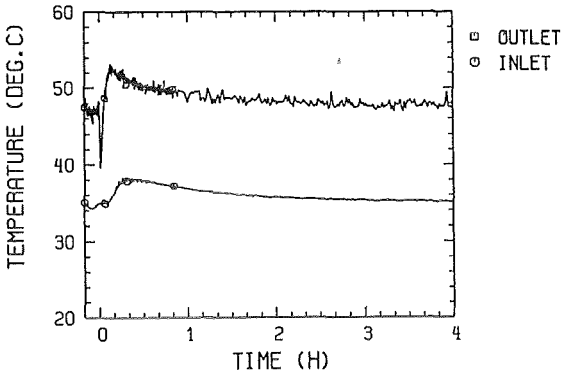

b) inlet and outlet temperatures of a core element, heating group 4

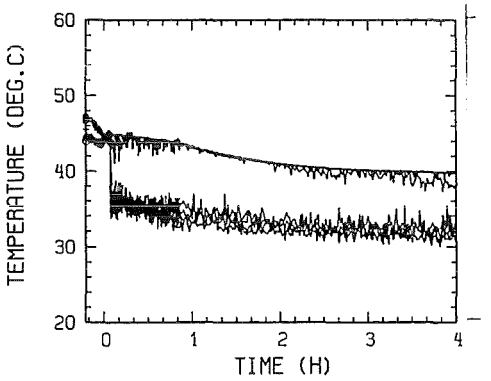

c) inlet and outlet temperatures at the primary side of the DHXs

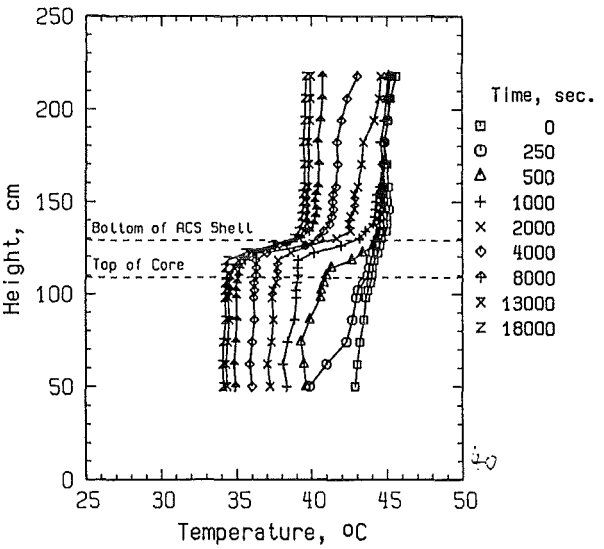

d) temperature profiles in the upper plenum

Fig.9-A Influence of the blocked primary flow paths of the IHXs on the transition from forced to natural convection (P =1600 kW,ACS imperm.)

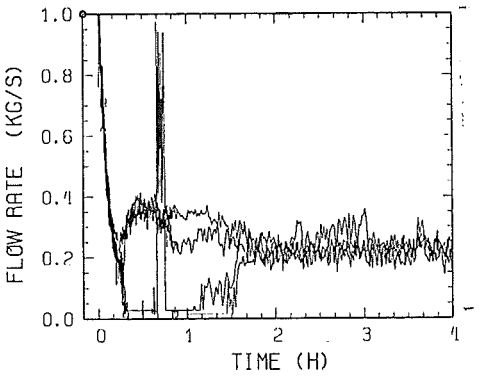

Test No.18

a) total core mass flow rate

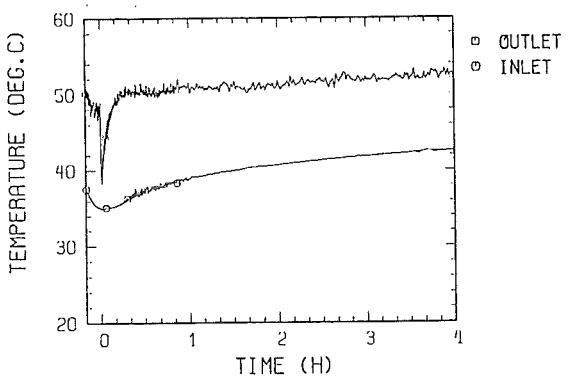

b) inlet and outlet temperatures of a core element, heating group 4

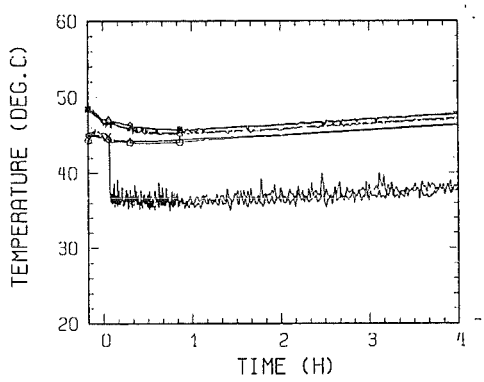

c) inlet and outlet temperatures at the primary side of the DHXs

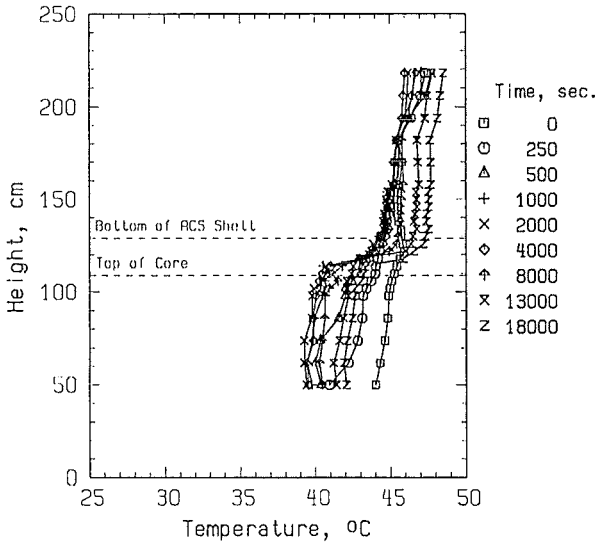

d) temperature profiles in the upper plenum

Fig.10-A Influence of asymmetric cooling mode on the transition from forced to natural convection (P =1600 kW,ACS permeable)

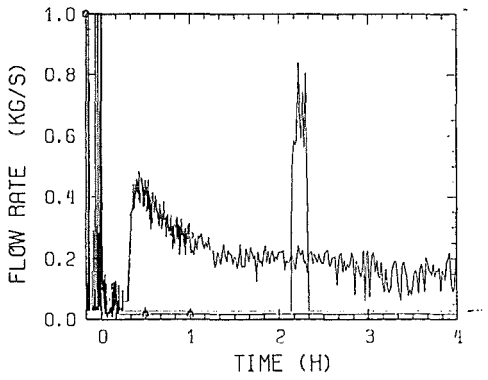

Test No.19

a) total core mass flow rate

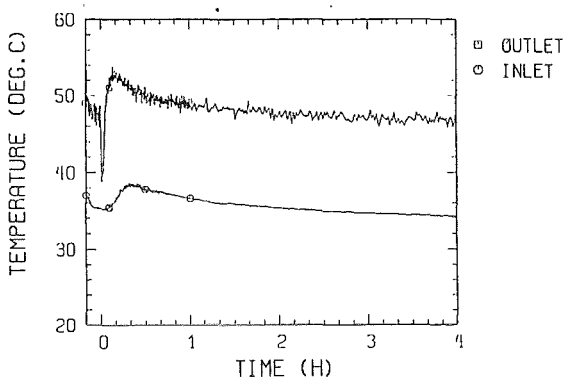

b) inlet and outlet temperatures of a core element, heating group 4

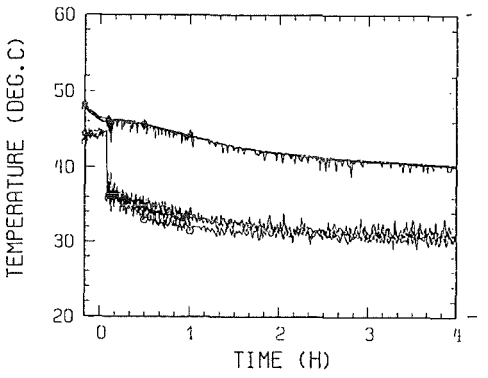

c) inlet and outlet temperatures at the primary side of the DHXs

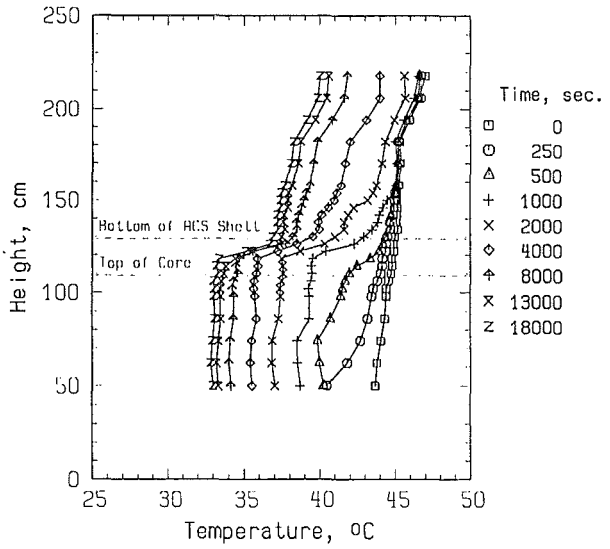

d) temperature profiles in the upper plenum

Fig.11-A Influence of the blocked primary flow paths of the IHXs on the transition from forced to natural convection (P =1600 kW, ACS perm.)